CHARACTERIZATION OF THE BACTERIOPHAGE LAMBDA HOLIN AND ITS MEMBRANE LESION

A Dissertation

by

JILL SAYES DEWEY

Submitted to the Office of Graduate Studies of
Texas A&M University
in partial fulfillment of the requirements for the degree of

DOCTOR OF PHILOSOPHY

August 2010

Major Subject: Biochemistry

CHARACTERIZATION OF THE BACTERIOPHAGE LAMBDA HOLIN AND ITS MEMBRANE LESION

A Dissertation

by

JILL SAYES DEWEY

Submitted to the Office of Graduate Studies of
Texas A&M University
in partial fulfillment of the requirements for the degree of

DOCTOR OF PHILOSOPHY

Approved by:

Chair of Committee,	Ryland Young
Committee Members,	Mary Bryk
	Christian Hilty
	Andreas Holzenburg
Head of Department,	Gregory Reinhart

August 2010

Major Subject: Biochemistry

ABSTRACT

Characterization of the Bacteriophage Lambda Holin and Its Membrane Lesion.

(August 2010)

Jill Sayes Dewey, B.S. Louisiana State University

Chair of Advisory Committee: Dr. Ryland Young

Bacteriophage holins are a diverse group of proteins that are responsible for the spontaneous and specifically-timed triggering of host cell lysis. The best-studied holin, S105 of phage lambda, is known to form lesions, or "holes", in the inner membrane of *E. coli* which are large enough to allow the endolysin through to the periplasm. S105 has been studied extensively by both genetic and biochemical approaches; however, little is known about the mechanism of hole formation or the structure of the lambda holin and its inner membrane lesion.

An in vitro system for reconstituting hole formation by S105 was developed in which liposomes containing a self-quenched fluorophore served as artificial cell membranes (1-2). Upon delivery of solubilized S105 to the liposomes, an increase in fluorescence was observed, indicating that the fluorophore within the liposomes had escaped into the surrounding media via an S105-mediated hole in the membrane. This in vitro system, which has been optimized in this work, has been a valuable biochemical tool for analysis and reconstitution of the pathway to S105 hole formation in the cell membrane.

Due to the difficulty associated with over-expression and purification of toxic membrane proteins, there are no solved structures of bacteriophage holins. Sample preparation and experimental conditions for NMR spectroscopy were optimized and structural information about a lambda holin mutant protein was obtained. Specifically, micellar contacts of transmembrane domain regions versus water contacts of the C-terminal region, secondary structure, and backbone dynamics were determined.

Cryo-electron microscopy was used to visualize the inner membrane lesions formed by phage holins λ S105, P2 Y, and T4 T. Therefore, the large holes initially seen in cells expressing S105 are not specific to the lambda holin, nor to class I holins. The S105 holes average ~340 nm (3), and are the largest membrane lesions ever observed in biology. They are stable at their original size, and are not localized to a specific region of the membrane. In addition, missense mutants of S105 were used to correlate hole size, protein accumulation, and lysis timing in a current model for the S105 hole formation pathway.

DEDICATION

To my husband, Ryan, for his love and support, and to my parents, Cathy and Mac, for believing in me.

ACKNOWLEDGEMENTS

I would like to thank my advisor, Dr. Ryland Young, and my committee members, Dr. Mary Bryk, Dr. Christian Hilty, Dr. Andreas Holzenburg, and Dr. Arthur Johnson for their insight and guidance throughout my time at Texas A&M University. I am also thankful for the support from the Young lab members, past and present. In particular, Dr. Christos Savva and Dr. Rebecca White, my fellow "S-group" members, who were instrumental in my success during graduate school, and I thank them whole-heartedly for their patience, advice, and encouragement. I would like to acknowledge our collaborators as follows: Dr. Christos Savva, Dr. Andreas Holzenburg, and Dr. Stan Vitha for microscopy, Dr. Christian Hilty and Youngbok Lee for NMR, Dr. Rebecca White and Chelsey Dankenbring for mutational analysis of the lambda holin, and Samir Moussa for visualizing cells expressing the T4 holin. Also, I would like to thank Greg Whitaker, who worked with me as an undergraduate, and Kenneth To and Jeremy Weaver, who worked with me during graduate school laboratory rotations.

I am indebted to my family and friends who have been extremely supportive of my education, especially my husband, Ryan Dewey, my parents, Catherine and Malcolm Sayes, my sister, Dr. Christie Sayes, and my in-laws, Cynthia and James Dewey.

TABLE OF CONTENTS

LIST OF FIGURES

FIGURE Page

FIGURE Page

FIGURE Page

CHAPTER I

INTRODUCTION TO BACTERIOPHAGE HOLINS

Bacteriophages, or just simply phages, are viruses that infect and kill bacterial cells. During the infection process, phages inject their DNA into the host cell, and progeny virions are assembled within the bacterium. To effect release of the virus particles, phages ultimately kill their host cells through a process called lysis. For lysis to occur, the host bacterial cell wall, or peptidoglycan layer, must be compromised in some way. The cell wall primarily serves to protect the intracellular contents, as well as maintain the overall shape of the cell (4), but during lysis, it is considered the barrier which keeps progeny virions from escaping the cell. For double-stranded nucleic acid phages, lysis is accomplished by a "holin-endolysin" system, and this strategy is referred to as the classic lysis paradigm (5-7). The endolysin, or lysozyme, is a murein-degrading, soluble enzyme that is responsible for the destruction of the cell wall peptidoglycan layer (4, 8). The holin, a membrane-bound protein which is credited with activating the endolysin, has roles in both membrane depolarization and precise timing of lysis (4, 9-10).

This dissertation follows the style of *Proceedings of the National Academy of Sciences of the United States of America*.

The Lambda Lysis Paradigm

Lambda is a double-stranded DNA phage with a long, non-contractile tail, belonging to the order *Caudovirales* and family *Siphoviridae*. In terms of lysis, lambda uses the classic paradigm of a holin-endolysin system. Within the genome, there are four separate lysis genes which comprise the lambda lysis cassette. The genes are located just downstream of the late promoter P_R' in the following order: *S* (holin), *R* (endolysin), *Rz*, and *Rz1* (Fig. 1.1). *S* has translational start sites at positions Met1 and Met3, which serve as the beginning residues of two separate proteins, S107 and S105, respectively (11) (Fig. 1.2). S105 is the holin and functions in both permeabilization of the membrane and lysis timing (6, 10). S107 is the antiholin and functions to inhibit hole formation by S105 (10). R, the endolysin, is responsible for degradation of the peptidoglycan layer, or cell wall, immediately preceding host cell lysis (12) (Fig. 1.3). Rz and Rz1 are two separate proteins, despite the fact that the *Rz1* reading frame is completely embedded within *Rz,* which function in destabilization of the outer membrane, and together they form a spanin complex (13).

During lambda lysis, S105 accumulates and oligomerizes in the inner membrane, and R is made in the cytoplasm, beginning with late gene expression. At a precisely-scheduled time that is genetically programmed, S105 forms a hole, or lesion, in the inner membrane, which allows the endolysin to bypass the cytoplasmic membrane and access its substrate, the peptidoglycan layer (6) (Fig. 1.3). Once R has degraded the cell wall,

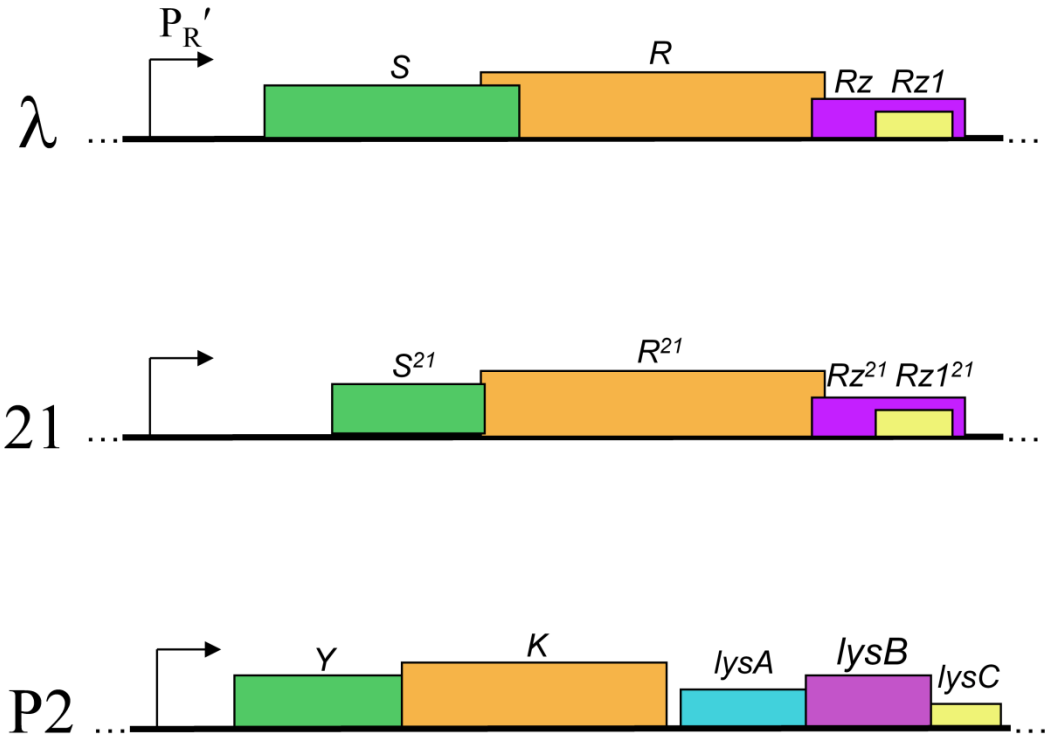

Figure 1.1. Lysis cassettes of bacteriophages lambda, 21, and P2. The following lysis genes are downstream of the late promoter, P_R' (arrow): holin (green), endolysin (orange), *Rz*-equivalent (magenta), and *Rz1*-equivalent (yellow). P2 has an additional gene, *lysA* (blue), which encodes the antiholin.

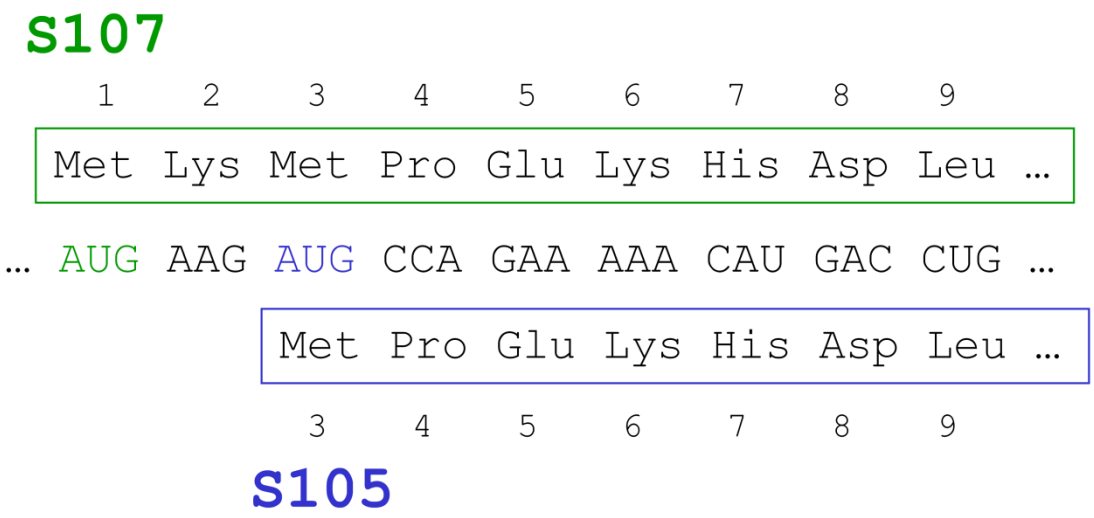

Figure 1.2. Dual-start motif of the lambda *S* gene. *S* encodes for two separate proteins: S107 (green), which is the antiholin, and S105 (blue), which is the holin. S107, which has two additional residues at the N-terminus, is 107 amino acids long, and its translation begins with Met1. S105 is 105 amino acids long, and its translation begins on Met3.

the outer membrane becomes destabilized with the help of Rz and Rz1 (13), and lysis ensues.

The Lambda Holin S105

The lambda holin gene product, S105, was first characterized by Altman et al. (1983) using two different models (9). The first model system was maxicells, in which the holin and endolysin genes were expressed from plasmids, and the second system involved UV-irradiated, lambda-infected cells. The results indicated the lambda holin gene product to be an 8.5 kDa protein (9). Isopycnic sucrose gradients containing lysates of infected cells were used to show that S105 localized to the inner membrane of *E. coli* cells (9). As shown in Figure 1.4, the lambda holin has three transmembrane domains (TMDs) which span the inner membrane of a bacterial cell (14). The N-terminus is located in the periplasm, and the C-terminus is located in the cytoplasm (14).

In order to determine the correct topology of S105 within the membrane, genetic and biochemical approaches were used. Random mutagenesis and site-directed mutagenesis were used to change single residues throughout the 105 amino acid protein (15-16). Studies with these mutants indicated that amino acid substitutions within all three TMDs of S105 changed the apparent lysis time (14). In fact, alanine at position 52, within the second TMD, was converted to both glycine and valine (14). The resulting mutants had very different phenotypes: $S105_{A52G}$ caused lysis of its host early at 19 minutes after induction; $S105_{A52V}$, in contrast, did not cause lysis of its host at all and

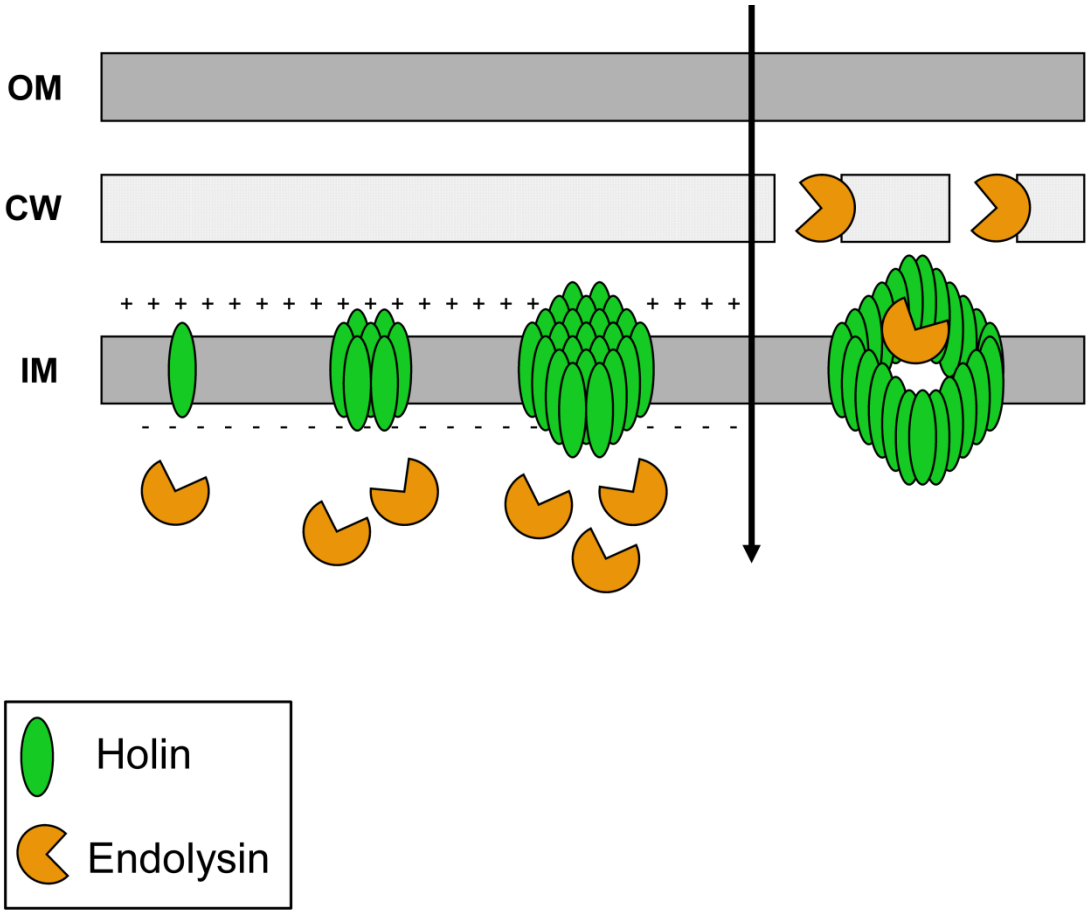

Figure 1.3. Model of holin-endolysin mechanism for lambda lysis. The cell envelope is composed of three layers: the outer membrane (OM), the peptidoglycan layer or cell wall (CW), and the inner membrane (IM). The holin (green) accumulates and oligomerizes in the inner membrane which has an associated pmf until the spontaneous time of triggering for hole formation (arrow). The endolysin (orange) accumulates in the cytoplasm, then passes through the inner membrane via the holin lesion.

was considered a non-hole-forming S mutant (17). Additional experiments involved cysteine substitutions of single amino acids, which allowed for chemical accessibility studies of S105. Specifically, the single Cys substitution alleles were expressed in cells so that inverted membrane vesicles (IMVs) and spheroplasts could be made and treated with the sulfhydryl-specific, membrane-impermeant reagent 4-acetamido-4′-((iodoacetyl)amino)stilbene-2,2′-disulfonic acid, disodium salt, or IASD (14). Three regions within the protein remained resistant to modification by IASD, and corresponded to the core regions of the predicted TMDs for S105 (14) (Fig. 1.4).

S105 has two distinct functions. The lambda holin is an inner membrane protein that oligomerizes upon accumulation until it forms a lesion in the membrane at an allele-specific time (9-10) (Fig. 1.3). The first biochemical evidence of S oligomerization in the inner membrane of *E. coli* cells was with detection of S-lacZ fusion proteins which had been extracted from membranes and crosslinked (18). Later, crosslinking data of DSP-treated membranes containing S105 demonstrated the presence of covalently-linked oligomers up to 6-mers (7).

In addition to hole formation, S105 has a second role in the timing of host lysis. In fact, S105 hole formation, which is due to a spontaneous, genetically-programmed triggering for lysis, has been characterized as the simplest biological clock (6). Although very little is known about the timing of phage lysis, it is considered extremely important from an evolutionary viewpoint. Extremely early lysis, such as before the first

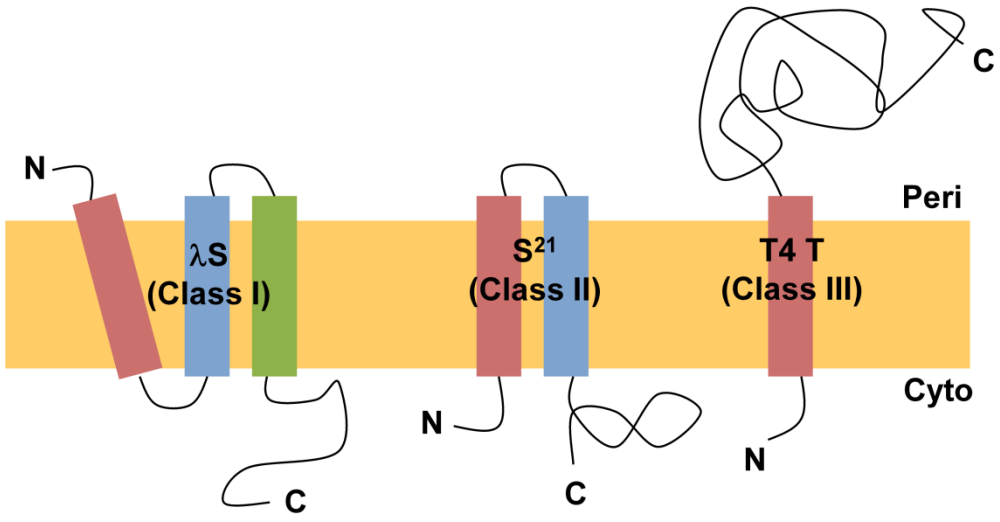

Figure 1.4. Three classes of holin proteins. Class I holins (left) have three transmembrane domains (TMDs) and an N-out, C-in topology. Class II holins (middle) have two TMDs and an N-in, C-in topology. Class III holins (right) have one TMD and an N-in, C-out topology.

virion phages are formed, would result in a non-productive infection. In this particular case, the absence of progeny virions would prevent subsequent infection of host cells. Alternatively, very late lysis is wasteful because progeny virions are trapped within a host and unable to infect more cells for the production of additional phage. Therefore, the tight scheduling of holin activity is essential for productive host cell lysis. The best way to illustrate this point is to compare the mutants $S105_{A52G}$ and $S105_{A52V}$, which have already been mentioned in terms of their different lysis phenotypes. $S105_{A52G}$ lyses very early at 17 min, while $S105_{A52V}$ is non-lytic (17). Both mutants are non-plaque-formers; however, the reasons for their non-productive phage infections are very different. $S105_{A52G}$ lyses too early for phage virions to be able to form, while $S105_{A52V}$ forms virions, but without lysis, is not able to release progeny.

A recent publication, featuring a modeling approach of phage-induced lysis, focuses on the inherent optimization of lysis timing by the lambda holin (19). According to the authors, lambda lysis involves a two step nucleation event; the first nucleation event being the condensation of holin "rafts", or inner membrane-associated aggregates of molecules, long before the time of lysis, and the second nucleation event, the formation of a hole within the holin raft. The modeling approach of the inner membrane holin molecules was used to assess the efficiency of phage lysis. The authors used variables to represent the holin interaction, the hole nucleation, the average lysis time, and the timing accuracy. The conclusions derived by the nucleation theory suggested that lambda lysis timing is optimal and cannot be improved upon by modeling. In fact,

the authors were unable to improve the lysis timing accuracy when they changed the holin interaction variable (19).

The structure of the S105-mediated lesion in vivo. Wang et al. (2003) used cells induced for expression of the fusion protein R, the lambda endolysin, tethered to full-length β-galactosidase (β-Gal), to determine the approximate size of the S105-mediated lesion (20). The hole formed by S105 was large enough to allow the R-β-Gal fusion protein, an active tetrameric β-Gal with a size larger than 480 kDa in mass, to bypass the inner membrane and degrade the cell wall, leading to host cell lysis (20). Experimental evidence, including lysis curves and plaque assays, showed that the R-β-Gal fusion was functional in lysis when expressed with the holin S105. In addition, the authors used a combination of immunoblotting and gel filtration to demonstrate the accumulation of R-β-Gal in its full-sized and active conformation. Therefore, this data suggests that the size of the lambda holin lesion is much larger than previously anticipated. In fact, to accommodate the size of tetrameric β-Gal, a protein that is 30 times the size of the 18 kDa endolysin, the S105-mediated hole must be larger than any known transmembrane channel constructed of intracellular proteins (20). To date, the largest documented membrane lesions are formed by the cholesterol-dependent cytolysins, a family of proteins which form pores with diameters of ~30 nm (21-22).

In addition to elucidating the large size of the holin lesion, Wang et al. (2003) also tested the R-β-Gal fusion protein for lysis in a prematurely triggered system (20). Specifically, the energy poison cyanide was added to a growing culture of cells induced

for expression of either R, or R-β-Gal, with S105. The results showed that R caused lysis as expected while R-β-Gal did not. In a separate experiment, R-β-Gal was expressed with an early lysing mutant of S105, $S105_{A52G}$, and was shown to cause efficient lysis. The experimental evidence suggested that prematurely triggered lysis resulted in smaller membrane lesions than spontaneously formed holes (20).

The structure of the lambda holin. Just as very little is known about the S105-mediated inner membrane hole, the same is true for the structure of the lambda holin in vitro. Historically, structural studies of holins have been very difficult because of the limitations during over-expression of toxic membrane proteins for purification purposes. Despite the challenges associated with large-scale purification of membrane proteins, Coomassie-blue detectable amounts of S were obtained with T7-based over-expression from a pET vector (23). In fact, 50-fold over-production of protein was achieved during the first 10 minutes following IPTG induction of such expression systems (6). The purified protein was shown to be localized to the membrane and the protein could be extracted from the membrane with either nonionic or zwitterionic detergents. An oligohistidine tag was incorporated within the sequence of S105 at position 94, and its presence was shown not to affect lysis timing or holin function (24). Before position 94 was tested, numerous oligohistidine insertions throughout S105, including both the N- and C-termini, were constructed. Most of the insertions changed the behavior of S105, sometimes even completely abolishing holin function. The presence of a His_6 tag allowed for successful purification of 1-3 mg protein per liter culture via immobilized

metal affinity ion chromatography (IMAC) (2). The ability to obtain purified S105 at relatively high levels for detergent-soluble membrane proteins, facilitated efforts to both study hole formation in vitro and determine the structure of the lambda holin.

Although there are currently no solved structures of holin proteins, either through X-ray crystallography or nuclear magnetic resonance (NMR), electron microscopy (EM) has been instrumental in obtaining structural information about detergent-purified S105. Savva et al. (2008) showed that S105 which was extracted from the membrane and purified in the presence of dodecyl maltoside (DDM) formed different oligomeric species, as evident from three separate gel permeation peaks (25). This was in contrast to Empigen BB (EBB)-purified S105 which was present in only a single oligomeric species, and only one gel permeation peak, after purification. The peak fractions from gel filtration of DDM-purified S105 were analyzed by EM, revealing the presence of ring-like structures which were present as monomers, dimers, and stacks of rings (Fig. 1.5). Single particle analysis of the rings showed that the majority had an inner diameter of 8.5 nm, an outer diameter of 23 nm, and a height of 4 nm, a height which is very similar to the thickness of the lipid bilayer (Fig. 1.5) (25). Additional experiments were carried out to assess the accessibility of S105 in rings to proteolysis and chemical modification. Unlike S105-associated inverted membrane vesicles (IMVs), which

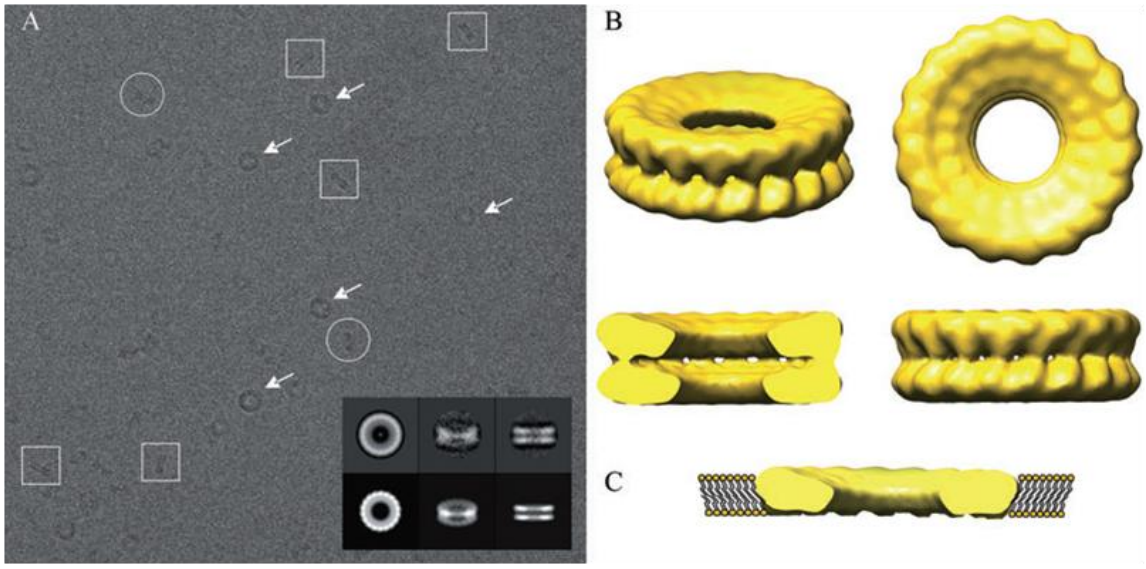

Figure 1.5. S105 rings in detergent. (A) EM image of ring-like structures, positioned in top-down view (arrows), or side-view (boxes/circles). Inset shows averages of the most common size classes for the rings. (B) Reconstructions based on single-particle analysis of the class averages. (C) The ring depth was similar to the depth of the lipid bilayer. Reprinted with permission from Savva et al. (25).

proved to be sensitive to proteinase K at both the N- and C-termini, S105 rings allowed for digestion of the C-terminus only. The authors suggested that the N-terminus in S105 rings was resistant to protease activity because it was protected by the formation of stacks (25). Similarly, the thiol-modification reagent, PEG-maleimide (PEG-mal), was used to further analyze the accessibility of strategically-positioned cysteines within S105 rings. It was determined that cysteines positioned at the termini were able to react with PEG-mal, whereas Cys51, which is positioned within the second TMD, was only accessible to PEG-mal after treatment with the detergent sodium dodecyl sulfate (SDS). These rings may represent the holes, or lesions, formed by S105 within the bilayer of the inner membrane just before host cell lysis, but additional in vivo studies of S105 holes are required to make this determination (25).

Classification of Holin Proteins

Holins have been classified into three groups based on size, number of TMDs, and topology (Fig. 1.4). It should be noted that actual TMDs have been experimentally demonstrated for only a few holins, while the majority of TMDs are identified by prediction programs such as TM hidden Markov model (TMHMM) (6). Class I holins, a group which includes S105, have three TMDs, an N-terminal periplasmic domain, and a C-terminal cytoplasmic domain (6-7) (Fig. 1.4). This group is also classified as having members with 90-125 amino acids. In addition to the lambda holin, other class I holins include, but are not limited to, the following: Y from phage P2, LydA from phage P1, and gp*13* from phage P22. Class II holins have two TMDs, cytoplasmic N- and C-

terminal domains, and 65-85 amino acid residues (4-5) (Fig. 1.4). Members of this group include S68 from phage 21 and gp*17.5* from phage T7, among others. Class III holins, a group which consists of T4 T as well as the holin proteins of all T4-related phages, have a single TMD, cytoplasmic N-terminus and periplasmic C-terminus, and share very few, if any, characteristics with other holins (7) (Fig. 1.4).

Although both Y from bacteriophage P2 and S105 from lambda are class I holins, the proteins differ considerably from one another. For instance, there is no detectable protein sequence similarity between the holin proteins. In addition, lambda *S* has a dual start motif, which contains two separate translation initiation sites, one for encoding S105 and the other for S107 (11) (Fig. 1.2). P2 *Y*, on the other hand, encodes a single protein, and therefore, only has one translational initiation site. In fact, there is a separate, unrelated gene, *lysA*, downstream of *Y* that is believed to encode the antiholin of phage P2 (26) (Fig. 1.1). This describes a system very different from that of many lambdoid phages with one gene encoding both the holin and the antiholin, which are two proteins of opposing function, despite the fact that they only differ by two or three N-terminal amino acids (27). Additional lysis genes have been identified for P2, which include the endolysin *K*, and *Rz/Rz1*- equivalent genes *lysB* and *lysC* (26) (Fig. 1.1).

The second class of bacteriophage holins includes two proteins which are not required for host cell lysis. gp*17.5* from phage T7 has been shown to effect sharp lysis in the context of the lambda phage, i.e. *17.5* expressed with lambda genes *R*, *Rz*, and *Rz1* (28). Unlike the lambda holin S105, gp*17.5* is not essential for host cell lysis. It was shown that cells infected with T7 phage, which were deleted for the *17.5* gene, were still

able to lyse host cells; however, lysis occurred at a slightly delayed time compared to cells infected with T7 phage containing gene *17.5* (29). The authors suggested that the reason why a *17.5* deletion mutant still lyses cells may be because there is another, not yet identified, T7 holin gene which is responsible for membrane depolarization (29).

$S^{21}68$ from phage 21 is another example of a class II holin that is not required for host lysis (Figs. 1.1, 1.4). This protein forms small holes, termed "pinholes", which are not large enough to accommodate the size of the phage 21 endolysin, R^{21} (30). Because the holin does not provide a lesion for R^{21} to use to bypass the inner membrane, the phage must have another mechanism for host lysis. Indeed, this mechanism describes a second mode of lysis which serves as an alternative to the paradigm holin-endolysin lambda lysis system. R^{21} is a Signal-Anchor-Release (SAR) endolysin which contains a signal sequence, directing it to the membrane and into the periplasm via the host Sec system (30-31) (Fig. 1.6). Once the membrane is depolarized by $S^{21}68$, the SAR endolysin is released from the membrane, undergoes refolding, and becomes catalytically active, allowing lysis (32).

The members of holin classes I and II are extremely diverse in terms of their primary structure, however this is not the case for class III holins. In fact, class III is comprised solely of T4 and T4-like phage holins (7). T, the holin from phage T4, is very large when compared to the average size of other holins. In fact, T is twice the size of

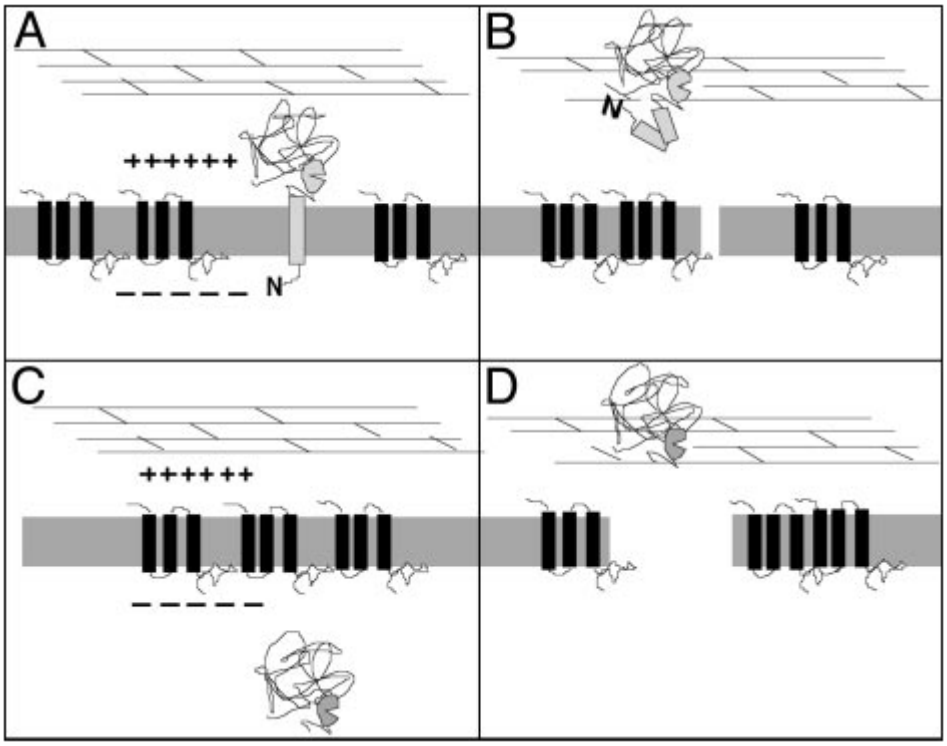

Figure 1.6. Modes of action for SAR endolysins versus soluble endolysins. (A) SAR endolysins are tethered to the membrane. (B) Depolarization of the membrane by the holin releases the SAR endolysin into the periplasm. (C) Soluble endolysins accumulate in the cytoplasm, and (D) are released into the periplasm upon hole formation by the holin. Reprinted with permission from Xu et al. (33). Copyright (2004) National Academy of Sciences, U. S. A.

the 105 amino acid lambda S, with an impressive 218 residues (34). In addition, T is largely hydrophilic in nature as it contains 49 acidic and basic amino acids (Fig. 1.4) (34). This describes a characteristic that is not shared by other holins belonging to the first two classes, which are largely defined by TMDs consisting of predominately hydrophobic residues. When *T* is expressed with the lambda lysis genes, *R*, *Rz*, and *Rz1*, it elicits sharp lysis at 20 min, showing that it is a functional holin within the lambda context (34). Much like S105, T-mediated lysis timing has some genetic malleability, as evident from single missense changes within T resulting in a wide range of lysis times (35).

Phage T4 is subject to a phenomenon known as lysis inhibition, or LIN (34, 36). Although lysis does not occur during LIN, the cell continues to experience secondary infections by T4 phage, and progeny virions continue to form. Lysis will eventually happen if secondary infections, or superinfection events, stop occurring. From an evolutionary viewpoint, LIN is believed to prevent the phage from releasing progeny into an environment that is host-deficient, which is just as disadvantageous as a non-productive infection. In a recent publication, it was shown that the periplasmic domains of T, the T4 holin, and RI, the T4 antiholin, are the major players in T4 lysis inhibition (37). The authors used a construct consisting of a PhoA fusion to the RI C-terminal domain to show that the periplasmic domain harbors the antiholin character. Similar constructs of the T C-terminal domain fused to PhoA were used to demonstrate interactions between the periplasmic domains of RI and T. In addition, co-immunoprecipitation experiments showed that RI and T form a complex (37). Although

the data demonstrate that the interaction between T and RI is involved in LIN, it is clear that the mode of LIN is not the same as that demonstrated by the lysis effector and inhibitor pair for lambda, S105 and S107, respectively, since T and R1 do not share sequence similarity.

Recent Advances in Lambdoid Phage Lysis

Phage 21 has a lysis cassette which is structured very similarly to the lysis cassette of lambda, with S^{21}, R^{21}, Rz^{21}, and $Rz1^{21}$ genes downstream of the late promoter (Fig. 1.1). Although the two regions of these phages appear to be the same, S^{21} and R^{21} are actually quite different than S^{λ} and R^{λ}. The former illustrate a second general type of holin-endolysin pathway, with the two major players being a pinholin and a SAR endolysin (30, 33). $S^{21}68$, the holin of phage 21, forms small holes and is thus referred to as a pinholin (30). It has been studied extensively, with recent evidence indicating that topological dynamics of the protein affect its lysis behavior. $S^{21}68$ has two TMDs (Fig. 1.7); the first TMD was shown to be unnecessary for host cell lysis (31). In fact, when all of the residues which comprise TMD1 were deleted, the resulting 44 residue protein was able to accumulate in the membrane and effect triggering for lysis by activating the endolysin R^{21}. Also, when the membrane was depolarized by the addition of DNP, $S^{21}68_{\Delta TMD1}$ prematurely triggered, indicating that it had retained its holin activity. With the addition of a highly charged RYIRS epitope tag on the N-terminus of $S^{21}68$ (Fig. 1.7), TMD1 was prevented from exiting the membrane, as evident by the

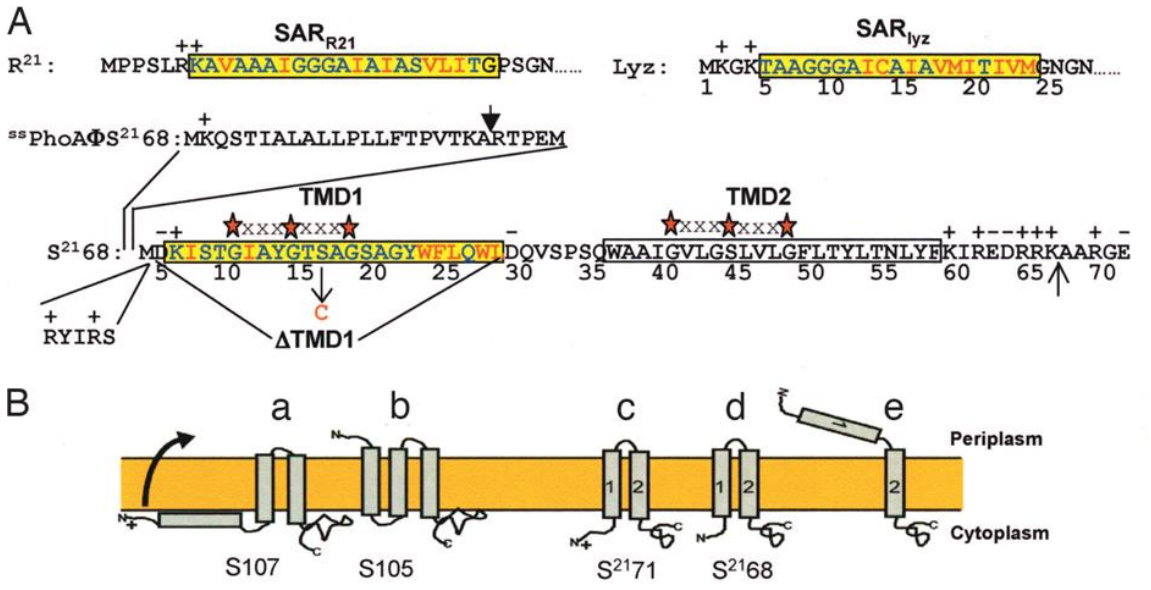

Figure 1.7. Sequences and topologies of lysis proteins. (A) The SAR domain sequences for $R^{21}$and Lyz (yellow boxes). S^{21}68 has 2 TMDs (boxes), and TMD1 is a SAR domain. (B) Topology of lambda antiholin S107 (a) and holin S105 (b), and 21 antiholin S^{21}68 (c) and holin S^{21}68(d) in the inner membrane. TMD1 of S^{21}exits the membrane to the periplasm (e). Reprinted with permission from Park et al. (31). Copyright (2006) National Academy of Sciences, U. S. A.

lack of disulfide bond formation and resistance to proteases in this region of the protein, ultimately preventing topological dynamics of TMD1 and lysis (31).

Phage 21 endolysin, R^{21}, has been characterized as a SAR endolysin (30). R^{21} contains an N-terminal signal sequence which targets the protein to the membrane. After R^{21} exits the membrane, it becomes an active enzyme which can degrade the peptidoglycan layer of the bacterial cell envelope (Fig. 1.6). Therefore, R^{21} can in fact function without the large hole-forming capability of the holin because the endolysin does not pass through the inner membrane lesion formed by the holin. In such a system, it may seem as though the holin does not play a role in lysis by SAR endolysins. However, it has been shown that S^{21} forms small holes, which depolarize the membrane, allowing the release of the SAR domain from the membrane (30). It has been suggested that pinholins, such as $S^{21}68$, may in fact represent an intermediate stage in the evolution of holin-endolysin systems.

Although pinholins require SAR endolysins, the converse is not true. Phage P1, like 21, has a SAR endolysin, and was shown to effect host cell lysis in the absence of the holin, LydA. Similarly to R^{21}, P1 Lyz has an N-terminal TMD that requires the Sec system for processing (33).

Review of Recent Holin Literature

Although the focus of this chapter has been on lambda S105 thus far, it is worth noting that there has been progress in the identification and characterization of putative holin genes among various bacteriophages. At the time of publication for the most

recent holin review in 2000, there were ~200 holins identified, with over 50 unrelated gene families (25). In the years since this review, that number has increased significantly, so much so that a current search in Genbank for the term 'holin' results in over 2000 protein sequences.

Unfortunately, the current criterion used as a basis for holin identification has not been useful. Many putative holins have been determined and characterized solely by their size, association with the membrane, or proximity to other lysis genes. There are distinct criteria which should be met in order for a protein to be definitively identified as a holin. The most important aspect of holin function is sharp host cell lysis upon membrane depolarization. Biologically, sharp lysis indicates that there is a specific, genetically-programmed time for hole-formation to occur, and that time, which is referred to as the triggering event, is dependent upon the holin (38). Before the triggering event, there is absolutely no effect on the membrane. This was demonstrated by the "spinning bug experiment", in which *E.coli* were tethered to a flagellar motor during expression of the lambda holin gene (38). The rotation of the cells, which was directly proportional to the proton motive force (pmf), stopped abruptly at the moment of lysis, but there was no decrease in flagellar velocity prior to triggering (38). Sharp lysis is defined as a rapid decrease in culture turbidity or optical density (OD) after a growing cell culture has been induced for expression of both the holin and endolysin genes. A slow decrease in optical density over a long time period is not characteristic of bacteriophage holin activity, but rather demonstrates a general deterioration of the membrane barrier, allowing endolysin to escape. To test potential holin proteins for

effecting sharp lysis, they must be induced along with the endolysin for expression, and the resulting lysis curve must show a dramatic, saltatory decrease in culture turbidity, as measured by A_{550}.

Holin activity can be further demonstrated by using an energy poison such as dinitrophenol (DNP) to de-energize the membrane of a growing culture that has been induced for holin expression. For true holins, addition of an energy poison will cause a premature triggering event. Until the time of triggering for hole formation, the pmf serves as the only barricade to lesion formation, and once the membrane has been de-energized by the addition of DNP, the cell lyses. The list of criteria for testing potential holins also includes successful complementation of a strain containing all necessary phage lysis genes except the holin. When a true holin is expressed at physiological levels *in trans* in a strain containing *Sam7* (39), a nonfunctional lambda holin gene, it will effect sharp, saltatory lysis.

Putative holins identified by sequence analysis. The genome of bacteriophage ε15 which infects Gram negative *Salmonella enterica* was recently sequenced (40). Comparative studies showed that regions of the ε15 genome share homology with known lysis genes from other phages. In particular, genes *23* and *24* were identified as putative holins, and gene *25* was designated as the endolysin (40).

Srividhya and Krishnaswamy (2007) produced a database containing information about prophages, including current sequence information and known annotations (41). At the time of publication, the database had a total of 47 prophages which exhibited two-

component lysis systems. The authors pointed out that there are no prophage-encoded holin proteins which have been characterized biochemically or structurally. The reasons were much the same as those described above for phage-encoded holins in that they are difficult to over-express and purify due to their toxicity. The defective lambdoid prophage of Gram negative *E. coli*, DLP12, has the putative holin, *essd*, with two predicted TMDs as well as a dual-start motif (41). Interestingly, this particular holin has 96% homology to phage 21 holin, S^{21}, the prototypical class II holin which encodes both a lysis effector and a lysis inhibitor. DLP12 putative endolysin, *ybcS*, is also very similar to phage 21 endolysin, R^{21}, in terms of both homology and presence of conserved SAR domains. In fact, this represented the first reported prophage-encoded endolysin with an N-terminal SAR domain. The authors concluded that DLP12 is only one of four prophages that have lysis cassettes similar to lambda, that is, containing not only the holin and endolysin, but also the *Rz* and *Rz1*-like genes, which they referred to as the endopeptidase and the endopeptidase precursor, respectively (41).

Phage holins of Gram negative hosts. The lysis genes of phage PM2, which infects Gram negative *Pseudoalteromonas* species, have been recently identified and characterized (42). The lysis system appeared to be unique when its components were compared to other lysis genes. For instance, gp*k*, a holin, has only a single TMD in its 53 amino acid sequence, and is therefore the smallest holin thus far identified. The topological characteristics of gp*k* do not allow it to fit into any of the current classifications for holin proteins. The authors suggested that the cell wall is degraded by

cellular components, not necessarily by a phage-encoded endolysin (42). In this work, another protein, gp*l*, was identified as being necessary for outer membrane destabilization and disruption, functions that have been ascribed to the proteins Rz and Rz1 of phage lambda (13). Mutations in both genes *k* and *l* resulted in turbid plaque formation as well as defective lysis. In addition, DNP was added to phage PM2-infected cells and induced premature lysis, indicating that a holin was produced. The authors were able to satisfy two of the three criteria for holin activity by successfully showing that gp*k* effects sharp, saltatory lysis and can be prematurely triggered with energy poisons, but they did not provide proof that gp*k* can complement a holin-deficient strain by effecting lysis *in trans* (42).

The pneumococcal J-1 phage holin, EJh, has 85 residues and two TMDs, categorizing it as a class II holin with no dual start motif (Fig. 1.8a) (43). Previously, EJh was shown to cause sharp lysis and complement *Sam7* (44). In a recent publication, authors created truncation mutants of EJh to determine which regions of the protein are important for holin activity. Through experiments involving fluorescence quenching, and both circular and linear dichroism, they were able to show that the N-terminal transmembrane helix retained the active holin region. In addition, fluorescence quenching was used to show oligomerization of the truncated protein (Fig. 1.8b). Pore-forming assays as well as atomic force microscopy (AFM) were used to assess the size of the holin-mediated lesion as ranging from 3 - 44 nm (43).

Phage holins of Gram positive hosts. Putative lysis genes of Gram positive *Oenococcus oeni* phages, or oenophages, have recently been studied and reported. One such gene is *orf117* from *Oenococcus oeni* phage fOg44, which was initially identified as a putative holin because of its downstream location with respect to the endolysin gene through comparative genomic studies (45) (Fig. 1.9). It was later shown to complement the non-lytic lambda holin allele, *Sam7*, by inducing lysis upon expression in *E. coli* cells. A second gene, *orf163*, shared homology with other putative holin genes, and therefore was tested for holin activity with *Sam7* complementation. Unlike *orf117, orf163*, a gene from fOg30, did not cause lysis when expressed *in trans* to the lysis-defective *Sam7* prophage (45).

By genome comparison, the authors determined that the endolysins of these phages exhibited N-terminal domains which serve as signal peptides and are believed to be processed by the Sec system (45). In light of the discovery that these phages contain secreted endolysins, it was suggested that the holin protein may in fact not be necessary for endolysin release from the cytoplasm. In turn, *orf163*, which has holin-like features, but does not complement *Sam7* with lytic activity, may still encode a holin that is responsible for membrane depolarization alone, instead of large hole formation, which is a characteristic of the pinholins. To test this possibility, *orf163* co-expressed with a

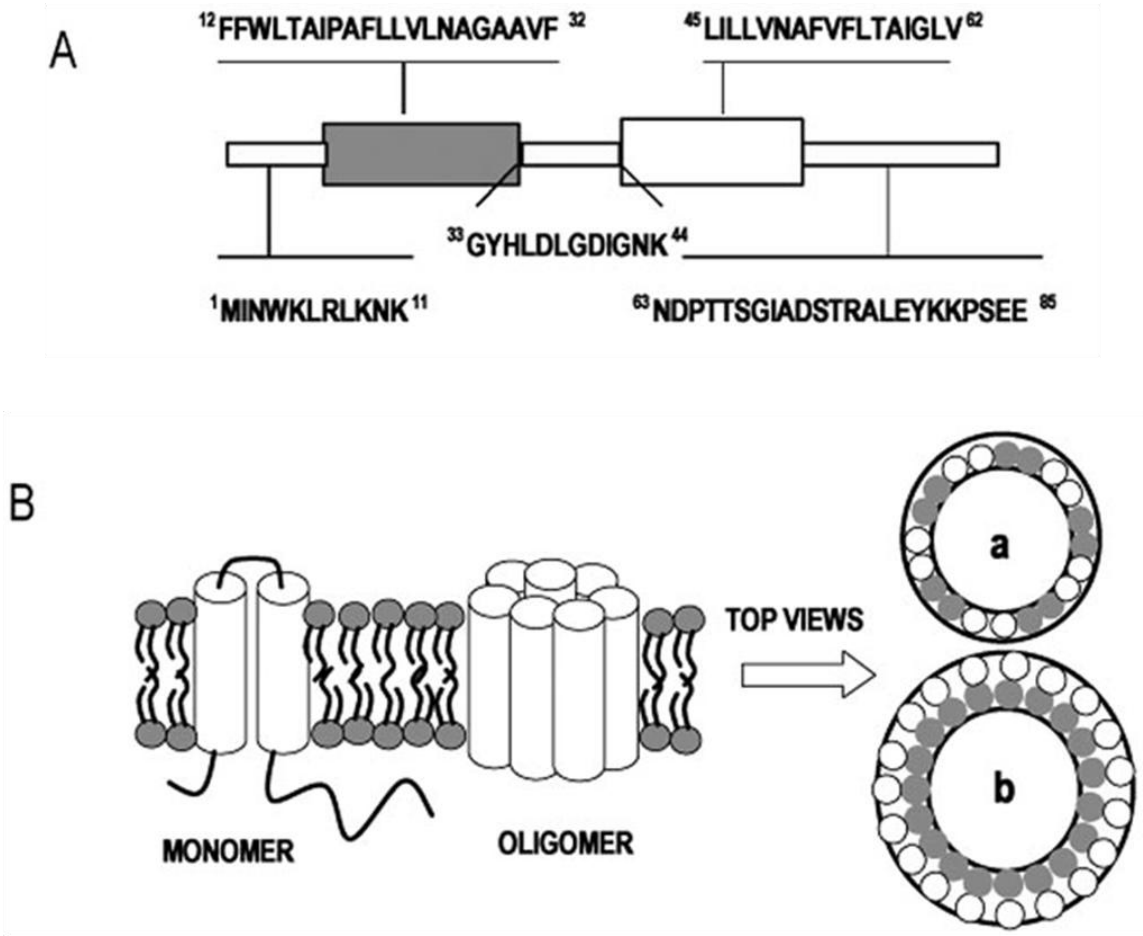

Figure 1.8. Sequence and predicted topology of EJh. (A) Protein sequence of EJh. The predicted TMDs are rectangles. (B) Predicted models of oligomerization and hole formation by EJh. This research was originally published in *The Journal of Biological Chemistry* by Haro et al. (43). © the American Society for Biochemistry and Molecular Biology. Reprinted with permission.

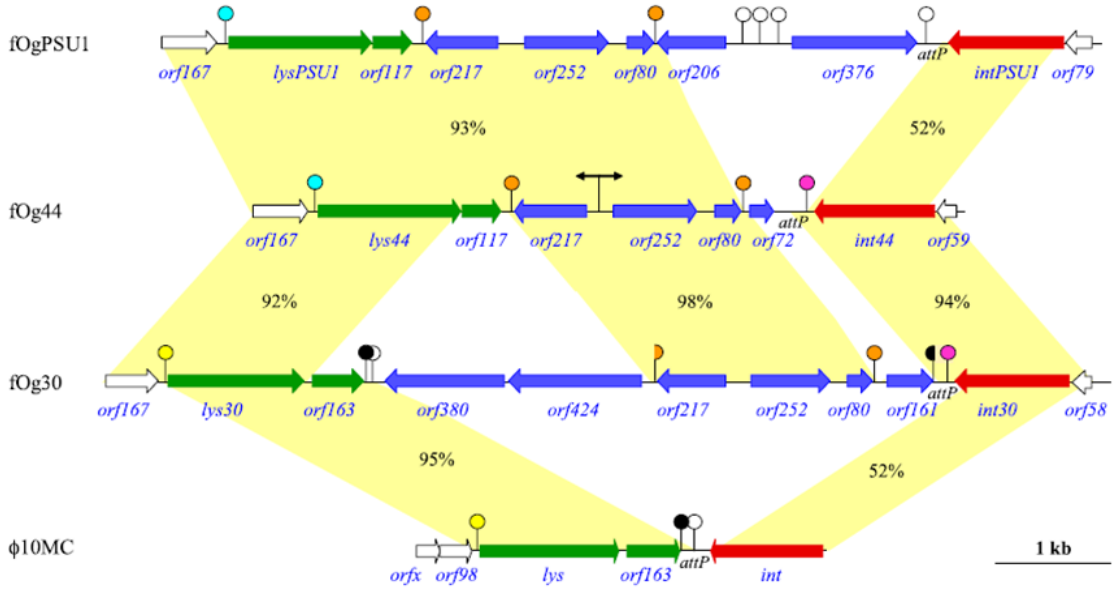

Figure 1.9. Lysis genes (green) for phages fOgPSU1, fOg44, fOg30, and phi10MC. Reprinted from Sao-Jose et al. (45), with permission from Elsevier.

known SAR endolysin, such as R^{21}, should effect lysis, while *orf163* co-expressed with a soluble endolysin, such as R^{λ}, would not cause lysis. Similarly, *orf163* and R^{21} should be susceptible to premature triggering with the addition of an energy poison, unlike *orf163* expressed with R^{λ}.

The authors satisfied two of the three criteria for holin characterization of *orf117* with the demonstration of sharp lysis after gene expression and *Sam7* complementation; however, experiments were not shown regarding premature lysis due to loss of the pmf, or protein expression levels. The level of holin gene expression is an important consideration here, especially since the system being used involves Gram positive genes expressed in a Gram negative host, a situation which can lead to problems associated with poor gene expression (or complete lack of expression) as well as inadequate protein production, improper folding, and protein instability. Additional experiments regarding further characterization of *orf163* as a potential pinholin were also lacking.

The lysis genes, specifically the holins, of 18 phages which infect Gram positive *Lactococcus lactis* have been recently reported and characterized (46). The three lactococcal phage groups include c2, 936, and P335. In the phages studied in this work, putative class I holins were identified for 936-like phages and c2-like phages, and putative class II holins were found in P335-like phages, based on sequence analysis. The authors focused on further characterization of the holin from a P335-like phage ul36, orf74B, by demonstrating that it could complement λΔ*S*, a lambda prophage which had been deleted for the holin gene, *S*, and effect lysis in *E. coli*. In addition, the lysis time demonstrated by orf74B was very similar to that of wild-type S105 when it was

expressed *in trans* to λΔ*S*. These experiments satisfied some criteria for characterizing orf74B as a true holin, but the authors did not demonstrate early lysis as a result of de-energizing the membrane. Labrie et al. (2004) addressed whether *orf74B* had a lysis clock component, given that it did not contain a dual start like λ*S* or other lactococcal phages by analyzing RNA isolated from phage-infected cells, and the results showed a delay in holin and endolysin gene expression (46). It is worth noting that, in general, Gram positive candidates suffer from poor physiological systems, which often cause low, or no expression yields in Gram negative hosts.

In a separate study, Yokoi et al. (2004) identified a two-component lysis system in the prophage ϕgaY from *Lactococcus gasseri* JCM1131^T through comparative studies (47). The endolysin gene was designated *lysgaY*, and was shown to have lytic activity toward autoclaved *L. gasseri* JCM 1131 cells by zymogram analysis. The holin was identified as HolgaY, based on its similarity to other holins. *holgaY*, located upstream of *lysgaY*, encodes a 143 residue protein with a molecular mass of 15.7 kDa, which contains three putative TMDs. When the authors over-expressed the construct p119gaY5, which contained both *holgaY* and *lysgaYΔC1* under P_{lac} control in *E. coli*, there was only a small decrease in culture turbidity, and this decrease occurred after 4 hours of induction. This result showed the effects of membrane toxicity, and not the effects of lysis due to holin activity (47). In fact, the authors were not able to demonstrate any of the necessary criteria for holin function, including expression of the holin gene product.

Recently, some *Staphylococcus* phages have been characterized in terms of their lysis genes. Gram positive *Staphylococcus warneri* M phage ϕWMY has a two-component lysis system which consists of a holin gene, *holWMY,* and an endolysin gene, *lysWMY*. These genes and the proteins that they encode have been recently sequenced and analyzed (48). HolWMY, located just upstream of LysWMY, has a molecular mass of 16kDa and is comprised of 148 amino acids (Fig. 1.10). In addition, it has two putative TMDs, which is typical of class II holins, a basic N-terminus and a highly-charged, acidic C-terminus (48). The authors stated that IPTG induction of HolWMY, under the control of the P_{lac} promoter, resulted in decreased culture turbidity; however, because the data are not shown, it is difficult to conclude whether HolWMY satisfied the criteria for sharp, saltatory, and timely host cell lysis. In fact, due to the absence of figures with lysis curves, it is not possible to evaluate the claim that HolWMY is a true holin. A separate, recent publication suggested that Gram positive *Staphylococcus aureus* bacteria have two genes, *cidA* and *lrgA*, which may encode holin proteins (49). Specifically, in vitro and in vivo data showed that mutations in *cidA* disrupted biofilm formation and resulted in decreased lysis. However, the authors did not present evidence that directly satisfied the criteria for testing holin function.

Gram positive *Staphylococcus aureus* phage P68 has the following lysis genes: two separate, putative holin genes, *hol15* and *hol12*, and an endolysin gene, *lys16* (50). Hol15 has three predicted TMDs, which is a characteristic of class I holin proteins, and Hol12 has two predicted TMDs, as is the case for class II holins. Both holin genes, expressed from plasmids by an in vitro transcription-translation system, were able

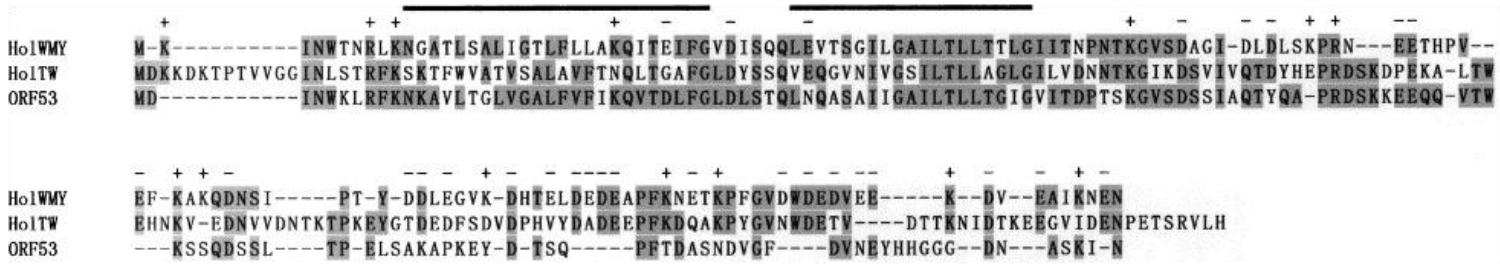

Figure 1.10. Alignment of phage sequences with HolWMY. Amino acid sequences of HolWMY, HolTW from *S. aureus* phage Twort, and ORF53 from phage phi11 are shown. Common residues are in gray, charged residues are indicated, and putative TMDs are denoted by black lines. Reprinted from Yokoi *et al*. (48), with permission from Elsevier.

to complement λ*Sam7* upon expression in *E.coli*, and therefore exhibited holin lytic activity. In addition, *hol15* has a dual-start motif very similar to wild-type λ*S* and it is suggested that it encodes both a lysis effector (Hol15-90) and a lysis inhibitor (Hol15-92). In fact, when Hol15-92 was present with Lys16, lysis only occurred upon membrane depolarization, whereas, the presence of Hol15-90 together with Lys16 was enough to effect lysis. Takac et al. (2005) addressed all of the before-mentioned essential criteria for testing holin activity, including demonstrating both sharp lysis and premature lysis by DNP, and characterized P68 Hol15 as a true holin protein (50).

CHAPTER II

IN VITRO CHARACTERIZATION OF THE LAMBDA HOLIN*

Part I: Protection of Holin Thiols During Protein Purification

Holins are bacteriophage-encoded membrane proteins that control the length of the infection cycle. They accumulate in the host membrane until a time programmed into their primary structure and then trigger to form lethal holes in the cytoplasmic membrane, allowing the phage-encoded lysozyme to degrade the cell wall. Lysis ensues within seconds. Holins are exquisitely malleable; that is, nearly every missense change alters the triggering time, either lengthening or shortening the infection cycle (11, 14, 17). The best-characterized holin is S105, so designated because it is a 105 amino acid product of the *S* gene of bacteriophage lambda (6). The extensive genetic and molecular data available for S105 made it an attractive target for biochemical and structural characterization. In general, membrane proteins pose special difficulties for purification, including toxicity in typical bacterial over-expression systems, but S105 is especially

---

*Reprinted in part with permission from Dewey JS, Struck DK, & Young R (2009) Thiol protection in membrane protein purifications: a study with phage holins. *Anal Biochem* 390(2):221-223.

problematical because its biological function is to kill *E. coli*. Moreover, it was not possible to fuse purification tag domains to either the N or C termini without compromising function in vivo (24). Chemical accessibility studies showed that most of the S105 sequence is occupied by three TMDs (14), so there were limited options for placing an oligohistidine tag. Ultimately, thirteen different positions within the S105 sequence were tested for the ability to support lysis with normal kinetics, and one allele, S105τ94, with GGHHHHHHGG inserted between residues 94 and 95, was obtained (24). Recombinant clones of *S105τ94* were constructed allowing the accumulation of 0.5 - 1 mg of S105τ94 per liter of induced over-expression culture (2). The subsequent purification of the extracted material involves immobilized metal affinity chromatography (IMAC), during which the protein is exposed to both detergent and divalent cations. Here, we report evidence that during extraction and purification, the S105 protein is damaged by covalent modification of its single cysteine sulfhydryl group Cys51 and document an approach for protection of this thiol using a reversible thiol-specific reagent.

Results

Modification of Cys51 sulfhydryls during membrane extraction. For the purposes of examining holin-mediated hole formation in vitro, preparations were made of the parental protein S105τ94, and also, as a control, $S105\tau94_{A52V}$, a missense mutant that is blocked in hole-formation in vivo. The production and purification of both proteins were identical, except that the initial levels of the $S105\tau94_{A52V}$ protein in the induced lysates

were substantially higher (not shown). The state of the Cys51 sulfhydryl in the purified preparations was assessed with Ellman's Reagent (5,5'-dithiobis (2-nitrobenzoic acid; DTNB) (51) (Fig. 2.1). The results show that more than 90% of the sulfhydryls had been modified. To determine when the cysteine modification was occurring, aliquots were removed at each step and treated with the sulfhydryl-specific PEGylation reagent, PEG-OPSS. The results clearly show that protein from the whole cell, lysate, and French press-disruption steps was fully PEGylated by PEG-OPSS (Fig. 2.2, lanes 1-6). This indicates that the Cys51 sulfhydryl group is accessible and unmodified through these steps. Modification was first apparent in the concentrated membrane material, which had been collected by high-speed centrifugation, resuspended in membrane extraction buffer, and incubated overnight with agitation. Quantification of the Western blot bands revealed that more than half of the S105 had been oxidized to intermolecular disulfides (double asterisk, Fig. 2.2), and about half of the remaining monomeric S105 was unable to react with the thiol-specific reagent PEG-OPSS at this stage of the purification (Fig. 2.2, lanes 11 and 12). The degree of modification increased in the final steps of IMAC purification, such that most, if not all, of the purified protein was modified (Fig. 2.2, lanes 13 and 14).

Protection of Cys51 sulfhydryls from modification. To prevent non-specific modification of the Cys51 sulfhydryl group and also artifactual intermolecular disulfide

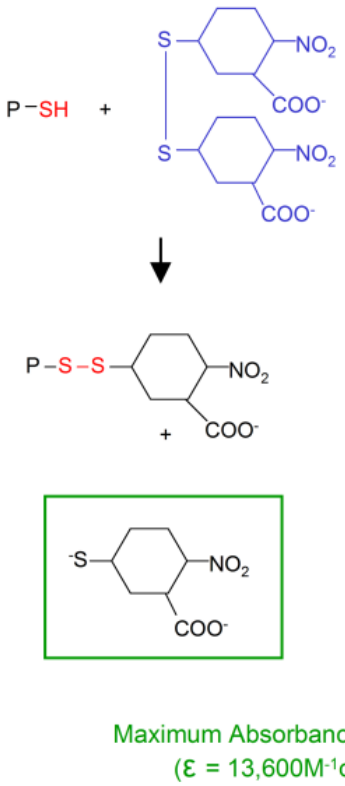

	Abs at 412nm	Free sulfhydryls (nmol)	% Non-reactive sulfhydryls
Reduced Glutathione	0.28 ± 0.02	1.96 ± 0.10	22 ± 4
Cystine	0.02 ± 0.01	0.16 ± 0.05	94 ± 2
S105τ94	0.02 ± 0.01	0.15 ± 0.09	94 ± 3
$S105\tau94_{A52V}$	0.02 ±0.01	0.13 ± 0.08	95 ± 3

Figure 2.1. Reaction of purified S105 with Ellman's Reagent, DTNB. Reduced glutathione was the positive control, and cystine was the negative control. 25 mM samples of reduced glutathione, cystine, S105τ94, and $S105\tau94_{A52V}$ were incubated with DTNB, and the absorbance of each of the samples at 412 nm, which indicated the presence of the reaction byproduct, was monitored to determine the state of the sulfhydryl groups in solution (52-53).

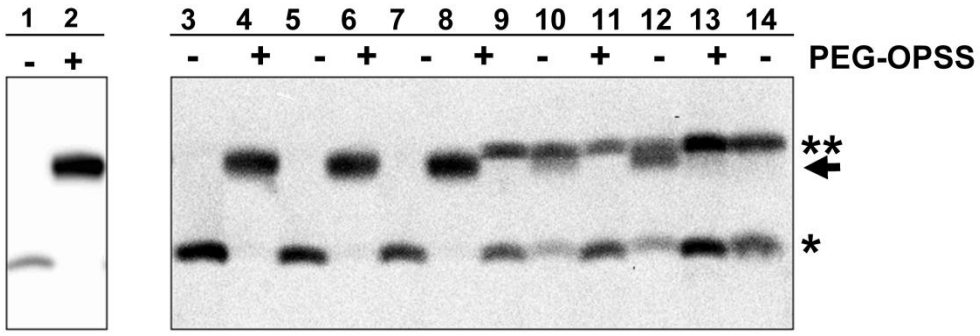

Figure 2.2. PEGylation of S105τ94$_{A52V}$ during the purification process. Samples incubated in the presence (+) and absence (-) of PEG-OPSS include TCA precipitated whole cells (lanes 1 and 2), resuspended cells (lanes 3 and 4), French pressate (lanes 5 and 6), clearing spin supernatant (lanes 7 and 8), resuspended membranes (lanes 9 and 10), extraction spin supernatant (lanes 11 and 12), purified protein (lanes 13 and 14).

bond formation, we selected another thiol reagent, 2,2'-dithiodipyridine (DTDP) (54), which was incorporated at a saturating concentration of 20 mM into the membrane extraction buffer. This reagent is small, making it less likely to be sterically restricted from access to thiol groups and fully reversible with Tris(2-carboxyethyl) phosphine hydrochloride (TCEP) (Fig. 2.3). The purification was conducted exactly as before, except that after elution from the IMAC column, the protein was reduced with 10 mM TCEP. PEGylation was again used to assess the degree of protection achieved, using the TCEP-insensitive thiol reagent PEG-maleimide. The results show clearly that the purified protein can be PEGylated to completion (Fig. 2.4A).

To demonstrate that this method may be applicable to other proteins with reactive thiol groups, DTDP-protection and PEGylation was carried out with a second protein, $S^{21}68_{G48C}{}^{his}$. $S^{21}68$ is the holin protein from the lambdoid phage 21 (55). Although it functions in the same two-component holin-endolysin lysis system as lambda S105, the two proteins have many differences. $S^{21}68$ has only two TMDs, and instead of sizable inner membrane lesions that allow passage of pre-folded proteins, it forms "pinholes" that cannot allow escape of endolysin (30). $S^{21}68_{G48C}{}^{his}$ is a non-lethal Cys-substitution mutant of the S^{21} holin. When DTDP was incorporated in the membrane extraction buffer during $S^{21}68_{G48C}{}^{his}$ purification, it reacted with the sulfhydryl side chain of Cys48. Only after the reduction of the bond between DTDP and the Cys48 thiol group of purified $S^{21}68_{G48C}{}^{his}$, was the protein able to react with a second sulfhydryl-specific reagent, PEG-maleimide (Fig. 2.4B).

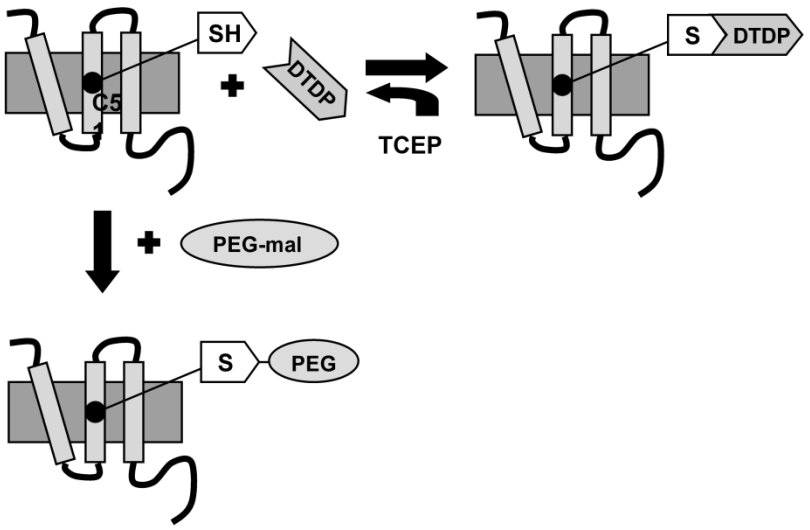

Figure 2.3. Diagram of DTDP-protection method for S105. Cys 51 thiol group reacts with DTDP during membrane extraction and remains bound until protein purification is complete. The DTDP is removed by reaction with the reducing agent TCEP. Successful protection is then determined by the ability of the thiol to react with sulfhydryl-specific PEG-mal.

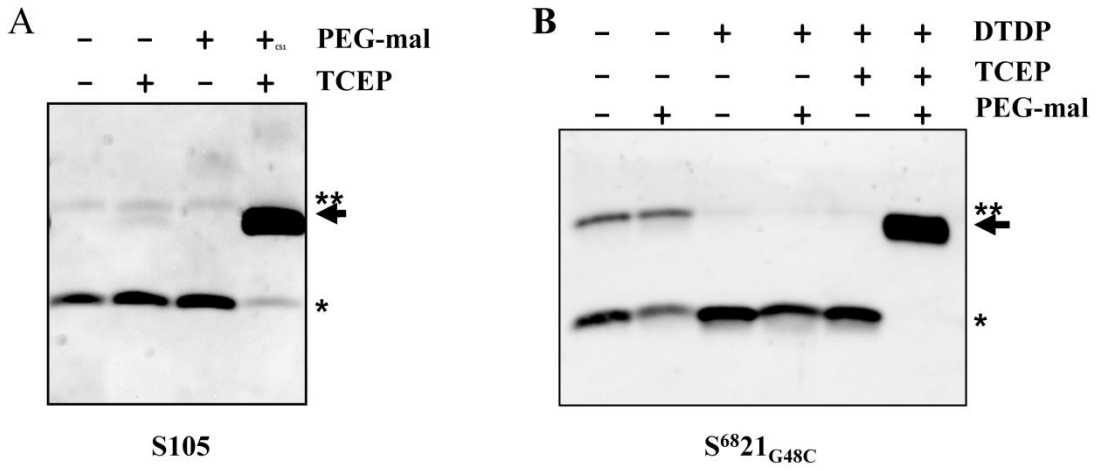

Figure 2.4. DTDP-protection of S105 (A) and $S^{68}21_{G48C}$ (B). Monomeric protein denoted by one asterisk (*); Dimeric protein denoted by two asterisks (**); PEGylation product denoted by an arrow.

Discussion

Currently, there are a variety of thiol-specific reagents commercially available for modification of free sulfhydryl groups within proteins. Some of these reagents have been used for thiol modification during protein purification in an effort to maintain free sulfhydryls (56-59). However, thiol protection during the rigors of detergent extraction and IMAC purification of membrane protein has not been specifically addressed. For the purposes of protecting the S105 Cys51 side chain during protein purification, we chose to use 2,2'-dithiodipyridine, also known as 2,2'-dipyridyldisulfide (PDS) or 2-PD (60). This reagent has been shown to react specifically and completely with thiols (54). In addition, it is considered stable under normal conditions, and has a broad, physiologically relevant pH range of 3.4 - 8.1 (54). DTNB, or Ellman's Reagent, on the other hand, is only effective within the pH range of 7.8 – 10.4 (54). Its utility as a thiol-protecting agent stems from the reversibility of the thiopyridine-cysteine disulfide linkage by the non-volatile reducing agent TCEP, as illustrated in this work. DTDP-protection has been described here for two holins, S105 and $S^{21}68_{G48C}$, but it is our expectation that it may be generally useful for application to cysteine-containing membrane proteins, which characteristically require extended biochemical manipulation during purification.

Materials and Methods

Reagents. The Talon metal affinity resin was obtained from Clontech Technologies, Inc. PEGylation reagents, PEG-OPSS and PEG-maleimide (PEG-mal), were purchased from

Nektar and Creative Biochem Laboratories, respectively. EmpigenBB (EBB) was purchased from Fluka. The Western blotting supersignal detection kit was obtained from Pierce. All remaining reagents were obtained from Sigma.

The over-expression strain *E. coli* C43(DE3)*tonA*::Tn*10* (61) was used for all protein production. The S105 plasmids pETS105H94 and pETS105H94$_{A52V}$ have been described previously (2), except the vector used for pETS105H94 was pET30b (25). For over-expression of $S^{21}68_{G48C}{}^{his}$, the plasmid $pETS^{21}68_{G48C}{}^{his}$, a derivative of the previously-described $pETS^{21}68^{his}$ (31), was constructed by Quickchange site-directed mutagenesis replacing Gly48 with a cysteine residue. $pETS^{21}68_{G48C}{}^{his}$ contains an oligohistidine tag between residues 66 and 67 (31). Antibodies directed against peptides which correspond to the C-termini of S105τ94 (62), as well as $S^{21}68^{his}$ (31), have been previously described.

Purification of S105. The details of the over-production of S105τ94 and S105τ94$_{A52V}$ have been described (2); production of $S^{21}68_{G48C}{}^{his}$ was done the same way. Briefly, C43(DE3)*tonA*::Tn*10* cells carrying the respective pET30b (or pET11a) derivatives were grown at 37 °C in batch cultures, induced with 1 mM IPTG at A_{550} = 0.6, harvested by centrifugation at 50 min (for S105τ94) or 90 min (for S105τ94$_{A52V}$ and $S^{21}68_{G48C}{}^{his}$) and stored at -20 °C. Frozen cells from 2 L of induced culture were resuspended in lysis buffer (20 mM Tris, pH 7.9, 150 mM NaCl, 1 mM EDTA, 1 mM DTT, and 1 mM PMSF) and disrupted by passage through a 30 mL Aminco French pressure cell at 16,000 psi. A low-speed clearing spin at 8,000 rpm in a Sorvall SS-34 rotor was used to

remove unlysed cells and cellular debris from the sample. The supernatant was centrifuged at 100,000 g for 1.5 h at 4 °C to collect the membranes. The supernatant was removed, and the membranes were resuspended in membrane extraction buffer (20 mM Tris, pH 7.9, 150 mM NaCl, 10 mM $MgCl_2$, 1 mM PMSF, 1% (v/v) EBB). The resuspended membranes were incubated with gentle shaking overnight at 4 °C and then centrifuged at 100,000 g for 1.5 h in a Ti 50.2 rotor at 4 °C to separate the solubilized material from the residual insoluble material.

For protein purification, the supernatant was applied to a Talon metal affinity (Clontech Technologies, Inc.) column that had been washed with distilled H_2O and equilibrated with buffer A (20 mM Tris, pH 7.9, 150 mM NaCl, 1% (v/v) EBB). The flow-through was reapplied to the column after a brief wash with 10 column volumes of buffer A. Thirty column volumes of buffer A, then five column volumes of low imidazole buffer (20 mM Tris, pH 7.9, 150 mM NaCl, 20 mM imidazole, and 1% (v/v) EBB) were used to wash the column after the second flow-through. The protein was eluted in 5 aliquots, each equivalent to the bed volume, in a buffer containing 20 mM Tris, pH 7.9, 150 mM NaCl, 500 mM imidazole, and 1% (v/v) EBB. The purity of the protein was assessed by Coomassie brilliant blue staining of a precast 16.5% Tris tricine criterion gel (Biorad) loaded with aliquots from the purification process, and protein concentration was calculated from A_{280}, using $\varepsilon = 11{,}460\ M^{-1}\ cm^{-1}$ for S105τ94 and $S105\tau94_{A52V}$. For PEGylation and DTDP-protection experiments, detection of the protein required Western blotting with antibodies directed either against a peptide

corresponding to the C-terminus of S105τ94 (62) or a peptide corresponding to the C-terminus of $S^{21}68^{his}$ (31).

Assaying free thiols with Ellman's reagent. Solutions of reduced glutathione, cystine, and purified S105τ94 and S105τ94$_{A52V}$ in TBS, pH 7.9 were prepared at final concentrations of 25 μM in a volume of 95 μl. Five microliters of 10 mM DTNB (dissolved in ethanol) was added to the above solutions. The samples were mixed by pipetting and incubated in the dark at room temperature for 30 min. The concentrations of free sulfhydryls in the assay solutions were determined by the presence of the anionic byproduct TNB (ε = 14,150 $M^{-1}cm^{-1}$ at 412 nm (51-52).

Monitoring sulfhydryl state with PEG-OPSS. Ten to fifteen fresh transformant colonies of C43(DE3) *tonA*::Tn*10* pETS105H94$_{A52V}$ (2) were used to inoculate a 200 ml LB culture supplemented with 100 μg/ml ampicillin. The culture was grown at 37 °C in a shaking waterbath and induced at A_{550} = 0.5 for 50 min. An aliquot of the culture was removed at 25 min for a whole cell sample, and the remaining culture was harvested for purification.

The expressed protein in the whole cell sample was precipitated with trichloroacetic acid (TCA). Five milliliters of the induced culture was added to 5 mL of cold 11.1% (v/v) TCA, vortexed, and incubated on ice for 30 min. The samples were centrifuged at maximum speed in a tabletop IEC clinical centrifuge at 4 °C for 15 min. The pellet was washed with 5 mL of cold acetone, vortexed, and centrifuged at 4 °C (see

above) for 15 min. The pelleted protein was air-dried for ~15 min and resuspended in 1 mL of PEGylation buffer (0.5 M Tris HCl, pH 7.0, 1% (w/v) SDS, 1 mM EDTA). Two hundred microliters of the resuspended protein was combined with 10 μL of 60 mM PEG-OPSS, incubated at room temperature for 30 min, treated with 1.4 mL of cold acetone for 10 min at -20 °C, and centrifuged at 14,000 rpm in a tabletop microcentrifuge for 15 min at 4 °C. The supernatant was carefully removed and the pellet thoroughly air-dried. The dry pellet was resuspended in non-reducing 2X protein sample buffer (0.5 mg/mL bromophenol blue in 0.25 M Tris, pH 6.8) and incubated at 37 °C for 10 min, then analyzed by SDS-PAGE and immunoblotted with the appropriate antibodies.

The harvested cells from the original culture were used for protein purification, and aliquots were removed after each step. The aliquots, which contained ~0.01 μg of purified protein, were diluted by 10-fold into PEGylation buffer. Ten microliters of 60 mM PEG-OPSS was added to each of the samples, and incubated at room temperature for 30 min. The samples were combined with an equivalent volume of non-reducing 2X protein sample buffer and analyzed by SDS-PAGE, then immunoblotted with the appropriate antibodies.

DTDP-protection. S105τ94 was purified as previously described, except a saturating concentration of 20 mM 2,2'-dithiodipyridine was included in the membrane extraction buffer. DTDP dissolved in the buffer only after the solution was incubated for a few minutes in a boiling waterbath, and the reagent remained in solution after the buffer

returned to room temperature. Membrane extraction was carried out overnight at room temperature instead of at 4 °C, to ensure that DTDP did not precipitate. After elution from the Talon metal affinity column and concentration determination by A_{280}, the protein was treated with 10 mM TCEP to reduce the bond between DTDP and the S105 Cys51 sulfhydryl (or Cys48 in $S^{21}68_{G48C}{}^{his}$). TCEP was added to the purified protein at a final concentration of 10 mM, and the samples were mixed by pipetting, and incubated for 5 min at room temperature.

The reduced protein was diluted 10-fold into PEGylation buffer. 14 μL of 10 mM PEG-mal was added to ~50-150 ng of reduced S105 protein for the +PEG samples. The reactions were mixed by pipetting and incubated for 30 min at room temperature. Aliquots of the samples were diluted at least 20-fold with 2X protein sample buffer containing β-mercaptoethanol. This dilution step was used to obtain samples with the appropriate protein concentrations for detection with the Supersignal West Femto Maximum Sensitivity Substrate (Pierce). In addition, the 20-fold dilution was necessary to reduce the high reaction concentrations of PEG-mal before the samples were loaded onto a gel, so that the reagent would not affect the mobility of the proteins during electrophoresis. The samples were boiled for 5 min, then analyzed by SDS-PAGE and immunoblotted with the appropriate antibodies. The procedure for protection of $S^{21}68_{G48C}{}^{his}$ was identical.

Part II: In Vitro Reconstitution of Hole Formation

The lambda holin, S105, has been studied extensively in vivo by both genetic and biochemical means, including mutational analyses, chemical accessibility studies, and chemical crosslinking experiments (14-16). These assays have proven to be invaluable in efforts to understand S105 form and function in the membrane; however, very little is known about the actual mechanism of hole formation. Specifically, the steps that are required for oligomers of S to transition into holes, or lesions, in the inner membrane of bacterial cells, are unknown. In vitro assays featuring purified S105 and artificial membranes are the ideal system to study the pathway to hole formation, especially given the variety of characterized holin mutants that are available. For example, the extensive collection of early and late lysing S105 mutants (15-16) provide a system for relating in vivo lysis time to in vitro hole formation. In addition, the S105 temperature-sensitive mutant, A55T (63), can be used to control the system with temperature changes, essentially turning hole formation "on" at permissive temperatures and "off" at non-permissive temperatures. Finally, the characterized non-hole-forming mutants of S105, including but not limited to A52V (16), can serve as valuable negative controls in such in vitro assays.

The in vitro approach for studying hole formation is dependent upon the ability to purify the lambda holin in a functional state. Previous research has indicated that during the purification procedure, the lambda holin is somehow being modified. For

instance, attempts to label the Cys51 sulfhydryl group in detergent-solubilized, purified S105 were unsuccessful, whereas labeling in the membrane, with whole cell samples, was efficient (14). In addition, preliminary in vitro calcein release experiments in which GroEL-solubilized, purified S was added to liposomes containing a quenched fluorophore, was inefficient. A large increase in intensity was expected when the quenched calcein was released from the liposomes through the holin lesion. However, Figure 2.5 shows that a large portion of the purified protein did not contribute to hole formation because there was only a small increase in fluorescence intensity after addition of S105. We hypothesized that inefficient hole formation by the in vitro system can be partially explained by chemical damage of the purified protein at its cysteine sulfhydryl group (64), which results in an inactive form of S. This work describes the optimization of an in vitro assay for demonstrating S105-mediated hole formation using a cysteine-less S105 mutant and artificial membrane vesicles.

Results

Purified S105 thiol modification and in vitro hole formation. For the dye release assays, cys-less versions of S105 and $S105_{A52V}$ were used to avoid any modification of the protein thiols during membrane extraction and purification (64). In an effort to find

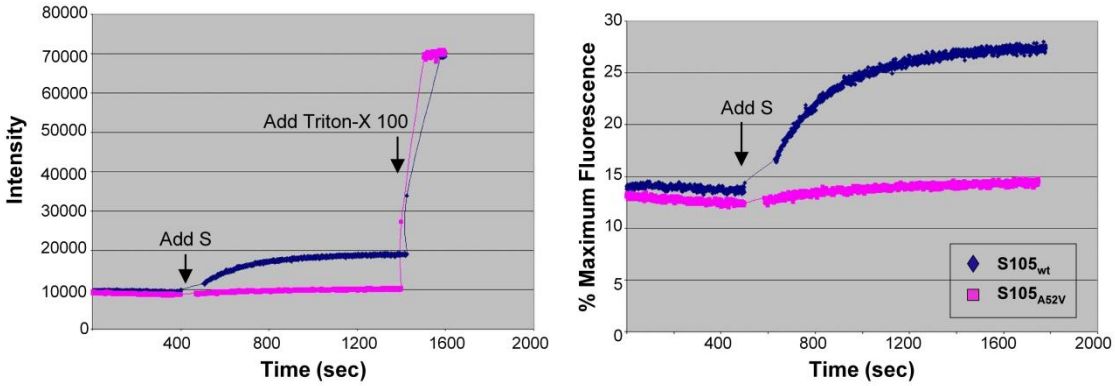

Figure 2.5. In vitro hole formation with GroEL-solubilized S105. Purified S/GroEL complex was added to calcein-loaded liposomes. Upon hole formation in these artificial membranes, there was an increase in fluorescence intensity for wild-type S105, but no increase for the non-hole-forming mutant, S_{A52V}. Triton X-100 is added at the end of the experiment to determine the maximum possible fluorescence.

a cys-less mutant which behaved similarly to the wild-type protein in terms of lysis, the single cysteine residue at position 51 of S105 was converted to several amino acids (Fig. 2.6). It was determined that C51A resulted in a missense change which had the least effect on lysis timing and was chosen for these studies. Since $S105_{C51A}$ was chosen as the wild-type protein for in vitro assays, it was important to test the non-hole-forming A52V mutation in the same background. Expression of $S105_{C51A\ A52V}$, like $S105_{A52V}$, did not cause lysis of cells, and therefore was used as the negative control for these experiments (Fig. 2.7).

S105 hole formation in vitro. An in vitro fluorescence assay was used to study the mechanism of hole formation by S105 (1-2). First, $S105_{C51A}$ was purified on Talon resin columns as previously described (see Chapter II, part I) in the presence of EBB detergent, then eluted in octylglucoside detergent. The detergent was then dialyzed away overnight, and the precipitated protein was dissolved in 6M Guanidine-HCl. 400 nm membrane vesicles containing the fluorophore, calcein, were made through extrusion of L-a-phosphatidylcholine (PC), 1,2-Dioleoyl-sn-Glycero-3-[Phospho-rac-(1-glycerol)] (DOPG), and rhodamine-labeled phosphoethanolamine (PE) lipids. Dye release assays were then carried out when the guanidine-solubilized S105 was diluted into a solution containing calcein-loaded liposomes (2). Upon hole formation, the calcein was released, and an increase in fluorescence was monitored with an ISS Koala spectrofluorometer. As a negative control, the non-hole-forming mutant $S105_{C51A\ A52V}$ was also tested

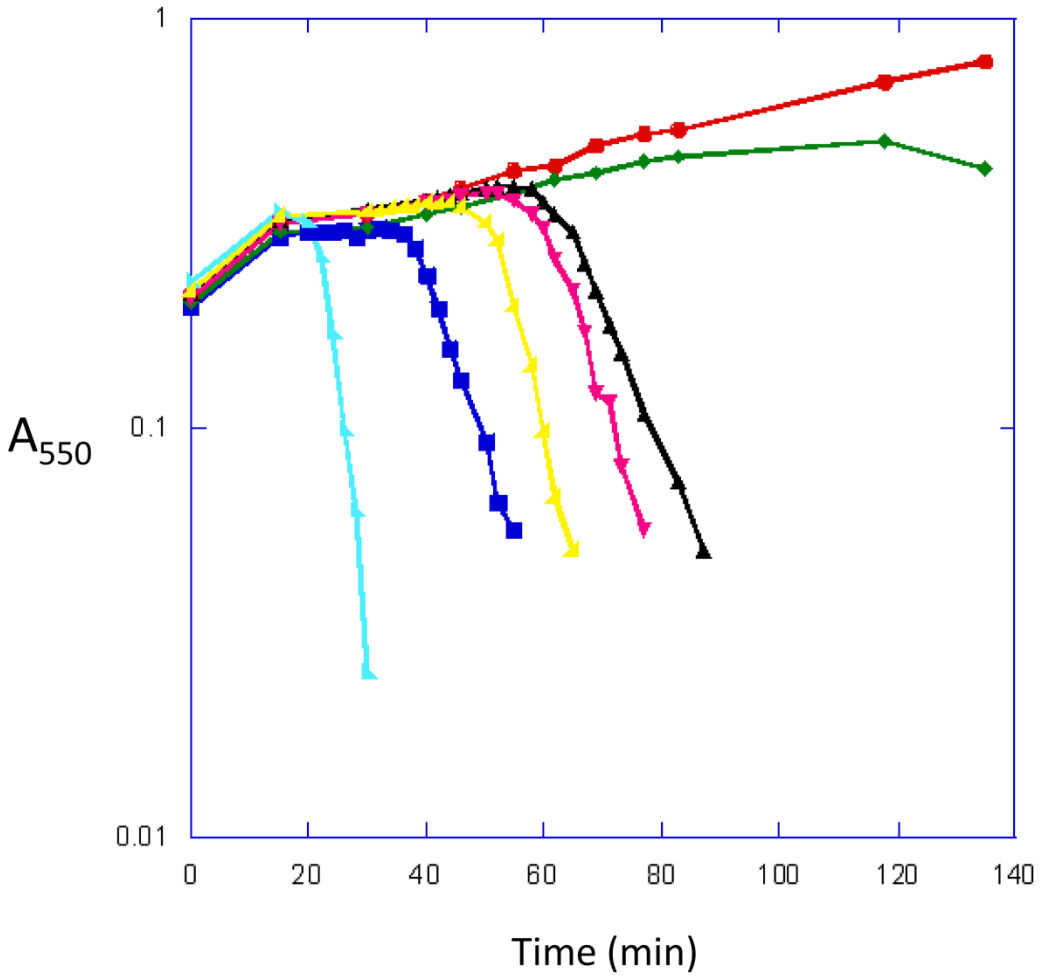

Figure 2.6. Lysis curves of initial S105 Cys51 missense mutants. All strains tested were MC4100 Δ*tonA* (λΔ*SR*); some strains expressed wild-type or mutant holin *in trans* from the plasmid pS105. The single cysteine residue of S105 was converted to 11 different amino acids. Only those mutants which lysed at a time similar to wild-type lysis are shown above: $S105_{C51M}$ (light blue), $S105_{C51A}$ (yellow), $S105_{wt}$ (dark blue), $S105_{C51L}$ (pink), $S105_{C51I}$ (black). Controls include MC4100 Δ*tonA* (λΔ*SR*) expressing pSam7 (green), and MC4100 Δ*tonA* (λΔ*SR*) with no S105 plasmid (red).

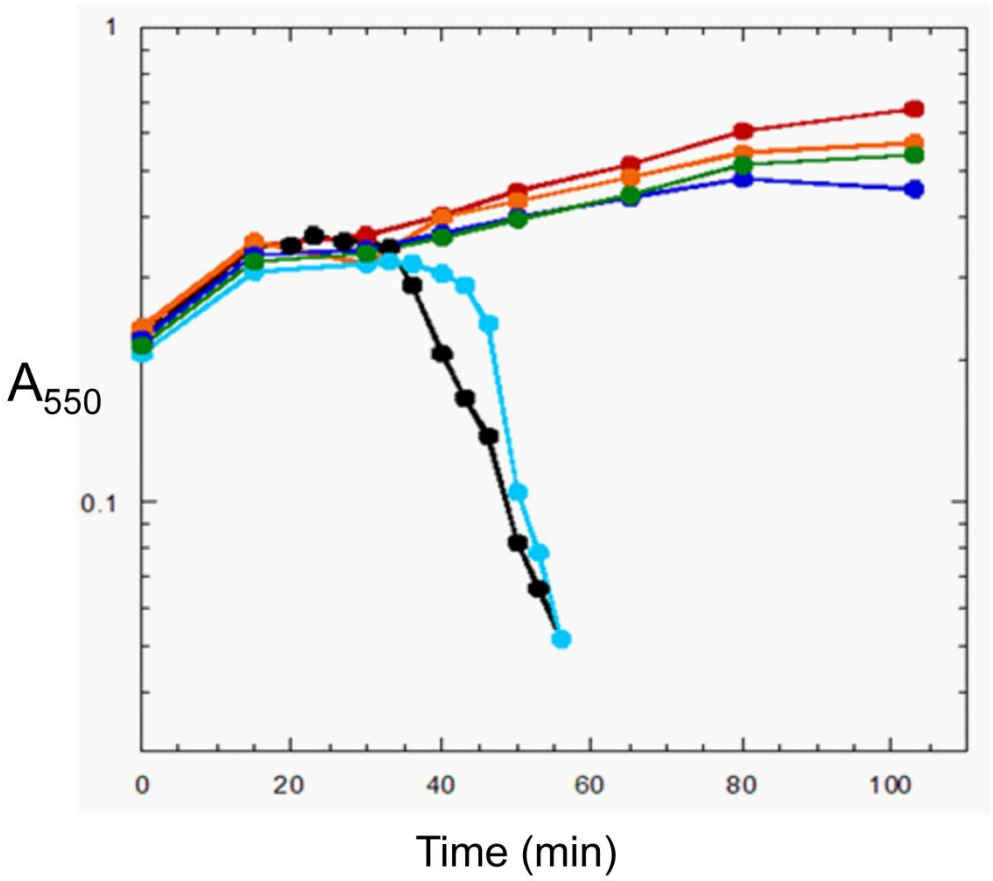

Figure 2.7. Lysis behavior of $S105_{C51A\ A52V}$. All strains tested were MC4100 Δ*tonA* (λΔ*SR*); some strains expressed wild-type or mutant holin *in trans* from the plasmid pS105. The following plasmids were expressed: $pS105_{wt}$ (black), $pS105_{C51A}$ (light blue), $pS105_{A52V}$ (dark blue), $pS105_{C51A\ A52V}$ (green). Controls include MC4100 Δ*tonA* (λΔ*SR*) expressing pSam7 (orange), and MC4100 Δ*tonA* (λΔ*SR*) with no S105 plasmid (red).

with the dye release assay, and shown to cause very little, if any, increase in fluorescence when added to preformed calcein-loaded liposomes. Surprisingly, the non-functional truncation mutant $S105_{\Delta TM1\ C51A}$, which lacks the first TMD and has antiholin character (65), caused intermediate fluorescence release (more than $S105_{C51A\ A52V}$, but less than $S105_{C51A}$) when added to liposomes in an end-point assay. The results of the in vitro fluorescence assay showed an average value of ~30% dye release upon the addition of purified $S105_{C51A}$ to calcein-loaded vesicles (Fig. 2.8).

The question remained as to why there was less than 100% fluorescence release for $S105_{C51A}$. To answer this question, it was important to determine how much of the purified S105 was actually associating with the liposomes. For this purpose, sucrose gradients were used. Purified $S105_{C51A}$ was incubated with liposomes and the protein-lipid mixture was loaded onto a pre-formed four-step gradient, ranging from 0 - 80% (w/v) sucrose. After the gradient was centrifuged at 100,000 g for 1 h at 4 °C, the lipid floated as expected and formed a tight band at the interface of 20% (w/v) sucrose and buffer (0% (w/v) sucrose) (Fig. 2.9). To determine how much S105 was associated with the lipid, fractions were collected from the top of the gradient and analyzed by immunoblotting. The results showed that the majority of S105 had formed large aggregates and were present in the most concentrated sucrose fractions, whereas only a small amount of S105 was present in the 0% (w/v) and 20% (w/v) sucrose fractions containing lipid (Fig. 2.9). Therefore, it was concluded that since only a small fraction of purified S105 was actually associating with the vesicles, it stands to reason that there would not be 100% dye release from calcein-loaded liposomes in the in vitro assay.

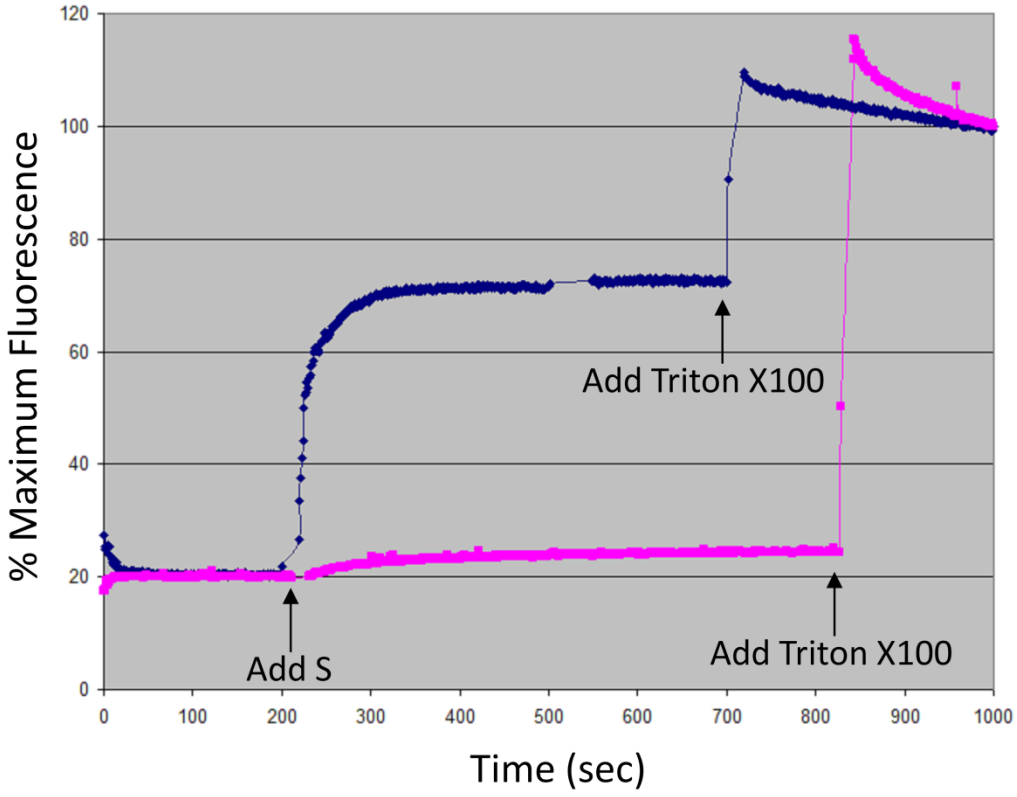

Figure 2.8. $S105_{C51A}$ in vitro hole formation results. At times 0-200 sec, background intensity was established with liposomes in buffer. At time 200 sec, purified S105 was added to the liposomes with constant stirring, and fluorescence change was observed. Triton X-100 was added to the liposomes to determine maximum fluorescence. $S105_{C51A}$ is shown in blue, and $S105_{C51A\ A52V}$ is shown in pink. The data shown is a representative result (the average increase after addition of $S105_{C51A}$ was ~30%).

Cryo-EM of liposomes incubated with S105$_{C51A}$. Cryo-electron microscopy (Cryo-EM) was used to observe liposomes in the presence and absence of S105$_{C51A}$. The hypothesis was that if there was in fact hole formation occurring in the in vitro system, there would be evidence of lesions in the vesicles, as imaged by cryo-EM. Liposomes were made as described and diluted appropriately for cryo-EM. S105$_{C51A}$ was purified as described and added to pre-formed liposomes. The samples, liposomes alone and liposomes incubated with S105$_{C51A}$, were plunge-frozen on EM grids in liquid ethane, then viewed under liquid nitrogen temperatures with cryo- EM, as later described in Chapter IV (3). The liposomes were prepared by extrusion using a 400 nm pore filter, but when the vesicles were viewed with cryo-EM, it was apparent that the liposomes were not all unilamellar. In fact, the majority of the liposomes were multilamellar (Fig. 2.10A). This may partially explain why only a percentage of the total dye was released in the in vitro fluorescence assays. Specifically, S105 hole formation would have only resulted in the release of calcein from the outermost layer of multilamellar liposomes, and any dye contained within interior liposomes would have remained trapped inside the vesicles in a quenched state. In any case, when the two separate samples, liposomes alone and liposomes incubated with S105$_{C51A}$, were compared with cryo-EM, there appeared to be no visible differences in the two samples (Fig. 2.10).

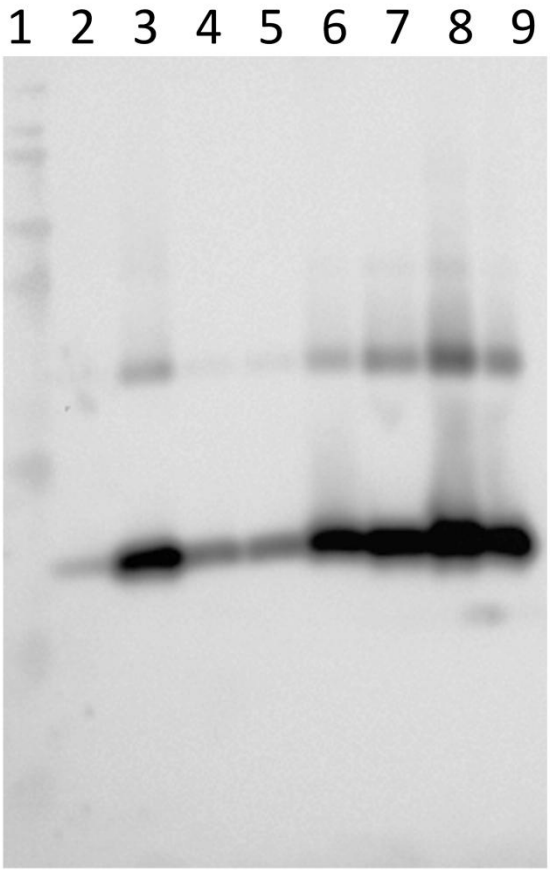

Figure 2.9. Western blot detection of $S105_{C51A}$ from liposome flotation fractions. Lane 1: molecular weight marker; lanes 2-9: aliquots from eight successive fractions (400 µl each) taken from the top to the bottom of the gradient after centrifugation.

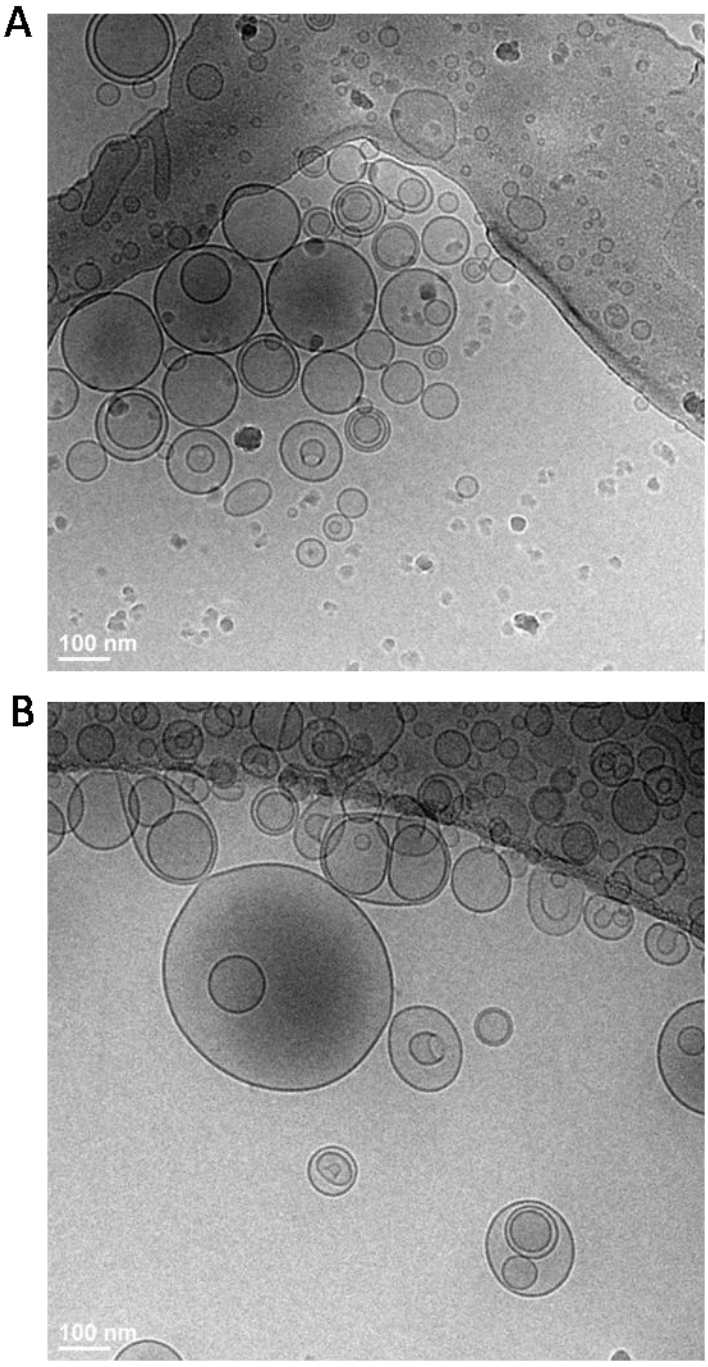

Figure 2.10. Cryo-EM images of liposomes in the absence (A) and presence (B) of $S105_{C51A}$.

Discussion

A completely in vitro system with purified lambda holin and artificial membrane vesicles, would be the ideal system for determining the pathway to hole formation by S105. Such a system, with purified S105 being delivered to liposomes, which released a fluorescent signal upon hole formation, was implemented (1-2) In this assay, S105, the functional lambda holin, was shown to cause hole formation when added to pre-formed liposomes, and the non-functional lambda holin mutant, $S105_{A52V}$, did not cause hole formation.

In this work, efforts were made to optimize the in vitro hole formation assay. Incremental advances were made in the optimization of the system. Specifically, using a cysteine-less version of the lambda holin that had been solubilized in guanidine prior to its addition to membrane vesicles resulted in increased fluorescence release, compared to cysteine-containing S105 solubilized with GroEL, indicating more efficient hole formation for the former. It became clear, however, that there were some remaining obstacles within the system. First, sucrose gradient results indicated that the majority of the purified protein was not associating with the liposomes. Instead, the protein appeared to form higher-order structures which were present with the most dense sucrose fractions after centrifugation instead of floating with the lipid. Second, cryo-EM analysis of the liposomes indicated that the vesicles were multilamellar instead of unilamellar. As a result, the fluorescence within the interior vesicles of a multilamellar liposome would not be released upon hole formation in the outermost layer. Finally, $S105_{\Delta TM1\ C51A}$, which is a non-functional mutant of the lambda holin, caused

fluorescence release when added to calcein-loaded liposomes in an end-point assay. This may reflect the ability of this truncated protein, with two TMDs, to insert efficiently within the membrane vesicles and cause leakage of the liposome contents.

Materials and Methods

Reagents. Lipids L-a-phosphatidylcholine (PC), 1,2-Dioleoyl-sn-Glycero-3-[Phospho-rac-(1-glycerol)] (DOPG), rhodamine-labeled phosphoethanolamine (PE), and cholesterol were purchased from Avanti Polar Lipids. Calcein, Empigen BB (EBB) and 6M guanidine HCl were obtained from Sigma. Octylglucoside (OG) was purchased from Anatrace. Lipid extrusion was carried out with a Liposofast extruder from Avestin. Fluorescence readings were done with an ISS Koala dual-excitation spectrofluorometer.

Protein purification. All protein samples used with the in vitro assay were purified as previously described (25, 64), except the protein was exchanged from Empigen BB detergent into octylglucoside detergent during Talon purification. Once the protein was bound to the Talon resin, and washed with Buffer A (20 mM Tris pH 7.8, 150 mM NaCl, 1 % (v/v) EBB), ~50 column volumes of Buffer B (20 mM Tris pH 7.8, 150 mM NaCl, 1.4 % (w/v) OG) were passed over the column. The remaining purification buffers were the same as previously described except they contained 1.4 % (w/v) OG instead of other detergents.

Liposome preparation. PC (4.9 mg), DOPG (2.1 mg), and cholesterol (0.7 mg) dissolved in ethanol were combined in a glass tube with 0.5 % (v/v) rhodamine PE, mixed, and dried with N_2 gas to form a thin film on the interior walls of the glass tube. The tube was left in a dessicator for at least 1 hour to completely dry the lipids. The dried lipids were then resuspended in 1 mL of 75 mM calcein, vortexed for ~5 min, and centrifuged briefly to bring all contents to the bottom of the tube. The lipids were passed through a 400 nm pore filter using a Liposofast extruder 21 times, then applied to a preparative Sepharose gel filtration column. The large orange-colored band from the void volume was collected because it contained the calcein-loaded liposomes. The unincorporated calcein and remaining lipid material were eluted later and discarded.

Sucrose gradient. Liposomes were made as described in the previous section, with the following exceptions. Dried lipids were resuspended in 1X TBS, pH 7.8. Gel filtration was not used to remove unincorporated calcein since no calcein was added to the dried lipid mixture. Sucrose solutions were made in 1X TBS buffer at the following concentrations (w/v): 20%, 60%, and 80%. Guanidine-solubilized S105 (4 μM) and liposomes (1.75 mg/ml) were combined in 1X TBS buffer in a final volume of 400 μl, and incubated at room temperature for 5 min. The liposome-protein mixture was combined with 400 μl 60% (w/v) sucrose, making the final concentration 30% sucrose. The sucrose gradient was made by carefully layering the following solutions from bottom to top in an ultracentrifuge tube: 600 μl of 80% (w/v) sucrose, 800 μl of 30% (w/v) sucrose (containing liposomes and protein), 1.2 ml 20% (w/v) sucrose, and 600 μl

1X TBS buffer. The tubes were centrifuged at 49,000 rpm (~100,000 g) for 1 hour in a Beckman TLS55 ultracentrifuge rotor at 4 °C. A visible pink band indicating the rhodamine-labeled lipid present in the liposomes was localized to the buffer/20% (w/v) sucrose interface. Fractions were collected from the gradient, top to bottom, in 400 µl aliquots, and aliquots from each fraction were used for SDS-PAGE and immunoblotting.

In vitro dye release assay. Purified $S105_{C51A}$ and $S105_{C51A\ A52V}$, eluted in 1.4% (w/v) OG, were dialyzed overnight against 1X TBS buffer (20 mM Tris pH 7.8, 150 mM NaCl) containing 1 ml Biobeads (Sigma). The proteins were removed from the dialysis cassettes the following day and spun down in an Eppendorf tube at 13,000 rpm in a tabletop microcentrifuge for 10 min. The precipitates, containing the proteins in the absence of detergent, were resuspended in 6 M guanidine HCl. The concentrations of the protein samples were determined by an A_{280} scan ($\varepsilon = 11{,}460\ M^{-1}\ cm^{-1}$).

A 2.5 ml glass cuvette with a small stir bar was used to house the sample within the spectrofluorometer (ISS). Two milliliters of liposomes in 1X TBS were added to the cuvette at a final concentration of 43.75 µg/ml. The cuvette was placed in the sample compartment of the fluorometer, and the magnetic stirrer was enabled. The absorbance and emission wavelengths, 490 nm and 520 nm respectively, were set according to the values used for the fluorophore calcein. The slow kinetics setting over a time period of ~ 10 min was used for data acquisition. Once a steady background was established indicating the stability of the liposomes (i.e. no leaking calcein, which would cause the fluorescence to increase over time), 47 µmol purified $S105_{C51A}$ was added to the

liposomes in buffer. The change in fluorescence intensity after protein addition was monitored until the intensity flatlined. Then, 1% Triton X-100, a detergent which solubilizes membrane vesicles, was added to the liposomes to obtain a value for maximum fluorescence. The experiment was repeated as described for $S105_{C51A\ A52V}$. The experiment was also repeated at varying liposome:protein ratios in an effort to optimize the assay.

GroEL solubilization and delivery of S105 was carried out as previously described (1).

In vitro calcein release endpoint assay. Protein and liposome concentrations were the same as for in vitro dye release assays. Purified protein was added to the bottom of a 5 ml Eppendorf tube and 2 ml of liposomes in buffer were pipetted directly into the tube so that the contents were mixed immediately. The tube was incubated for at least 5 min at RT, then the sample was moved to a cuvette and single-point intensity readings were taken with the ISS Koala spectrofluorometer. Ten microliters of 10% (v/v) Triton X-100 was added to the sample, and another single-point intensity reading was taken for the sample to determine maximum fluorescence.

Cryo-EM. Five microliters of a mixture of liposomes and purified $S105_{C51A}$ were applied to C-FLAT (CF-4/2-2C) or home-made lacey carbon-coated grids that had been glow-discharged just prior to use. Grids were then plunge-frozen in ethane using an FEI Vitrobot. Specimens were observed in an FEI Tecnai G^2 F20 TEM equipped with a

GATAN Tridiem GIF-CCD using zero-loss imaging and low-dose conditions with typical doses of 5-10 $e^-/Å^2$ per image. A GATAN 626 cryo-holder was used for all experiments (3).

CHAPTER III

NMR STUDIES OF A LAMBDA HOLIN MUTANT

Structural information for the lambda holin would be extremely valuable for determining the mechanism of hole formation. For example, a solved structure would inform investigators of protein subunit interactions, helical packing, and TMD interaction with lipid or lumen. However, due to the difficulties associated with over-expression and purification of membrane proteins, there are very few solved structures of such proteins (64). In fact, there are currently no solved structures of bacteriophage holins, either by x-ray crystallography or nuclear magnetic resonance (NMR) spectroscopy. In collaboration with Dr. Christian Hilty and Youngbok Lee (Chemistry Department, Texas A&M University), we sought to solve the NMR solution structure of the bacteriophage lambda holin protein mutant, $S105_{\Delta TM1\ C51A}$. This holin truncation mutant lacks the first TMD and lacks any Cys residues where oxidative damage could occur during preparation. It was used for structural studies because it is small and relatively non-toxic to the membrane, can be produced in large quantities, and remains soluble for weeks at 4 °C. $S105_{\Delta TM1}$ contains only two TMDs, and is thought to mimic the canonical lambda antiholin, S107, in the membrane (65). Both S107 and $S105_{\Delta TM1}$ delay hole formation when expressed in trans to S105 (65), and therefore are considered to be functionally relevant proteins. In addition, the structure of the holin-antiholin complex would likely mimic holin-holin interactions.

NMR has become a prominent method for solving membrane protein structures. Until recently, x-ray crystallography was considered the optimal method because there were restrictive protein size limitations with NMR (66). This is especially problematical for membrane proteins because in the purified form, they are embedded within detergent micelles, which adds considerably to the overall protein mass. The experiment which was specifically designed to overcome the NMR size restrictions is called Triple Resonance Optimized Spectroscopy (TROSY) (66). TROSY allows for large proteins to be analyzed via NMR with the same resolution as would be possible for small proteins. Large protein samples usually have significant interfering transverse relaxation, which can reduce the overall signal and cause broad, poorly-resolved peaks. TROSY filters out the interfering signals so that only the true signal, and none of the transverse relaxation, contributes to the overall signal (66). Therefore, the resulting peaks are narrow and well-resolved, as would be the case with small protein samples.

Results

Assessing the behavior of the lambda holin for NMR. Before beginning structure determination of the lambda holin, it was important to first assess whether the conditions required for NMR were suitable for the protein. After determining that the holin mutant $S105_{\Delta TM1}$ and the cys-less variant, $S105_{\Delta TM1\ C51A}$, were successfully over-expressed and purified at the acceptable concentration for NMR (~1 mM), the sample was subjected to a range of temperatures that would be required for obtaining the necessary spectra. In addition, there was extensive optimization of sample conditions, which included buffer

composition, pH, and selection of detergent micelles for protein solubility. These preliminary experiments were carried out with unlabeled $S105_{\Delta TM1\ C51A}$, and with buffers containing the detergents SDS or DDM, at pH ranging from 6.0 to 7.8, and temperatures of 15 - 35 °C. The resulting 1D spectrum suggested that SDS would be an appropriate detergent for $S105_{\Delta TM1}$ structure determination, and lowering the pH may improve the peak resolution (Fig. 3.1). The DDM spectrum contained less well-resolved peaks, as well as variations due to temperature changes (Fig. 3.2). In fact, when $[^{2}H][^{15}N]$ labeled $S105_{\Delta TM1}$ was analyzed under the same conditions, there were more detectable peaks for the protein in DDM when tested at the lower temperature of 15 °C, as compared to the increased temperature of 35 °C (Fig. 3.3). The 2D spectrum of $[^{2}H][^{15}N]$ labeled $S105_{\Delta TM1}$ in SDS proved to be very promising indeed. The spectrum had 92 well-resolved peaks, each one corresponding to a single amino acid within the protein, which has a total of 92 residues. From this spectrum, preliminary assignments for some of the peaks were made, specifically the 13 glycine residues and the single tryptophan residue which have distinct chemical shifts (Fig. 3.4).

In an effort to screen additional detergents for NMR studies of the holin mutant, the $[^{2}H][^{15}N]$ $S105_{\Delta TM1}$ originally prepared in SDS and DDM was exchanged into buffers containing the detergents dodecyl phosphocholine (DPC) and

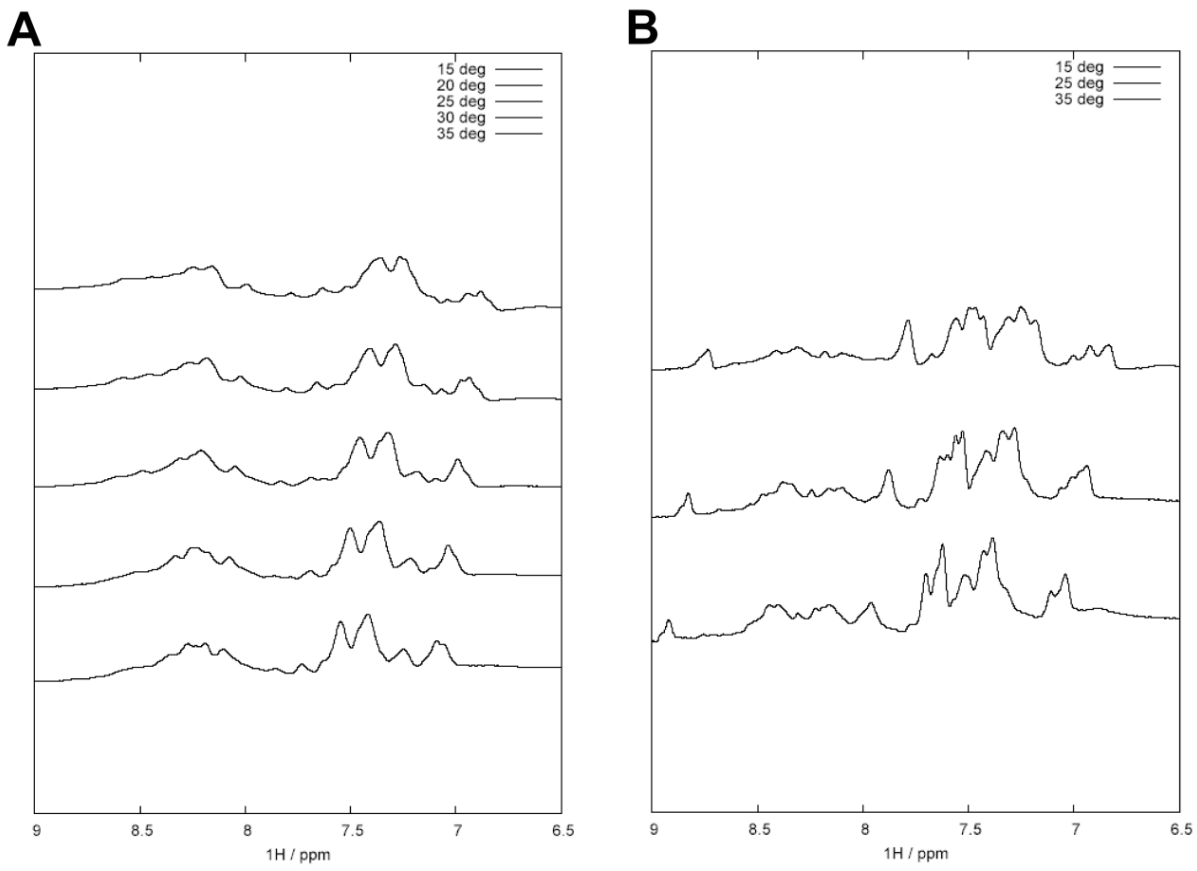

Figure 3.1. 1D spectra of unlabeled $S105_{\Delta TM1\ C51A}$ in SDS micelles at varying temperatures. (A) Sample pH of 7.8; (B) Sample pH of 6.0.

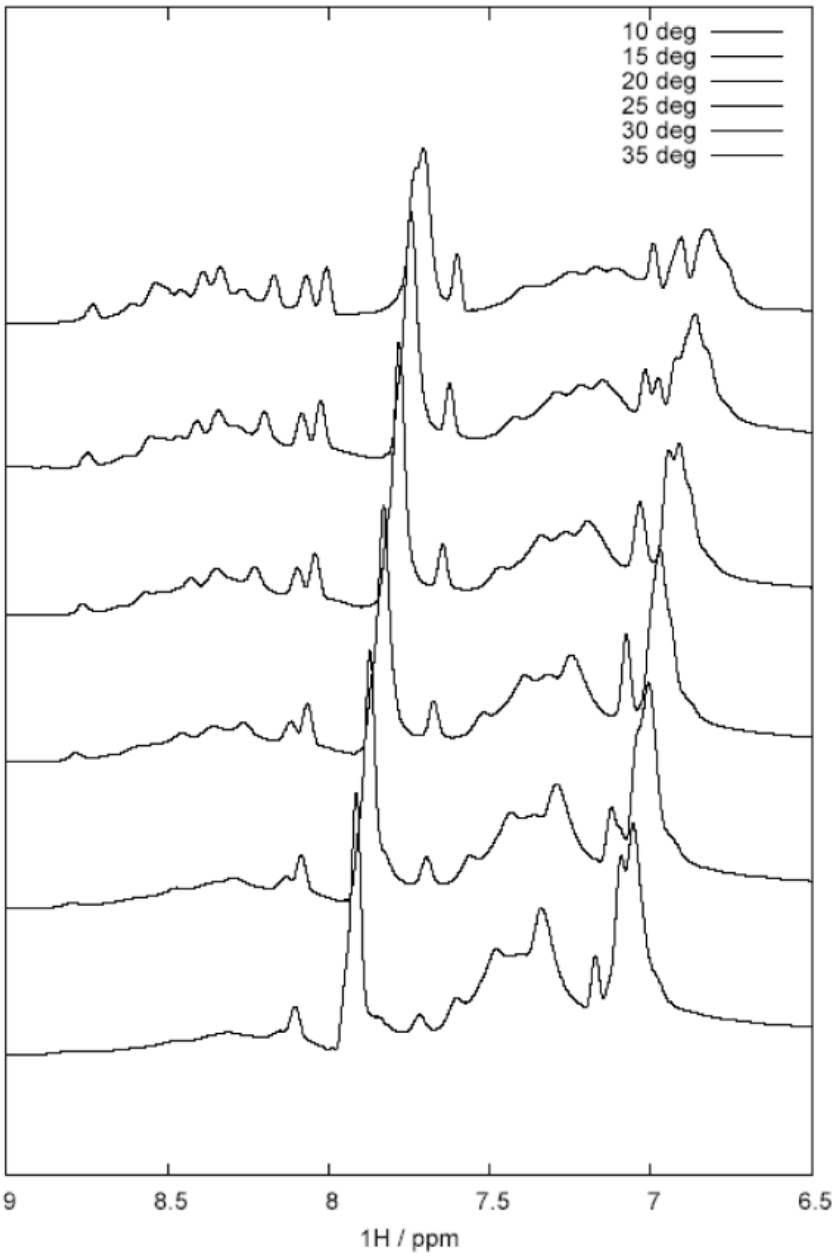

Figure 3.2. 1D spectrum of unlabeled $S105_{\Delta TM1}$, pH 7.8, in DDM micelles at varying temperatures.

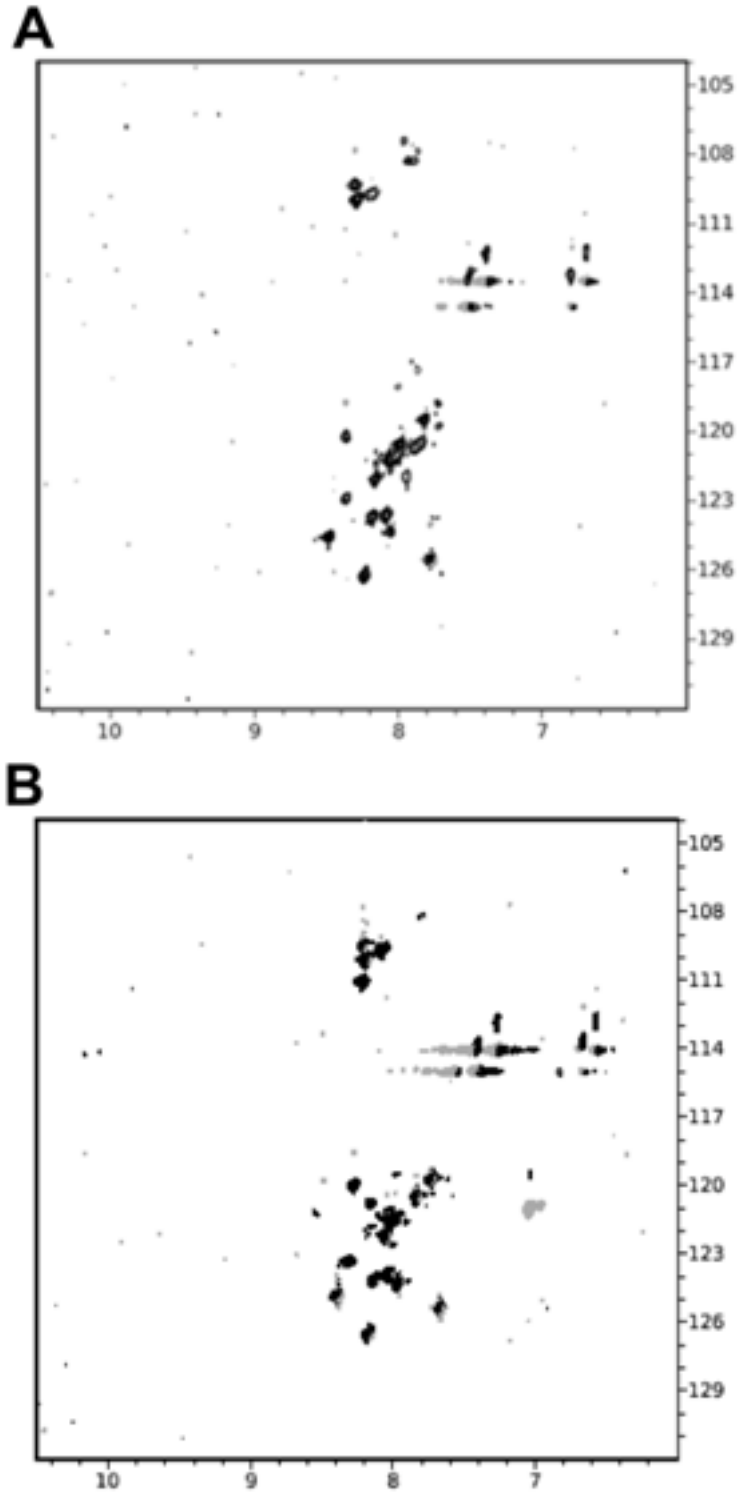

Figure 3.3. 2D spectra of [^{2}H][^{15}N] labeled S105$_{\Delta TM1}$ in DDM micelles at varying temperatures. The following temperatures were used: 35 ℃ (A) and 15 ℃ (B).

lauryldimethylamine-oxide (LDAO) by gel permeation chromatography. The 2D spectrum of [^{2}H][^{15}N] labeled S105$_{\Delta TM1}$ in DPC micelles showed most of the amino acid peaks, but indicated sample degradation due to the presence of two additional tryptophan peaks (Fig. 3.5A). The protease degradation was verified by analyzing the sample with a Coomassie-stained gel and immunoblotting with an antibody that specifically recognizes the C-terminus of the S protein (Fig. 3.5B,C). Regardless of the protease degradation for the samples in DPC and LDAO detergents, it was apparent that the overall distribution of peaks in the DPC spectrum was much broader than the pattern of peaks in the SDS spectrum (Fig. 3.6), which provides clues as to the state of the protein. A protein which is folded properly will have a broader distribution of residue peaks, whereas an unfolded species will exhibit a narrower spectrum. Therefore, it was determined that SDS, an ionic detergent considered to be harsh, may in fact cause the protein to be unfolded, and, despite the fact that it provided promising preliminary data, it should not be used for additional studies. Instead, LDAO, a detergent which has successfully been used in the NMR solution structure determination of other membrane proteins, such as Mistic (67) and VDAC-1 (68), and resulted in a broad spectrum for S105$_{\Delta TM1}$ similar to DPC, was chosen for future experiments.

Testing the functionality of S105$_{\Delta TM1\ C51A}$. The remaining NMR results were carried out with the cys-less version of S105$_{\Delta TM1}$ so as to avoid any modification of the thiol at Cys51 during purification (see Chapter II) (64). The functionality of this particular

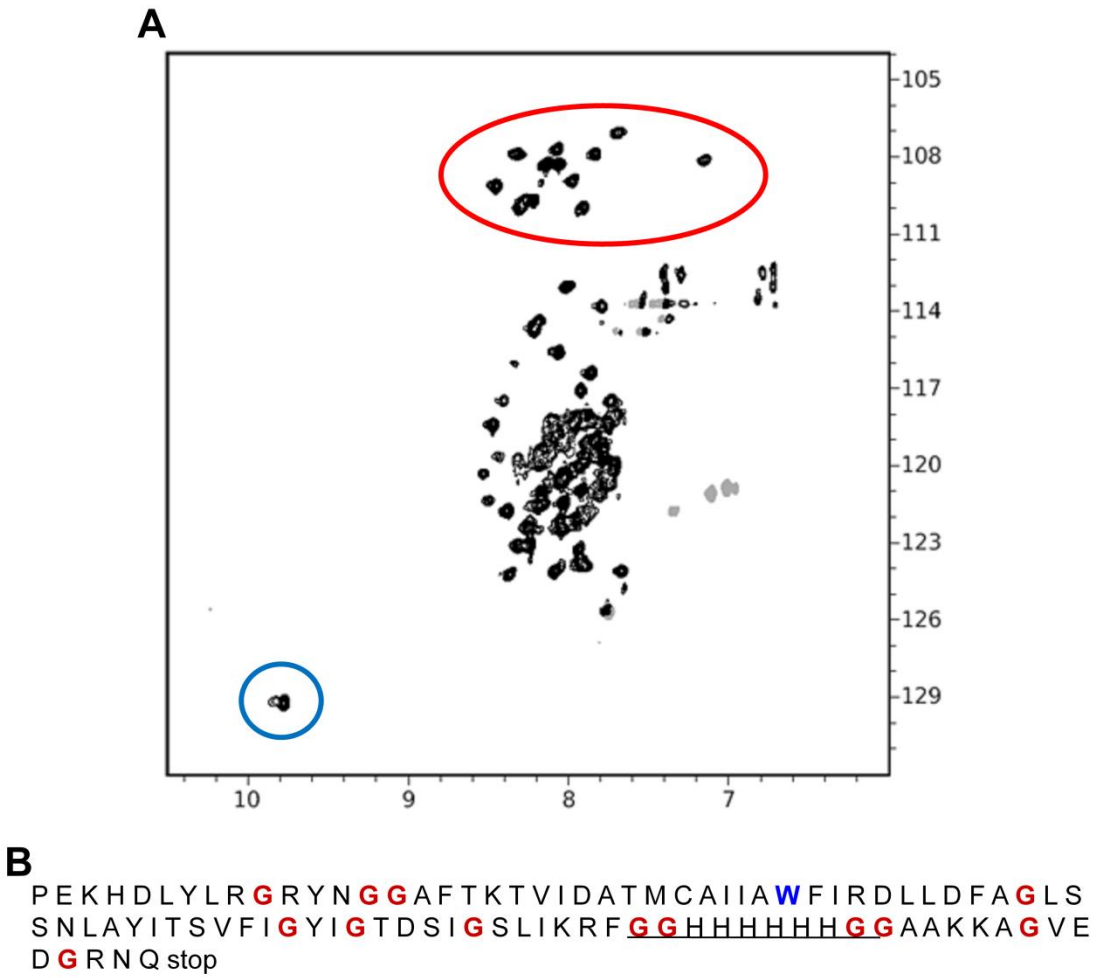

Figure 3.4. 2D spectrum of [^{2}H][^{15}N] labeled S105$_{\Delta TM1}$ in SDS micelles at 35 °C (A). The 13 glycine residues are circled in red and the single tryptophan is circled in blue. The amino acid sequence of S105$_{\Delta TM1}$ (B). The oligohistidine tag is underlined; the glycines are in red, and the tryptophan is in blue.

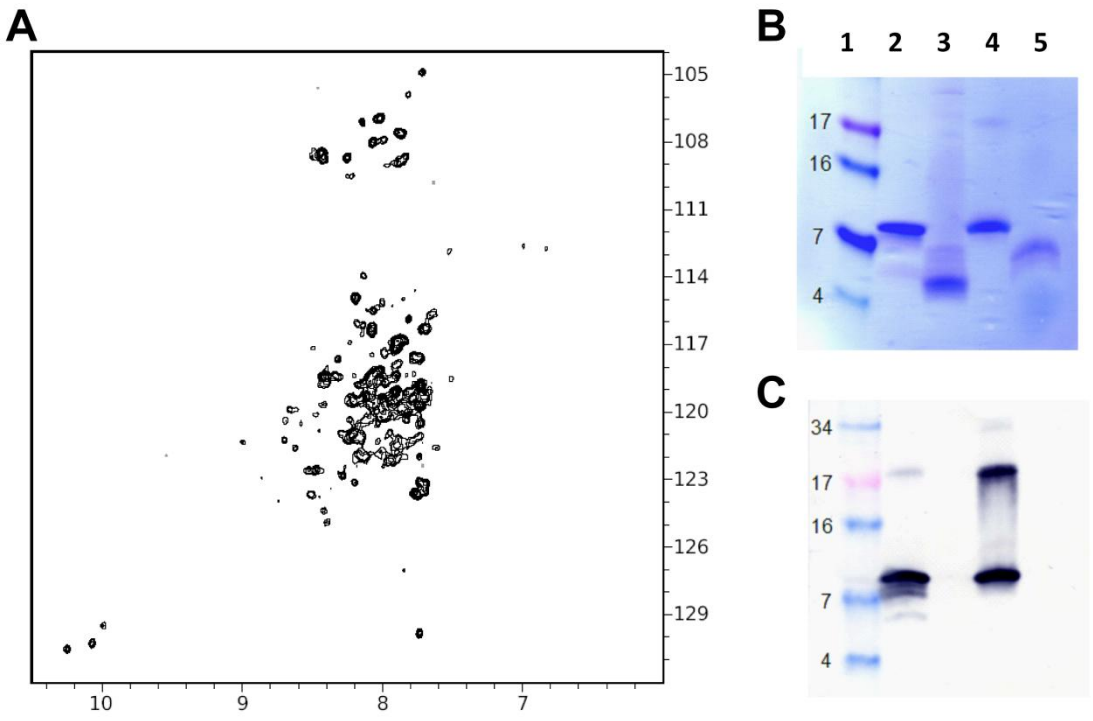

Figure 3.5. NMR sample degradation. 2D spectrum of [^{2}H][^{15}N] labeled S105$_{\Delta TM1}$ in DPC micelles (A). Coomassie-stained gel of samples used for NMR (B). Western blot of samples used for NMR, detected with an antibody directed against the C-terminus of S105 (C). Lanes in gel and blot are as follows: (1) molecular weight marker, (2) unlabeled S105$_{\Delta TM1}$ in SDS, (3) [^{2}H][^{15}N] labeled S105$_{\Delta TM1}$ in DDM, (4) [^{2}H][^{15}N] labeled S105$_{\Delta TM1}$ in SDS, (5) [^{2}H][^{15}N] labeled S105$_{\Delta TM1}$ in LDAO.

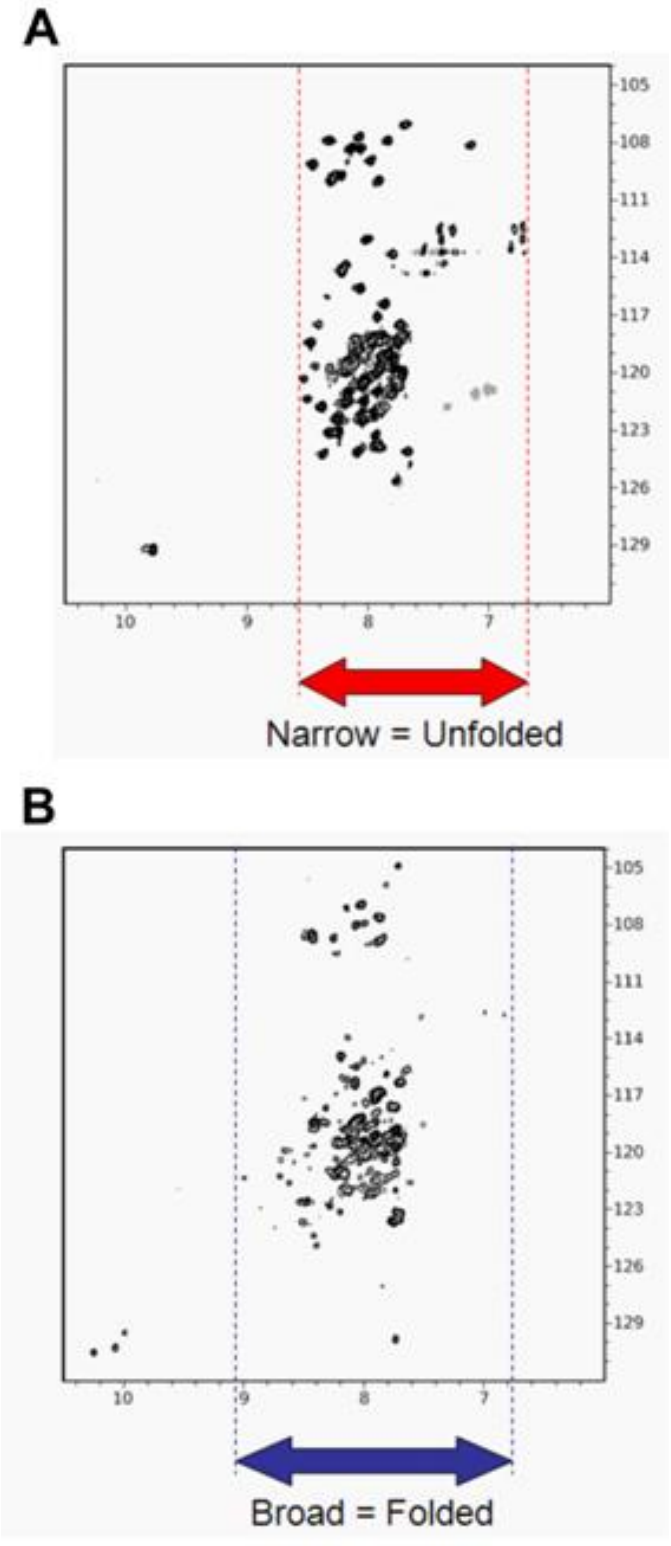

Figure 3.6. 2D spectra of [^{2}H][^{15}N] S105$_{\Delta TM1}$ in SDS (A) and DPC micelles (B). The dotted lines and arrows indicate the overall distribution of peaks.

mutant was tested for inhibition of the full-length cys-less lambda holin by first constructing a strain containing a lysogen with $S105_{C51A}$. When the cys-less lambda holin mutant, $S105_{C51A}$, is present on the prophage, and $S105_{\Delta TM1\ C51A}$ is expressed in trans from a plasmid, lysis is inhibited (Fig. 3.7). The solved structure of this particular protein, because it resembles the holin S105 in form, and functions like the antiholin S107, would be invaluable toward efforts to elucidate the mechanism of hole formation.

Three dimensional NMR of $[^2H][^{15}N][^{13}C]$ labeled $S105_{\Delta TM1\ C51A}$. Nuclear Overhauser Effect Spectroscopy, or NOESY, was used for many of the experiments described in this work. NOESY allows for detection of protons within the same amino acid, protons on sequential residues, and protons that are not linked through bonds, but rather close in space (69). The first successful NMR run with triple-labeled protein yielded two continuous fragments of assigned residues. Using NOESY, it was clear that one fragment had significant contacts with the detergent micelle, and therefore should be in one of the transmembrane segments (70) (Fig. 3.8). In fact, the peaks belonging to those particular residues, with their associated chemical shifts, were ultimately assigned to the third TMD of the holin. The second fragment lacked these same micellar contacts, but instead had significant interactions with water, indicating that this region must be either at the termini or in the loop region between the two TMDs (70) (Fig. 3.9). These peaks were assigned to the C-terminal tail region, which is believed to have very little ordered structure and is non-essential (17, 71-72).

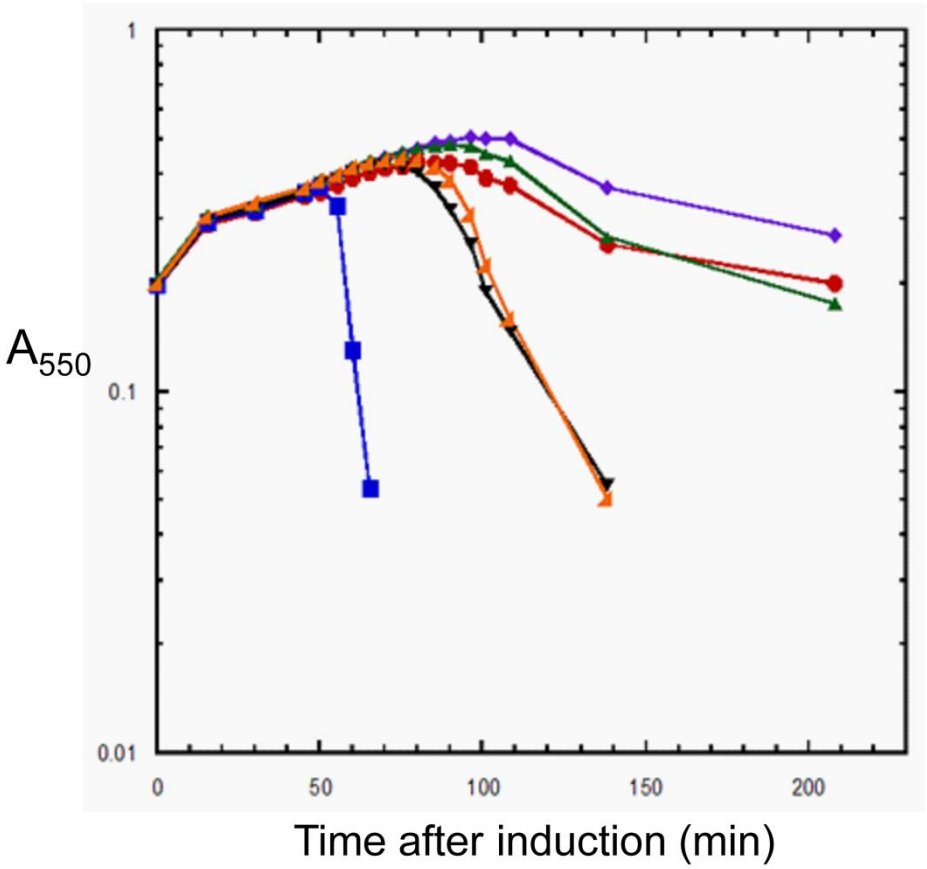

Figure 3.7. Functional test of $S105_{\Delta TM1\ C51A}$. The curves correspond to the following strains ("λ" indicates prophage and "p" indicates plasmid): $\lambda S105_{C51A}$ + $pS105_{\Delta TM1}$, purple; $\lambda S105_{C51A}$ + $pS105_{\Delta TM1\ C51A}$, green; λS105 + $pS105_{\Delta TM1}$, red; $\lambda S105_{C51A}$ + pSam7, black; λS105 + $pS105_{\Delta TM1\ C51A}$, orange; λS105 + pSam7, blue.

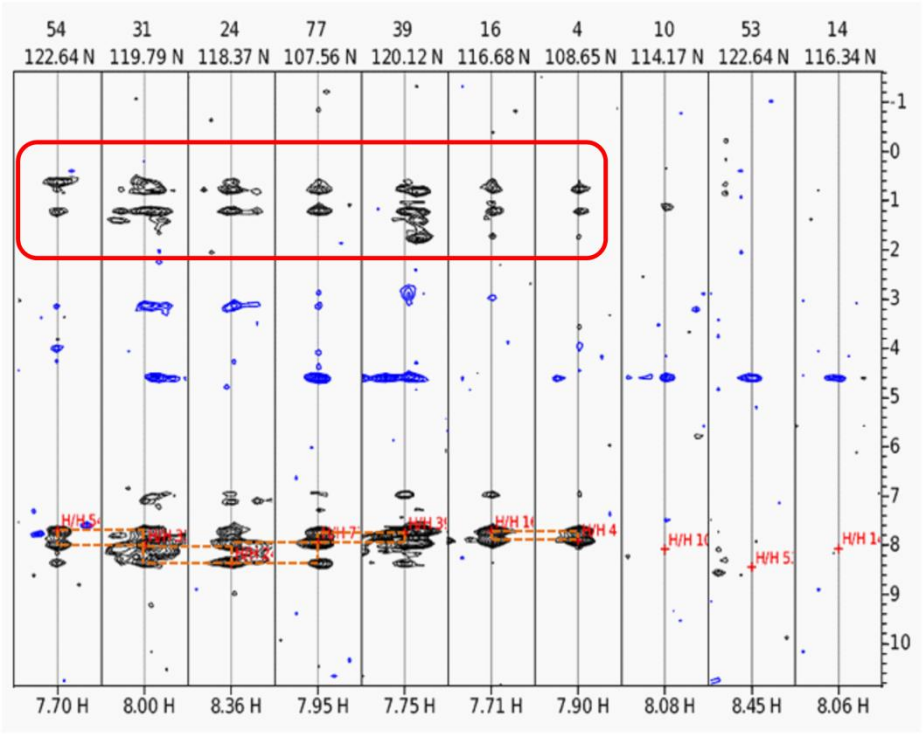

Figure 3.8. NOESY spectrum of residues within TMD3. The red box indicates contacts with the micelle (70).

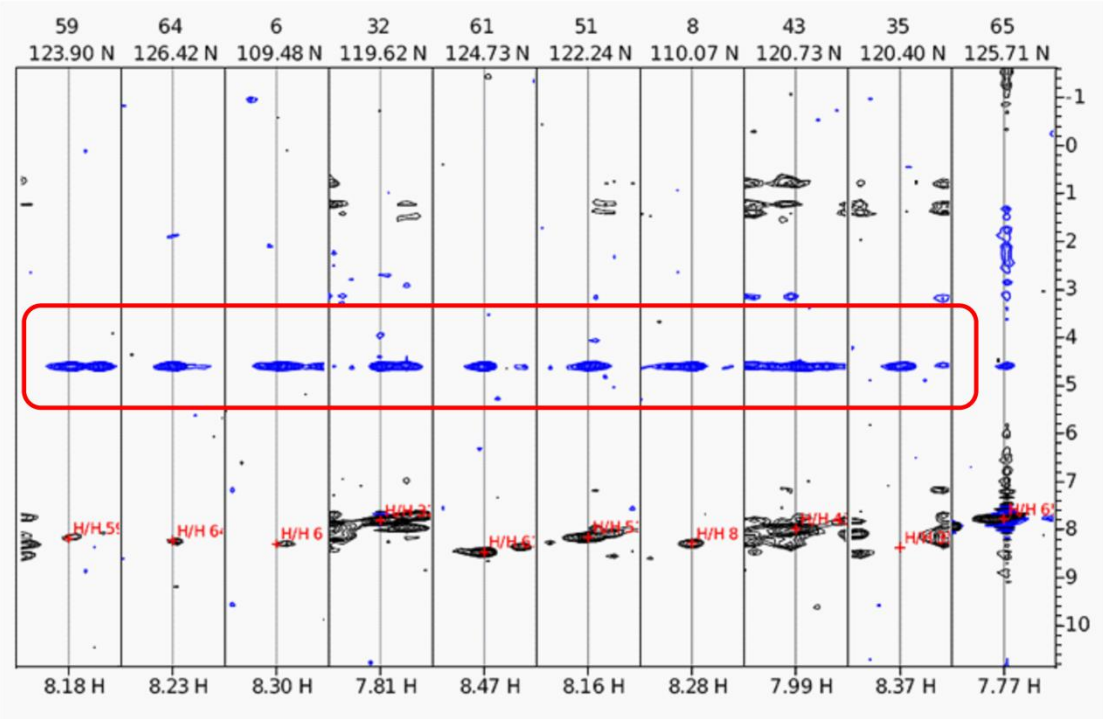

Figure 3.9. NOESY spectrum of residues in the C-terminus. The red box indicates contacts with water (70).

Transverse Relaxation Optimized Spectroscopy, or TROSY, was also used in this work, in an effort to filter transverse relaxation from the overall signal and improve peak resolution (66). Figure 3.10A shows the TROSY spectrum for [^{2}H][^{15}N][^{13}C]-labeled $S105_{\Delta TM1\ C51A}$ in LDAO micelles. Some of the peaks were distinct and well-resolved, but others were close to one another, making it difficult to determine where one peak ended and the next began (Fig. 3.10B). In an effort to better resolve the peaks throughout the entire protein, improvements were made to the sample preparation. First, the question of sample quality was addressed. For these experiments, the optimal concentration of protein was 1 mM (or ~10 mg/ml for S) in a volume of at least 250 μl. Although this seems simple enough for soluble proteins, this was not so easy to accomplish with a toxic membrane protein. Nonetheless, the purification method was marginally streamlined and the buffer conditions were optimized so as to produce the highest concentration of protein possible. Secondly, non-distilled D_2O was used for all remaining experiments to ensure that deuteration levels remained high. Finally, and perhaps most importantly, higher field magnets, with extremely sensitive cryoprobes, were used for future experiments, resulting in more peaks and better resolved peaks. Dr. Christian Hilty and Youngbok Lee used the Varian 800 MHz spectrometer with triple resonance probe and the Bruker 800 MHz NMR spectrometer with cryoprobe for collecting data from a number of experiments, including: 2D-TROSY-HSQC, 3D-HNCA, 3D-NOESY, 3D-HNCACB, 3D-HNCO, 3D-HN(CA)CO, 3D-HN(CO)CA, ^{1}H^{15}N heteronuclear NOE, and T1/T2 relaxation. These experiments resulted in the

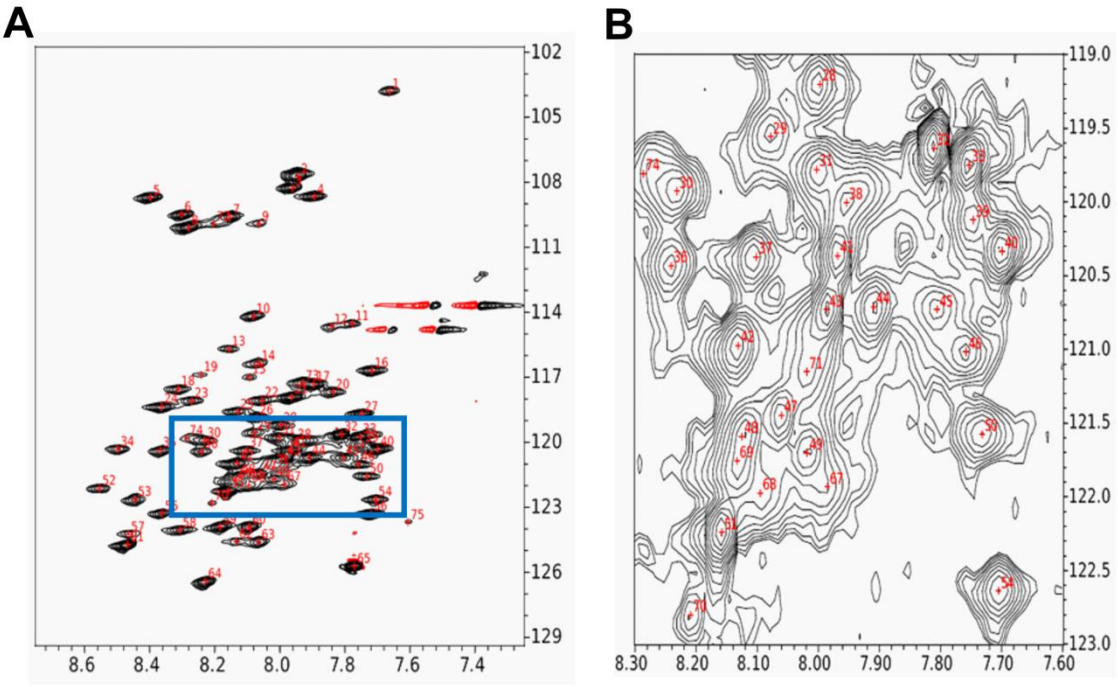

Figure 3.10. TROSY spectra of [^{2}H][^{15}N][^{13}C] labeled S105$_{\Delta TM1\ C51A}$ in LDAO micelles. (A) The entire spectrum; the blue box indicates the region zoomed-in for panel B; (B) close-up view of region with poorly-resolved peaks.

assignment of 85 out of the total 92 amino acid residues (70). Chemical shift assignments for residues within the protein sequence still remain missing, however, for portions of TMD2 and TMD3, as well as the associated linker region and the 6XHis tag. Figure 3.11 shows a side-by-side view of some of the resulting data with the 600 MHz NMR (Fig. 3.11A) versus the 800 MHz NMR (Fig. 3.11B).

Secondary structure and backbone dynamics of S105$_{\Delta TM1\ C51A}$. Collaborators Dr. Christian Hilty and Youngbok Lee analyzed the NMR data and obtained information about the secondary structure, as well as backbone mobility, for the protein sample. Deviations in random coil values for C_α chemical shifts can be used to determine secondary structure, i.e. positive values are indicative of alpha-helical character, and negative values are unstructured (73). In the case of S105$_{\Delta TM1\ C51A}$, residues 16-35 and 41-61, which correspond to regions of TMD2 and TMD3, had positive values (70). In addition, similar deviations in random coil values for C_α chemical shifts were determined for residues 62-71, indicating alpha helical character for this region as well. In contrast, negative values were determined for regions at the N- and C-termini, which suggest these regions are unstructured (70). Secondary structure can also be determined by medium-range NOEs, based on ^{1}H-^{1}H distances (74). For alpha-helical structure, NOEs d_{NN} and $d_{NN}(i,i+2)$, which correspond to distances between backbone amide protons on neighboring residues and distances between the alpha proton of one residue

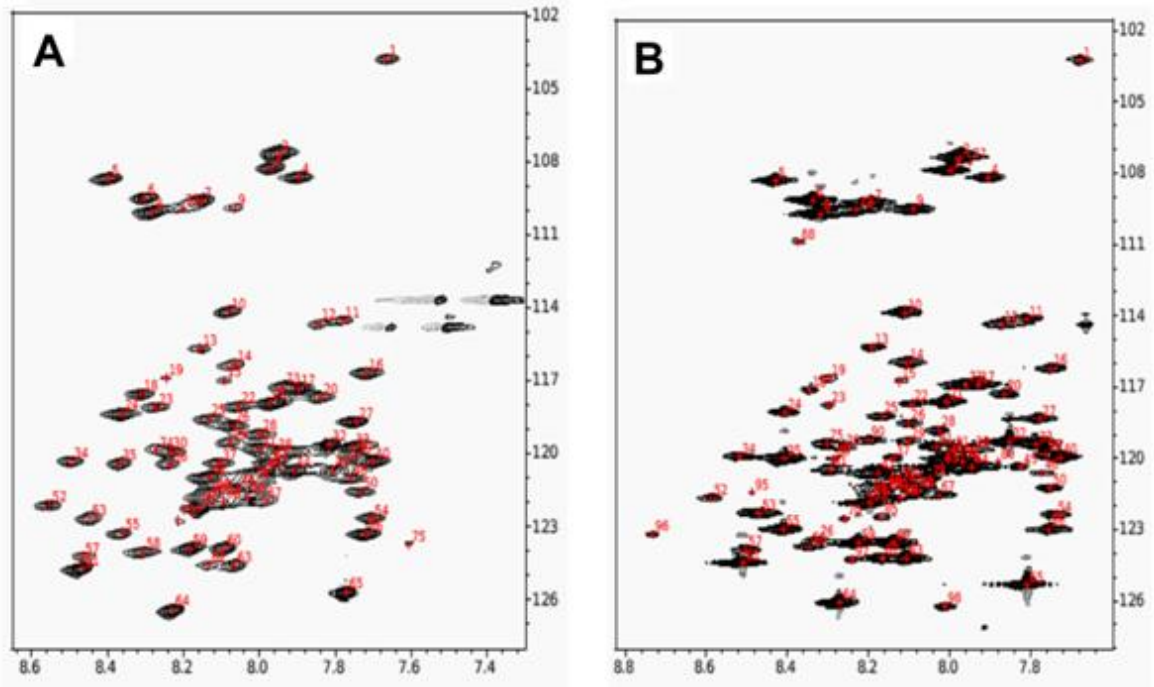

Figure 3.11. [^{1}H][^{15}N] TROSY-HSQC spectra of triple-labeled $S105_{\Delta TM1\ C51A.}$ The following instruments were used: 600 MHz NMR (A) and 800 MHz NMR (B).

and the amide proton of a residue two positions away, respectively, can be observed in deuterated protein samples. For $S105_{\Delta TM1\ C51A}$, both d_{NN} NOEs and $d_{NN}(i, i+2)$ NOEs, which are characteristic of alpha helical structures, were found in the TMDs, and at the region beginning with residue 62 (70).

Heteronuclear $^{15}N\{1H\}$-NOE enhancement and ^{15}N-T_1 and T_2 relaxation times were used to determine the backbone mobility of $S105_{\Delta TM1\ C51A}$. Enhancement values indicate the relative flexibility of a polypeptide chain (75). Specifically, rigid regions of the backbone give enhancement values of +0.8 and less rigid regions have negative values. According to the results, residues within the TMDs of $S105_{\Delta TM1\ C51A}$, as well as residues 62-71, have enhancement values which indicate rigid structure. In contrast, residues 69-94, which correspond to the C-terminus, have negative enhancement values, or less rigid structure (70). In addition to enhancement values, T_1 and T_2 relaxation measurements can also be used to assess backbone dynamics, i.e. increased T_1 and decreased T_2 are associated with rigid structure (75). For $S105_{\Delta TM1\ C51A}$, T_1 and T_2 values for both termini suggest increased flexibility or mobility. However, the T_1 and T_2 relaxation times for the TMDs were significantly different (70).

Due to the appearance of additional NMR peaks in aging samples, there were indications that the protein was undergoing conformational changes (70) (Fig. 3.12). The changes did not appear to be consistent with degradation, but rather a slow process of dimerization and/or oligomerization. To determine whether the protein was changing

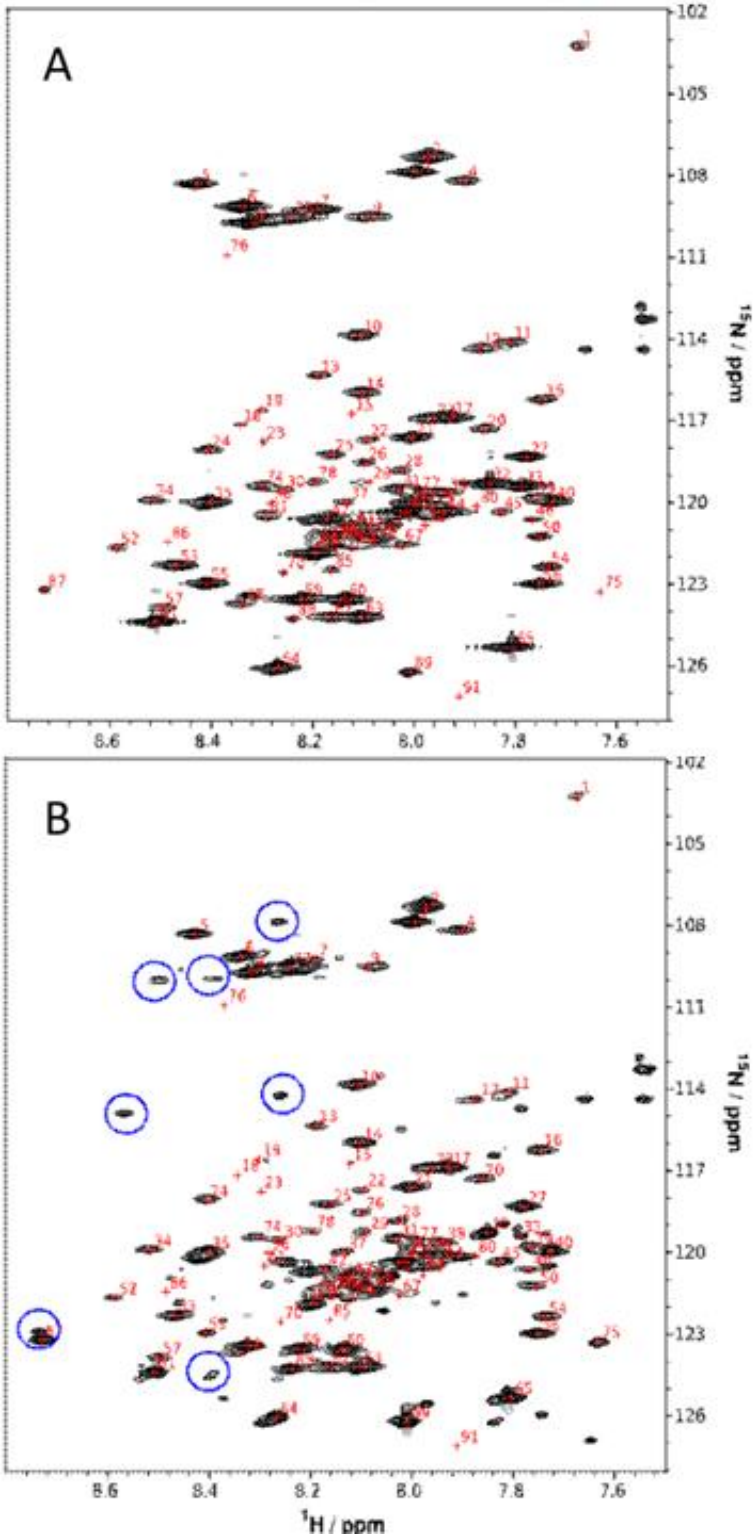

Figure 3.12. 2D-TROSY spectra of newly-prepared sample (A) and aged sample (~10 days) (B). Blue circles indicate new peaks (70).

over time, gel filtration and chemical crosslinking were used to assess the oligomeric state of $S105_{\Delta TM1\ C51A}$. Specifically, dithiobis (succinimidyl-propionate) (DSP) crosslinking was performed on the labeled NMR sample, and gel permeation chromatograms were compared for 3-month old aged and freshly-prepared protein samples. DSP-crosslinking of the NMR sample indicated that there was some dimer formation in the aged sample (Fig. 3.13). The gel permeation results indicated that although the majority of the protein remained in a monodisperse peak which seemed to be consistent with a monomeric species, the secondary peaks differed depending on the age of the sample (Fig. 3.14). In the newly-made sample, the secondary peak was positioned consistent with a dimer, whereas the aged sample had a secondary peak consistent with a larger-sized oligomer.

Discussion

As a result of these collaborative studies, there has been significant progress in the effort to determine the solution structure of the lambda holin mutant, $S105_{\Delta TM1\ C51A}$. Over 60% of the amino acids have been identified as spin systems; however, there are still a number of residues without assignments. The data confirm the placement of at least one of the TMDs within the protein, as well as the placement of the highly charged and less structured C-terminal tail. In addition, both micelle-embedded and water-exposed regions have been differentiated and identified. NMR studies have also provided evidence of secondary structure in the form of the alpha-helical character

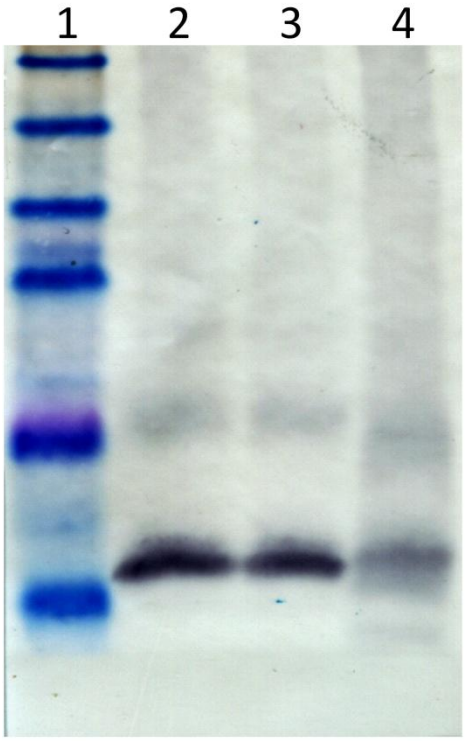

Figure 3.13. Western blot of DSP-crosslinked $S105_{\Delta TM1\ C51A}$. Lane 1: molecular weight marker; lane 2: NMR sample; lane 3: NMR sample, -DSP; Lane 4: NMR sample, + DSP

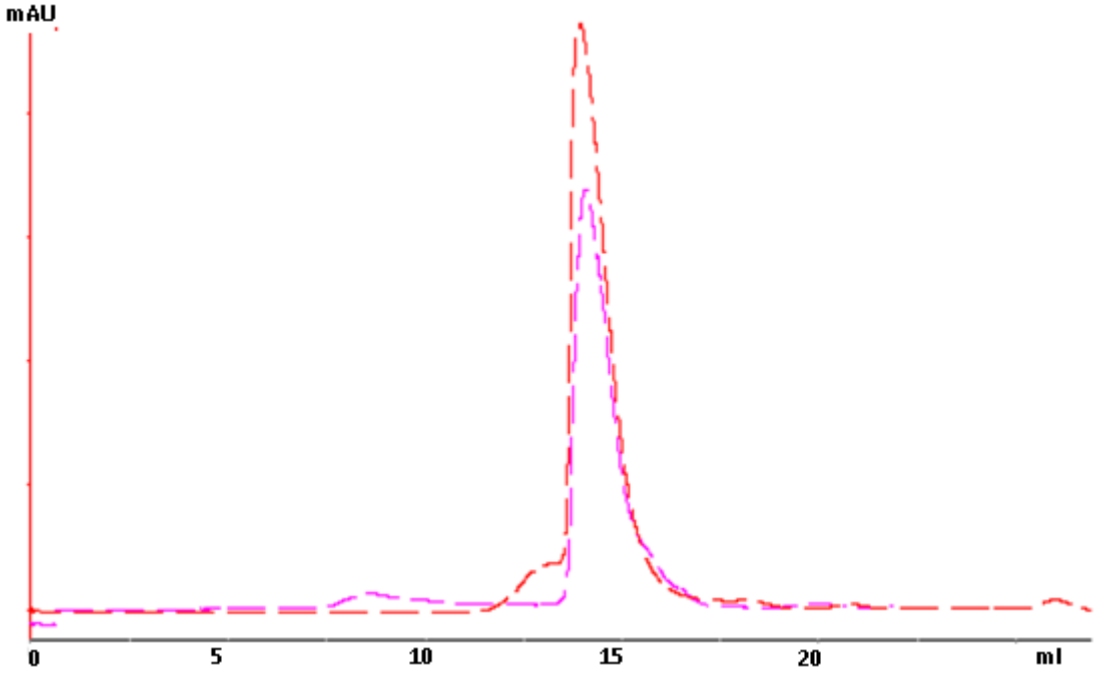

Figure 3.14. Gel permeation chromatograms for $S105_{\Delta TM1\ C51A}$ (comparison of aged and newly-made samples). Aged (3-month old sample), pink; newly-prepared sample, red.

for the TMDs and the possibility of an extended helix at the bottom of TMD3. In addition, these studies have indicated regions involved in backbone dynamics for the lambda holin mutant $S105_{\Delta TM1\ C51A}$ (70).

Although significant progress has been made on this project, there are several experiments still to be done so that the NMR solution structure of the lambda holin mutant, $S105_{\Delta TM1\ C51A}$, can be completed. To begin, future work on this project will involve selectively-labeling amino acids within the protein, in an effort to verify current assignments, as well as acquiring the remaining chemical shift assignments. The strain DL39(DE3) (76-77), which is auxotrophic for the following amino acids: leucine, isoleucine, aspartic acid, valine, phenylalanine, and tyrosine, will be used to express the selectively-labeled protein. Secondly, paramagnetic relaxation reagents will be used to more definitively determine which parts of the protein are exposed to water or actually embedded in the lipid micelle. Specifically, the reagent Gd-DTPA is a water-soluble spin label which only affects water-exposed regions of the protein, and lipophilic 16-doxyl stearic acid only affects micelle-embedded regions. Finally, and perhaps most importantly, the optimized conditions for sample preparation and NMR spectroscopy of $S105_{\Delta TM1\ C51A}$ will be used to study the structure of the wild-type lambda holin, S105, as well as other bacteriophage holin proteins.

Materials and Methods

Plasmids and strains. The plasmid used for this work was pET11a $S105_{\Delta TM1\ C51A}$, which has ampicillin resistance. pET11a $S105_{\Delta TM1}$ is the same as pET11a S105 (2) with

the sequences encoding residues L9 through A30, which comprise TMD1 of S105, deleted. pET11a $S105_{\Delta TM1\ C51A}$ was made by Quickchange site-directed mutagenesis of pET11a $S105_{\Delta TM1}$, converting the cysteine residue at position 51 to alanine. The strain used for protein expression was C43(DE3) *tonA*::Tn*10* (61).

Reagents and instruments. All labeled NMR reagents for minimal media, including D_2O, ^{13}C-glucose, and ^{15}N-ammonium chloride were purchased from Spectra Stable Isotopes (Cambridge). The remaining reagents used for minimal media were obtained from Sigma. All NMR experiments were carried out with the following instruments: the Varian 500 MHz NMR with triple resonance probe (Texas A&M University), the Varian 600 MHz NMR with triple resonance probe (Texas A&M University), the Varian 800 MHz spectrometer with triple resonance probe (Pacific Northwest National Lab) and the Bruker 800 MHz NMR spectrometer with cryoprobe (The University of Houston).

Media preparation. One liter of solution Q was made according to the following recipe: 8 ml HCl, 5 g $FeCl_2\ 4H_2O$, 184 mg $CaCl_2\ 2H_2O$, 64 mg H_3BO_3, 18 mg $CoCl_2\ 6H_2O$, 4 mg $CuCl_2\ 2H_2O$, 340 mg $ZnCl_2$, 605 mg $Na_2MoO_4\ 2H_2O$, 25.4 mg $MnCl_2$ in H_2O at a final volume of 1 L. The solution was filter-sterilized and stored at room temperature. One hundred milliliters of vitamin mix was made according to the following recipe: 50 mg thiamine, 10 mg D-biotin, 10 mg choline chloride, 10 mg folic acid, 1 mg niacinamide, 10 mg D-pantothenic acid, 10 mg pyridoxal, and 1 mg riboflavin in H2O at a final volume of 100 ml. The vitamin mix was filter-sterilized and stored at -20 °C.

Two liters of minimal media were made according to the following recipe: 25.6 g Na_2HPO_4 $7H_2O$, 6 g KH_2PO_4, 1 g NaCl, dissolved in ~1.9 L D_2O. Two milliliters of solution Q, 4 ml 1M $MgSO_4$, 20 ml vitamin mix, 4 g $^{13}C_6$-D-glucose, and 2 g $^{15}NH_4Cl$ were added and stirred gently until all contents dissolved. D_2O was added to the media to bring the final volume to 2 L. The media was filter-sterilized and stored at 4 ºC.

Culture growth for protein purification. Cultures were grown as previously described with some changes (25, 64). C43(DE3) *tonA*::Tn*10* cells were transformed with pET11a $S105_{\Delta TM1}$ and plated on LB agar containing 100 mg/ml ampicillin. Ten-fifteen colonies were used to inoculate a 30 mL LB culture containing 100 mg/ml ampicillin. This starter culture was grown to OD = 0.6 at 37 °C with gentle shaking, then used to inoculate two 1 L culture flasks of [^{2}H][^{13}C][^{15}N]-labeled minimal media at a dilution of 1:100. The large cultures were grown to OD = 0.6 at 37 °C with gentle shaking, then induced for expression of $S105_{\Delta TM1}$ or $S105_{\Delta TM1\ C51A}$ with 1 mM IPTG. The induced cultures were grown for 3 additional hours, then the cells were harvested and stored at -20 °C.

Protein purification. Protein purification was carried out as previously described, (25, 64) with the following exceptions. 20 mM Phosphate pH 7.8, instead of 20 mM Tris, was used for the following purification buffers, including lysis buffer, extraction buffer, buffer A, low imidazole buffer, and elution buffer. The detergent used for purification was LDAO, at a final concentration of 20 mM in the extraction buffer and 4 mM in the

purification buffers. Following Talon purification, the protein was applied to a Sephadex 200 gel filtration column and eluted at 0.5 ml/min into 1 ml fractions of buffer containing 20 mM Phosphate pH 6.5, 150 mM NaCl, 4 mM LDAO. The fractions containing protein were concentrated with a 3 K MWCO Amicon centrifugal concentrator (Millipore) to a final volume of 250 µl. The final protein concentration was ~1 mM in buffer containing 20 mM phosphate, 150 mM NaCl, and 128 mM LDAO.

NMR spectroscopy and data analysis. All NMR spectroscopy and associated data analysis was carried out by Dr. Christian Hilty and Youngbok Lee. A Bruker 800 MHz NMR spectrometer with cryoprobe was used for triple resonance experiments, with specified parameters such as carrier frequency, spectral width, time-domain data size, maximum evolution time, and number of scans. The following experiments were carried out: 3D-TROSY-HNCA, 3D-TROSY-HNCACB, 3D-TROSY-HNCO, 3D-TROSY-HN(CA)CO, 3D-TROSY-HN(CO)CA, 3D-^{15}N-resolved [^{1}H,^{1}H]-NOESY. A Varian 800 MHz spectrometer with triple resonance probe was used for determination of backbone dynamics. All of the data were collected at 35 °C. Data were processed using the NMR pipe software (78). Some of the data acquired on the Bruker spectrometer were processed directly with the Topspin software. The program CARA (79) was used for chemical shift assignments and peak integration (70).

CHAPTER IV

MICRON SCALE HOLES TERMINATE THE PHAGE INFECTION CYCLE*

Bacteriophage lysis, the most frequent cytolethal event in the biosphere, is a precisely scheduled process controlled by proteins of the holin family (4). Holins are an extremely diverse class of small, phage-encoded membrane proteins (6). The best studied holin is S105, a 105-residue polypeptide with three TMDs encoded by the *S* gene of phage λ (14). Throughout the period of late gene expression and particle assembly, S105 accumulates in the cytoplasmic membrane of *E. coli* without any effect on its integrity (38). Suddenly, at a programmed time, S105 triggers to form a lesion, or hole, in the membrane; this allows the λ endolysin, R, to escape from the cytoplasm and attack the cell wall (6). In phages of Gram-negative hosts, there is a third step to complete the lysis pathway involving a protein or protein complex, the spanin, which connects the cytoplasmic and outer membranes (13, 80). In λ, the spanin complex consists of the cytoplasmic membrane protein Rz and the outer membrane lipoprotein Rz1. This complex is essential for lysis in media containing millimolar concentrations of divalent cations and thus is thought to act by disrupting the

---

*Reprinted with permission from Dewey JS,Savva, CG, White, RL, Vitha, S, Holzenburg, A, and Young, R. (2010) Micron-scale holes terminate the phage infection cycle. *Proc Natl Acad Sci U S A* 107(5) 2219-2223.

outer membrane, possibly by fusion with the inner membrane (13).

Although the S105 holin has been extensively studied using genetic and biochemical approaches (10, 14, 16, 25, 38), nothing is known about the membrane holes except that they are non-specific and large enough to allow escape of fully folded, tetrameric R-β-galactosidase chimeras (>450 kDa), indicating that they are of unprecedented size for channels made by integral membrane proteins (20). Recently, cryo-electron microscopy (cryo-EM) studies of detergent-purified S105 revealed large ring assemblies with two main size groups consisting of 18 and 20 protomers respectively, with the majority class, 18mers, having an inner diameter of ~ 8.5 nm (25). S105 in these purified complexes retained α-helical content and protease sensitivity consistent with the membrane topology in vivo, as determined by genetic and biochemical experiments (14). However, the nature of the S105 lesion in the host membrane has remained elusive. The lumenal diameters observed are not consistent with the ability to release endolysin-β-galactosidase chimeras of ~0.5MDa mass. Attempts to visualize the membrane lesions by conventional ultra-thin-section electron microscopy have been unsuccessful (81), in part because of the structural deformations associated with the multiple fixation, dehydration and staining steps (82).

Rapid freezing at liquid ethane temperatures allows complete preservation of biological material below ~2 μm in size, in a native hydrated environment (83-84). Furthermore, the millisecond fixation allows time-dependent biological processes to be captured essentially instantaneously (85). We reasoned that by examining cells

expressing *S105* in the absence of *R*, *Rz* and *Rz1*, we could observe the sole effect of the holin on the host cell. Furthermore, by utilizing cryo-EM, we would be able to image the cells in a physiologically relevant state. The results of these studies are discussed in terms of a model for the molecular pathway of holin-mediated lysis.

Results

Expression of S105 leads to large membrane gaps in the E. coli inner membrane. To examine the effect of S105 on the host, we used *E. coli* strains expressing the holin in the presence and absence of the endolysin R and the spanin complex proteins, *Rz* and *Rz1* (Fig. 4.1A). It was important to characterize the lysis behavior of the strains prior to their imaging by cryo-EM. Cultures expressing *S105* with and without *R*, were grown and induced for expression of the lysis genes (Fig. 4.1B). The strain harboring pSRRzRz1, with functional alleles of all the genes of the λ lysis cassette, lysed as expected at approximately 50 min. The strain carrying pS, expressing *S105* alone, ceased growth at 50 min, indicative of hole formation in the cytoplasmic membrane, but, because of the absence of endolysin activity, did not undergo lysis. In order to visualize the effect of S105 alone on the host membrane, a 60 minute sample of an induced pS culture was plunge-frozen into liquid ethane without any further manipulation (i.e. concentrating or washing). Specimens were then imaged under liquid nitrogen temperatures and low-dose conditions, revealing rod-shaped cells with intact outer membranes. Upon closer examination, about half of the cells displayed an apparent discontinuity in the inner

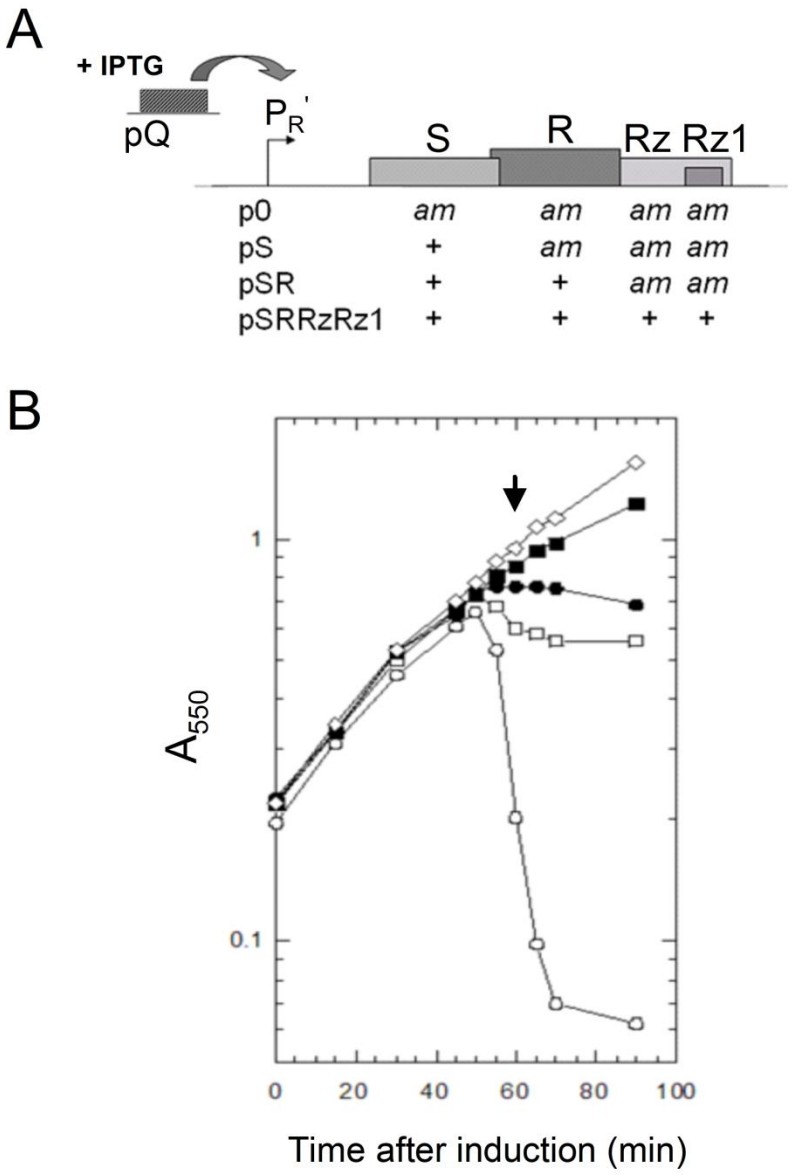

Figure 4.1. Plasmids used in this study (A). Lysis curves of cultures carrying (B): no S105 plasmid, (◊); p0 (■); pS,(●); pSR, supplemented with 10 mM $MgCl_2$ (□); pSRRzRz1 (○).The arrow shows the 60 minute timepoint at which samples were taken for cryo-EM.

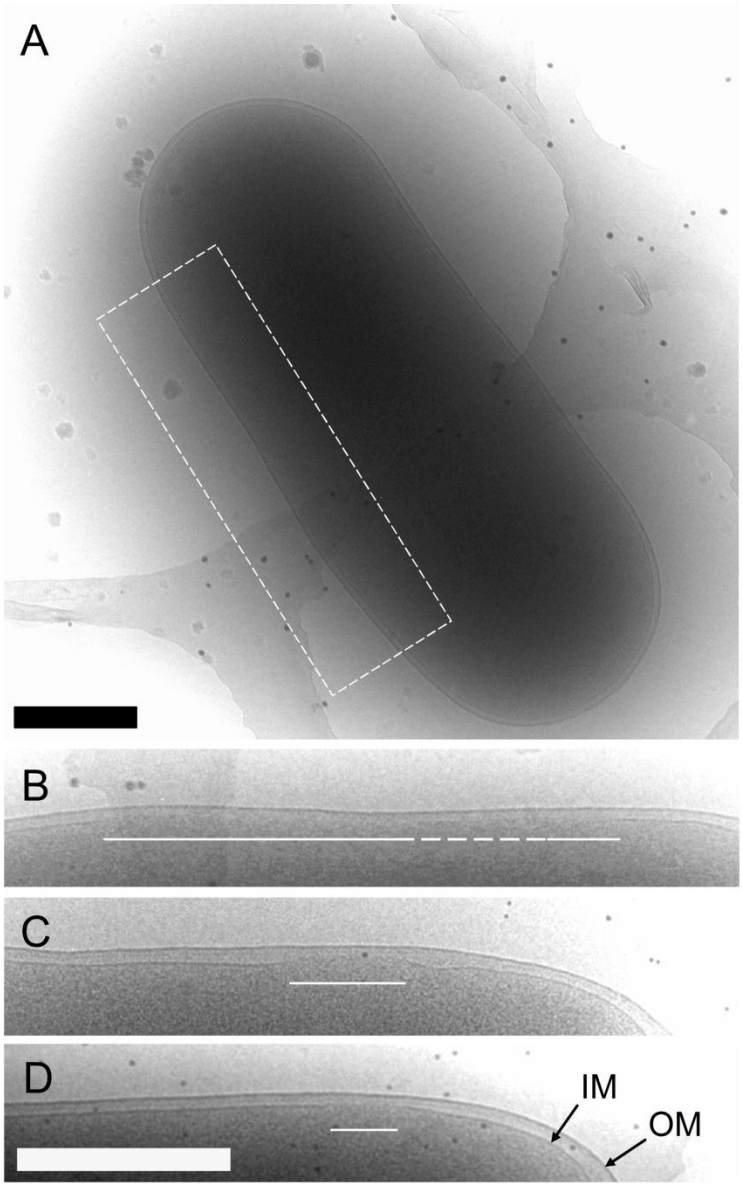

Figure 4.2. Cryo-EM of the S105 lesion. Cells were grown and imaged as described. A cell expressing *S105* is shown in A. The area enclosed in the white-dashed box is shown enlarged in B. The white solid lines indicate the location and extent of the lesion. The dashed white line indicates an area of semi-continuous membrane density. Close-up views of the S105 lesions from two other cells (C, D). Scale bar corresponds to 500 nm.

membrane density (Figs. 4.2, 4.3A). These gaps ranged in size from 88 nm to 1.2 μm, with an average size of ~340 nm (Figs. 4.2B-D, 4.3B). The lesions were not localized to a specific region in the inner membrane but appeared randomly throughout its periphery, irrespective of size (Fig. 4.3C, D). Taking into account the geometry of viewing in the vitreous ice, the observed diameters, and the random positioning of the lesions, calculations indicated that there must be ~2 holes per cell (Fig. 4.4). In order to confirm that these inner membrane gaps were associated with S105 function, cells expressing an isogenic null *Sam* plasmid (p0) were also visualized. Among 45 cells from two different experiments, none displayed an inner membrane discontinuity (Figs. 4.3A, 4.5B). These data indicate that the large gaps observed in the cells expressing *S105* are in fact the lethal holes that allow the endolysin access to the cell wall immediately prior to cell lysis. The unprecedented size of the holes, more than 10-fold larger than those formed by pore-forming cytolysins (21), accounts for the ability of S105 to cause release of unrelated, prefolded endolysins with heterologous structure (6) and of the megadalton scale R-β-galactosidase chimeras (20).

Cryo-tomography of the S105 lesions. To visualize the overall structure of the S105 lesion, cryo-electron tomography was carried out on *E. coli* cells expressing *S105*. Initial attempts were complicated by the large size of the LB-grown cells; the electron path through the specimen at 60° is twice that at zero tilt. Hence, a cell of ~ 1 μm width results in images of very poor signal due to the multiple inelastic scattering events

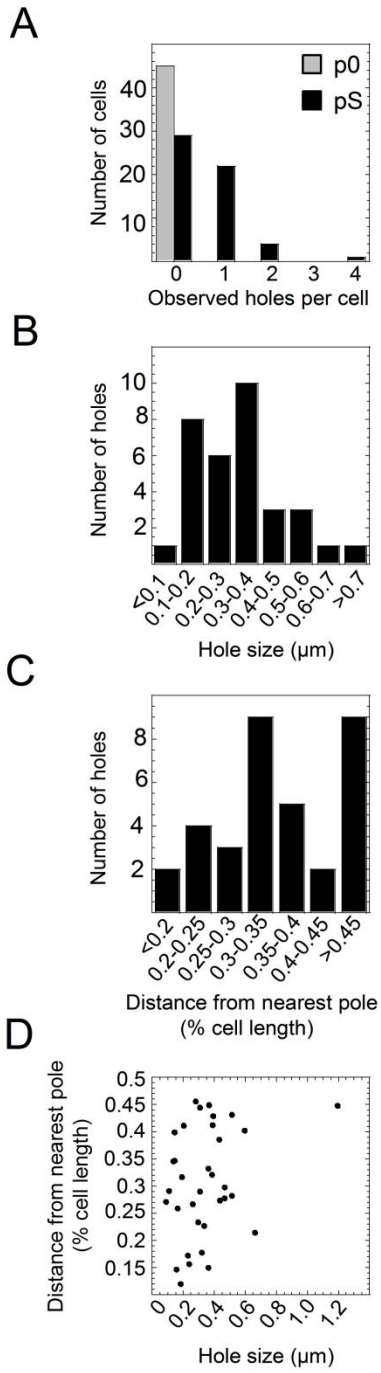

Figure 4.3. Quantification of (A) the number of S105 holes per cell, (B) hole size variation, (C) hole localization, and (D) relationship of hole size to location.

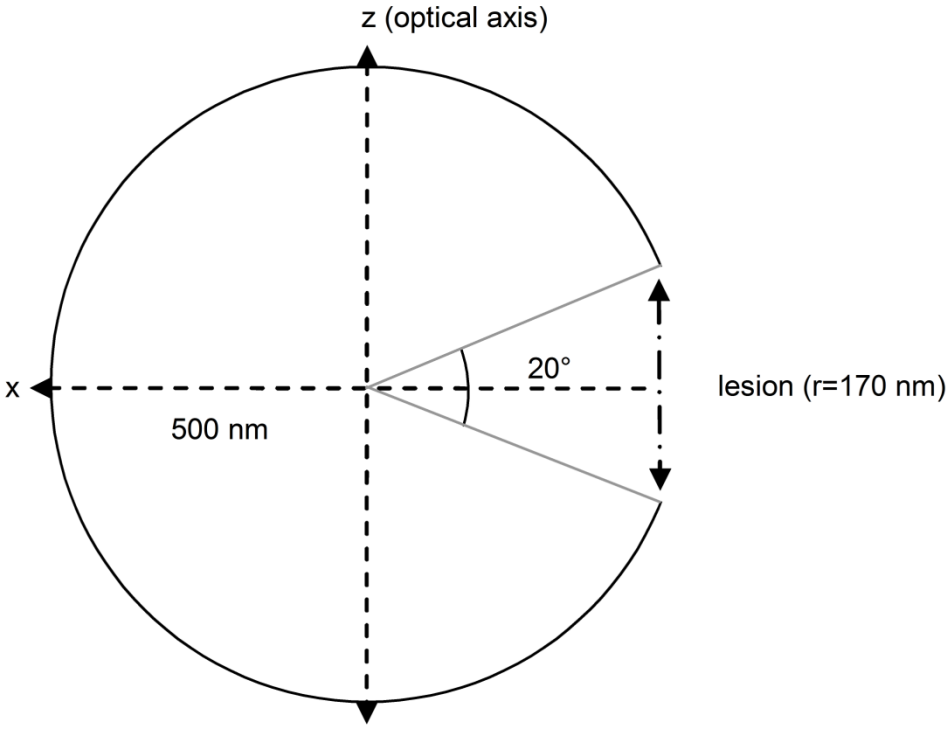

Figure 4.4. Diagram depicting the calculations for the probability of observation of a 340 nm lesion (at a 0° tilt). The circle represents the circumference of a rod-shaped cell along its width (cells observed had an average width of ~1000 nm). A 340 nm lesion (which spans ~40° range) can be observed when part of it is located at the xy plane.

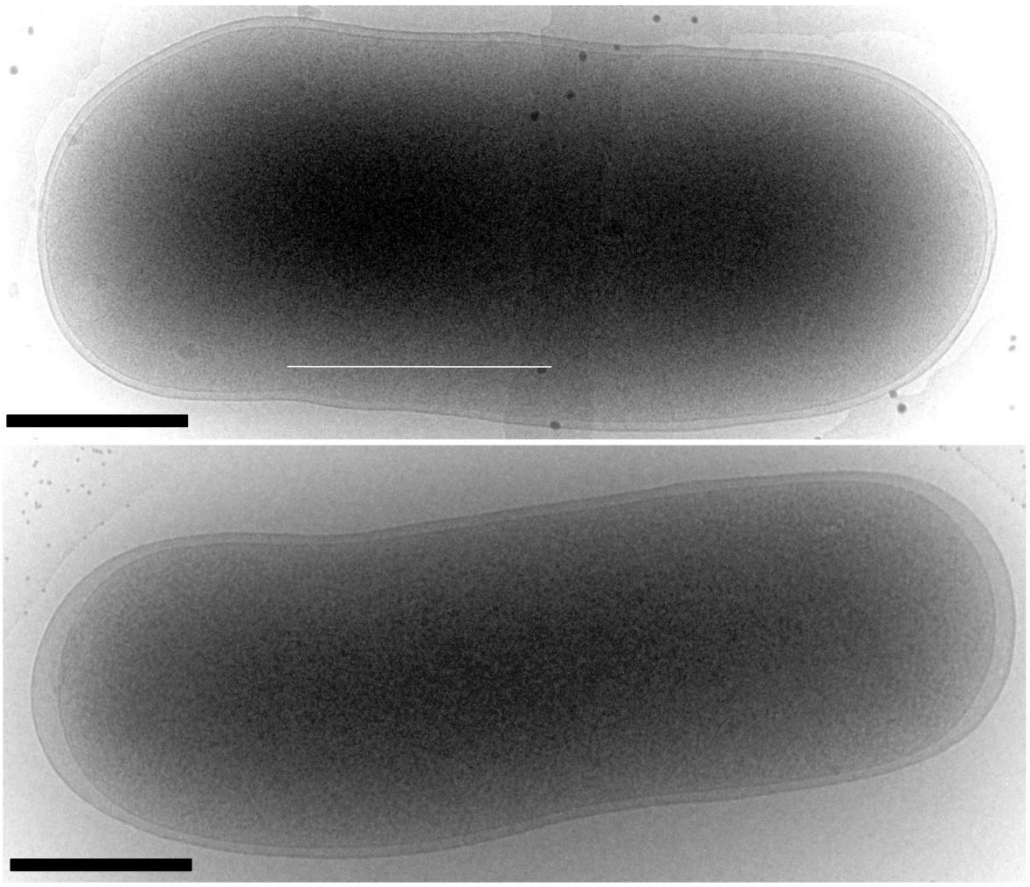

Figure 4.5. Cells expressing *S105* (pS) (top) or *Sam7* (bottom). A continuous inner membrane was characteristic of all cells expressing *Sam7*. Scale bars correspond to 500 nm.

despite the use of an energy filter. In an attempt to reduce the size of the cells, we took advantage of the coupling between cell mass and growth rate (86) and tested several minimal medium conditions (87) for the ability to support the slowest possible growth rate but still allow the precisely-scheduled lysis characteristic of cells grown in rich medium. Among several carbon-sources tested, succinate was found to support a doubling time of 80 min and preserved rod-shaped morphology; induction of the fully functional lysis cassette led to a sharply-defined lysis at 30 min after induction (Fig. 4.6). Phase-contrast microscopy as well as cryo-EM examination revealed that the average cell length and diameter were reduced by >30%, leading to a final relative volume of ~20% of that observed in LB (Fig. 4.7). We examined induced cells for lesions smaller than ~200 nm in order to acquire tomographic data completely spanning a hole. Two 3D reconstructions of cells induced in succinate minimal medium were obtained (Fig. 4.8; Fig. 4.9). Slices through the tomogram shown in Fig. 4.8 show the appearance of a lesion with a maximum diameter of ~130 nm across the xy plane and its subsequent disappearance over a z range of ~125 nm. The actual height of the lesion is less when taking into account elongation effects along z due to the missing wedge (88-89). Segmentation of the cell envelope densities in both tomograms (Fig. 4.8B; Fig. 4.9C) revealed that the lesion in each case was irregular in shape. Although irregular, the lesions resemble a roughly circular shape; i.e. they are not elongated along a particular axis.

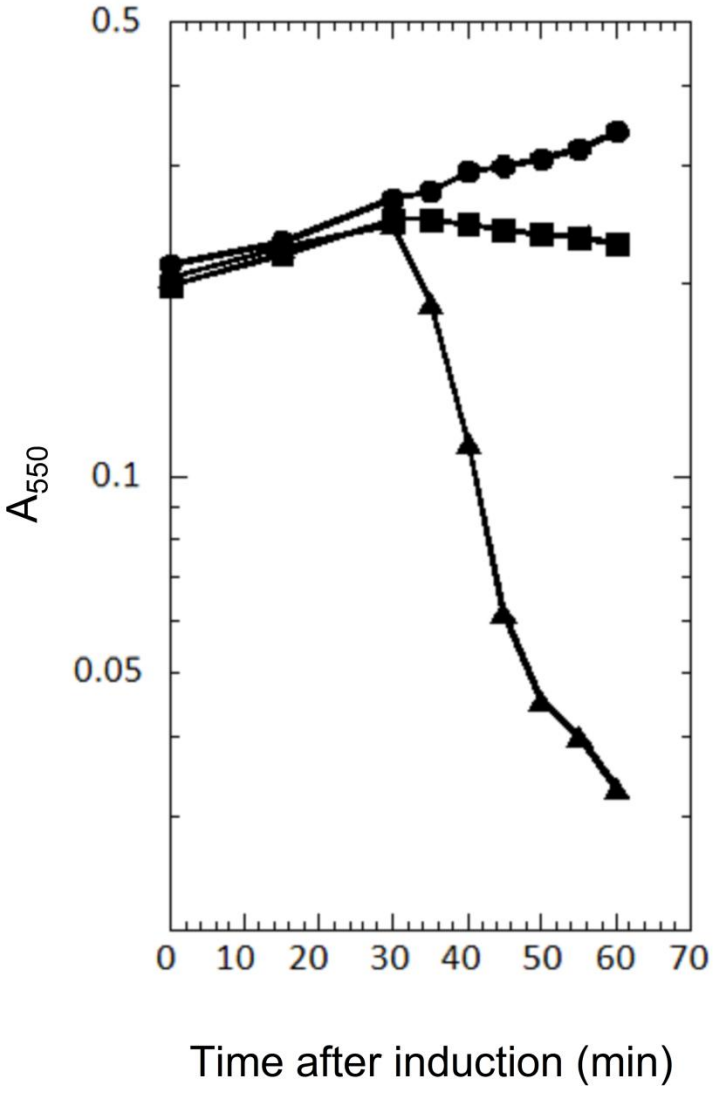

Figure 4.6. Growth curves of cultures carrying no S105 plasmid (●), pS (■), or pSRRzRz1(▲), grown in succinate-minimal media and induced with IPTG at t=0.

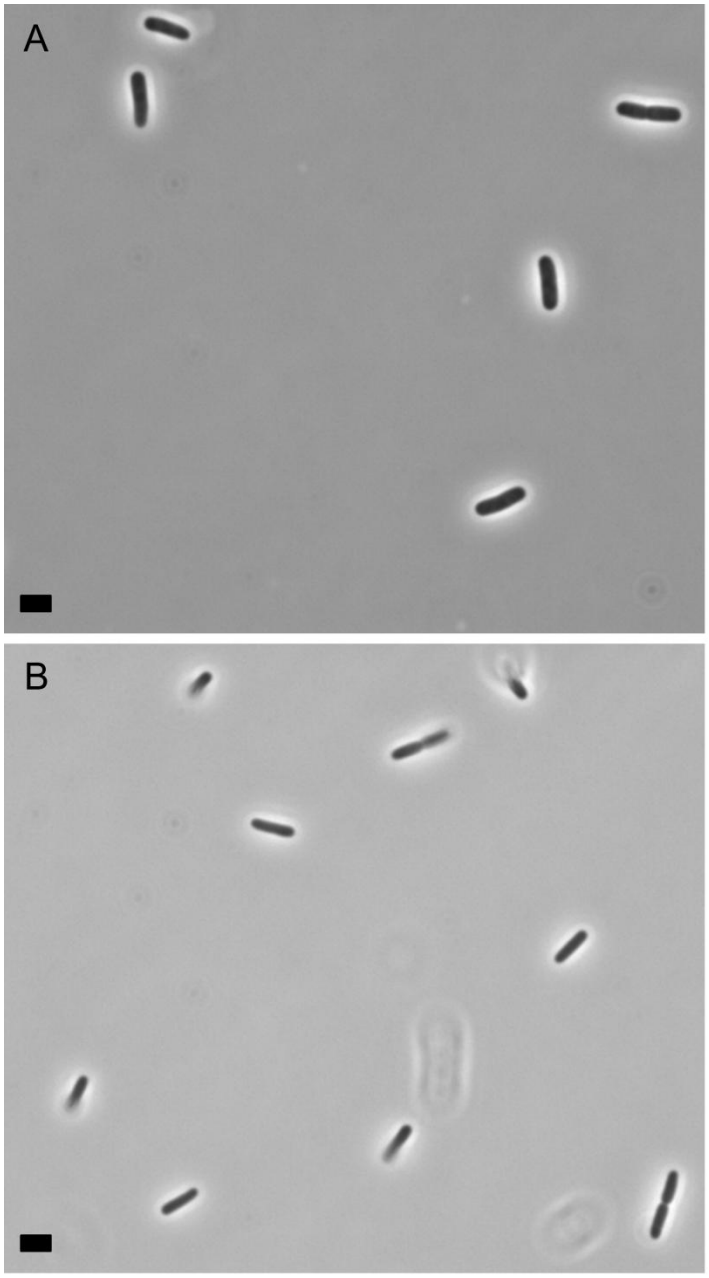

Figure 4.7. Light micrographs of cells grown in LB (A) and succinate media (B). The average length of cells grown in LB and succinate is 3.8 μm and 2.9 μm respectively, while the average width measures 0.97 μm in LB and 0.77 μm in succinate (as measured by cryo-EM). Measurements using light microscopy closely matched the above results. Scale bars correspond to 2 μm.

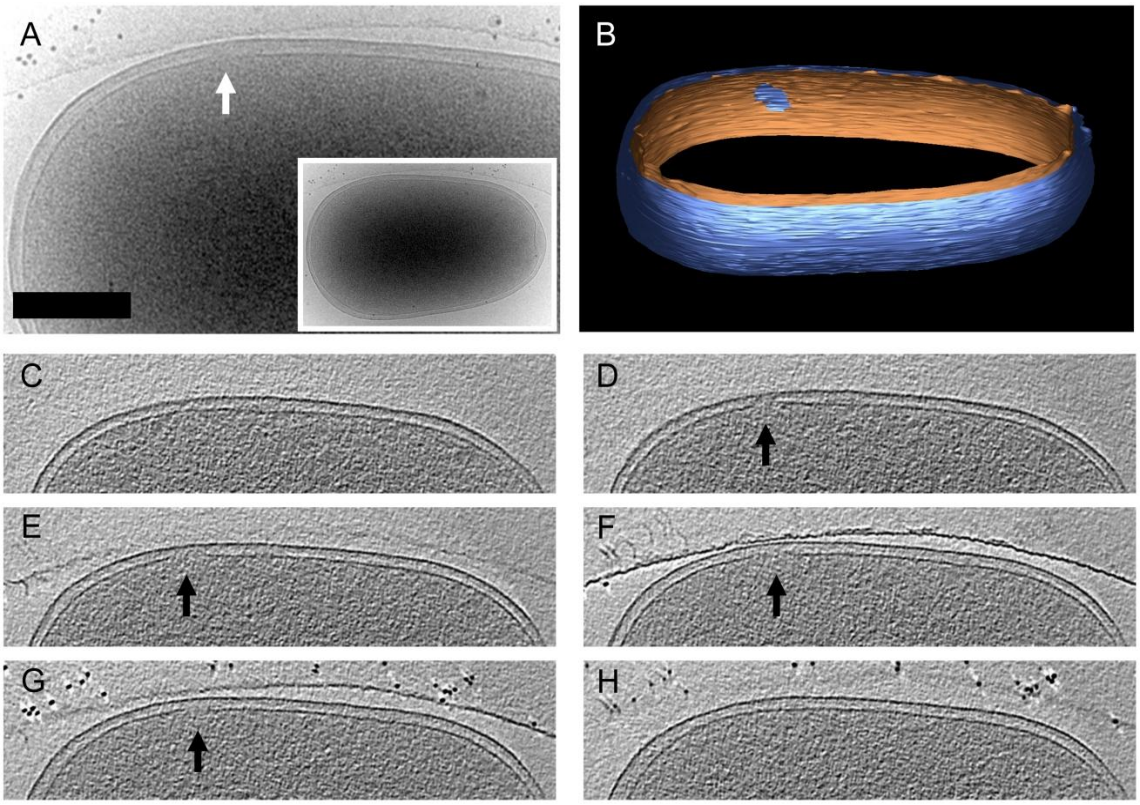

Figure 4.8. Cryo-electron tomography of an S105 lesion. The cell shown (A, inset) expressing *S105*, was tilted +/- 55º and a three-dimensional reconstruction was calculated. A close-up of the lesion in projection is highlighted by the white arrow. Segmentation of the envelope densities (B) shows the outer membrane (blue) and inner membrane (orange). 2.6 nm-thick slices along z (C-H, spaced by 26 nm) show the appearance of a lesion and its subsequent disappearance over a z-height of ~125 nm. Arrows indicate the S105 lesion. Scale bar corresponds to 250 nm.

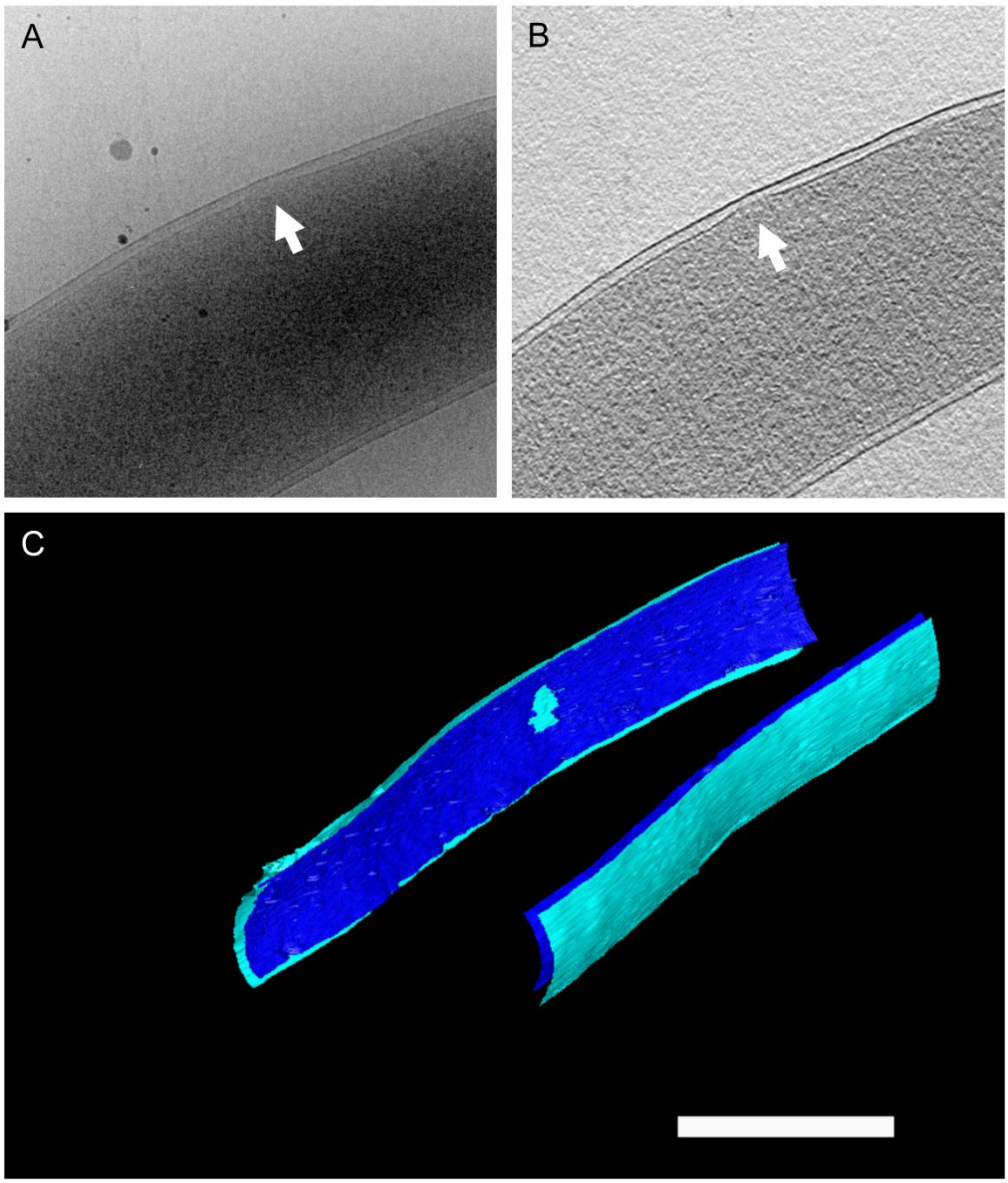

Figure 4.9. Cryo-electron tomography of a cell expressing S105. A zero tilt projection image (A) and a ~25 nm thick slice through the tomogram (B). The observed lesion is highlighted by arrows and displayed in 3D (C) after segmentation of the inner (dark blue) and outer membrane (light blue) densities. Scale bar corresponds to 500 nm.

The holin-endolysin system effects dramatic changes on E. coli, immediately prior to lysis. Having observed the effect of S105 alone on the cell envelope, we sought to visualize cells under conditions that permit complete host cell lysis, i.e., with co-expression of the endolysin R (Fig. 4.1). In images of samples taken at 60 min, the great majority of these cells had undergone complete lysis, as evident from the presence of cellular debris. However, we were able to capture rare instances of cells that had not yet lysed. These cells had lost the characteristic rod shape of *E. coli* and were completely spherical (Fig. 4.10). Because neither *Rz* or *Rz1* is functional, the outer membranes of these cells were still intact. Nevertheless, the inner membrane sacs were collapsed, with evident release of cytoplasmic contents. As shown in Fig. 4.11, in the absence of *Rz* or *Rz1* function, lysing cells can be stabilized in this spherical morphology if millimolar concentrations of divalent cations are supplied in the medium (90-91). Samples taken from an induced pSR culture in medium supplemented with 10 mM $MgCl_2$ were imaged and found to contain a significantly larger number of intact, yet spherical cells similar to the rare unlysed cells in the absence of metal ions. This allowed us to capture various levels of inner membrane disruption, ranging from large membrane gaps to a total collapse of the inner membrane sac (Fig. 4.11). In addition, as a result of the destruction of the murein, most cells exhibited a significant separation of the inner and outer membranes. No instances of punctate zones of adhesion, or Bayer's patches (92-93), between the membranes were observed, supporting the notion that either they require the presence of the murein or that they may be artifacts of sample preparation (82, 94).

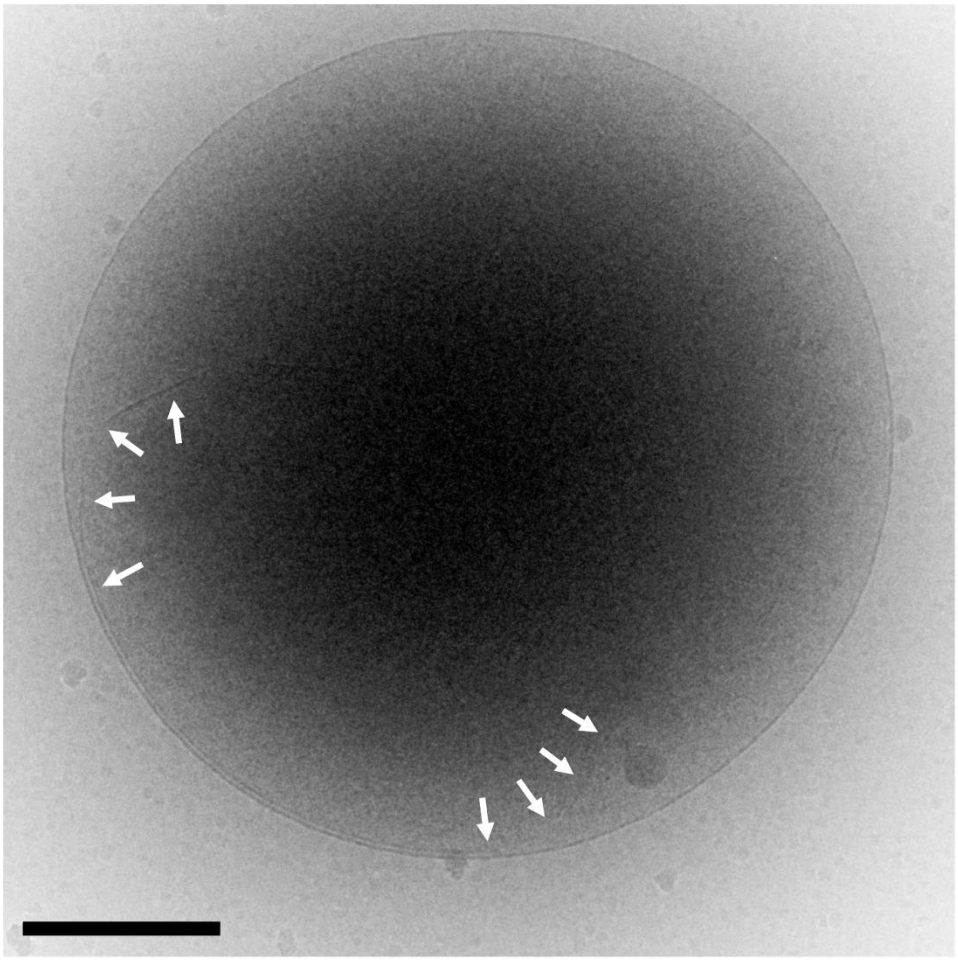

Figure 4.10. Cell expressing *S105* and *R*, without divalent cations present. For these conditions, most cells had undergone complete lysis as evident from the observed cell debris. Arrows trace the discernible inner membrane at the point of separation from the cell envelope. Scale bar corresponds to 500 nm.

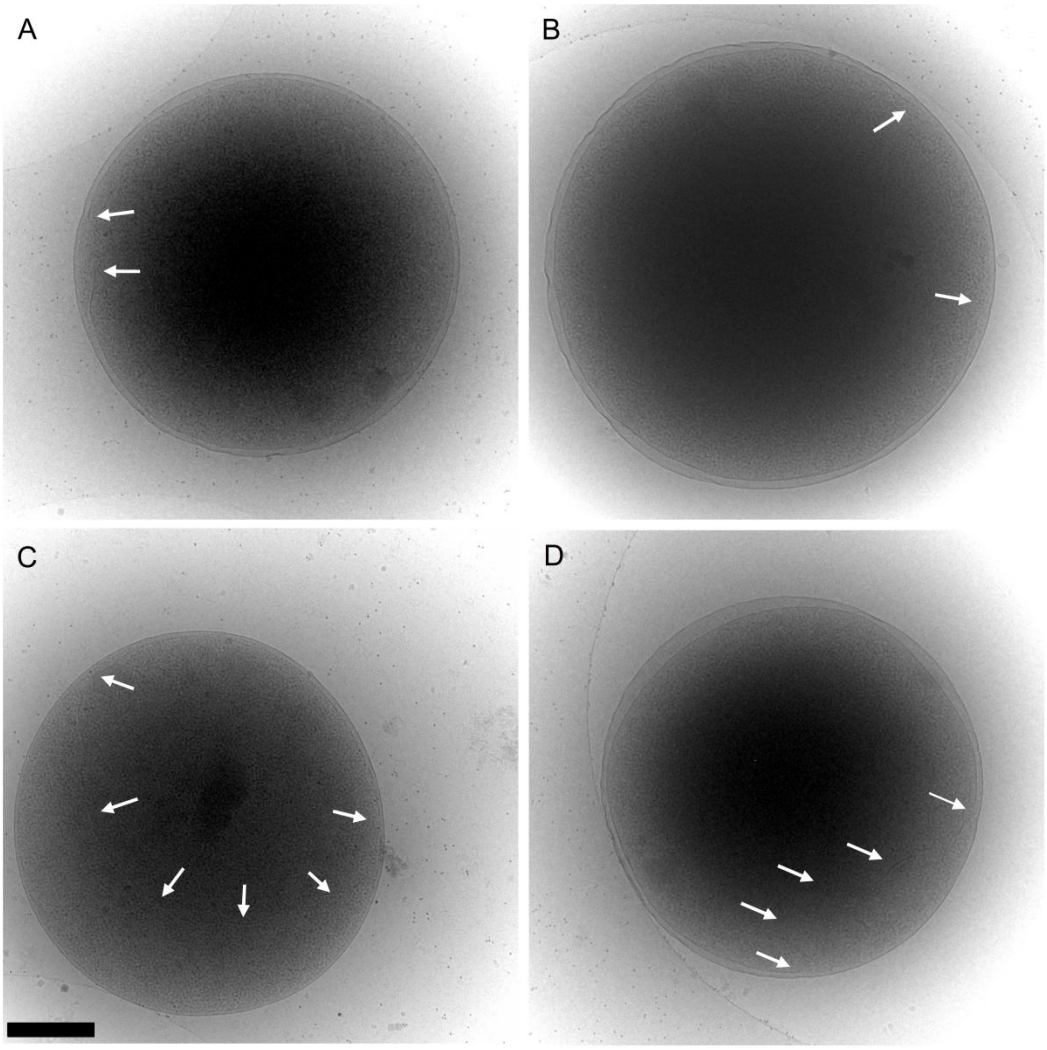

Figure 4.11. Cryo-EM of cells co-expressing the holin (*S105*) and endolysin (*R*) in the presence of Mg^{2+} ions. Cells were captured at different stages of inner membrane disruption including gap formation (A, B) and a more pronounced collapse of the inner membrane (C, D). White arrows indicate the border of membrane discontinuity (A, B) or the trace of the collapsed membrane (C, D). Scale bar corresponds to 500 nm.

Stages of early cytoplasmic leakage through the S105 hole were also observed. An example is shown in Fig. 4.12, where a cloud of density proximal to the inner membrane suggested cytoplasmic leakage through a hole. Tilting of the microscope stage confirmed that the leakage originated from a lesion of ~100 nm diameter (Fig. 4.12B-D)

Discussion

For the first time, the lethal holes caused by the holin-endolysin lysis system of bacteriophages have been directly observed in cells. Unexpectedly, the size of the membrane holes caused by the S105 protein in terminating the λ infection cycle exceeds by more than an order of magnitude that reported for any other membrane lesion in biology, the largest of which are the ~30 nm pores formed by the cholesterol-dependent cytolysins (21, 95). Tomographic analysis confirmed that membrane gaps observed in projection represented actual holes, rather than invaginations or deformations. In addition, it could be established that the holes were irregular in shape, unlike the highly symmetric cytolysin pores which make the next largest membrane holes observed to date (95). These results contradict the previous ultrastructural study, which failed to detect any interruptions in the integrity of the cytoplasmic membrane after function of the S holin (81); however, the previous work used thin-sections of cells subjected to harsh fixation and dehydration steps.

The existence of holes of such unprecedented size is even more remarkable,

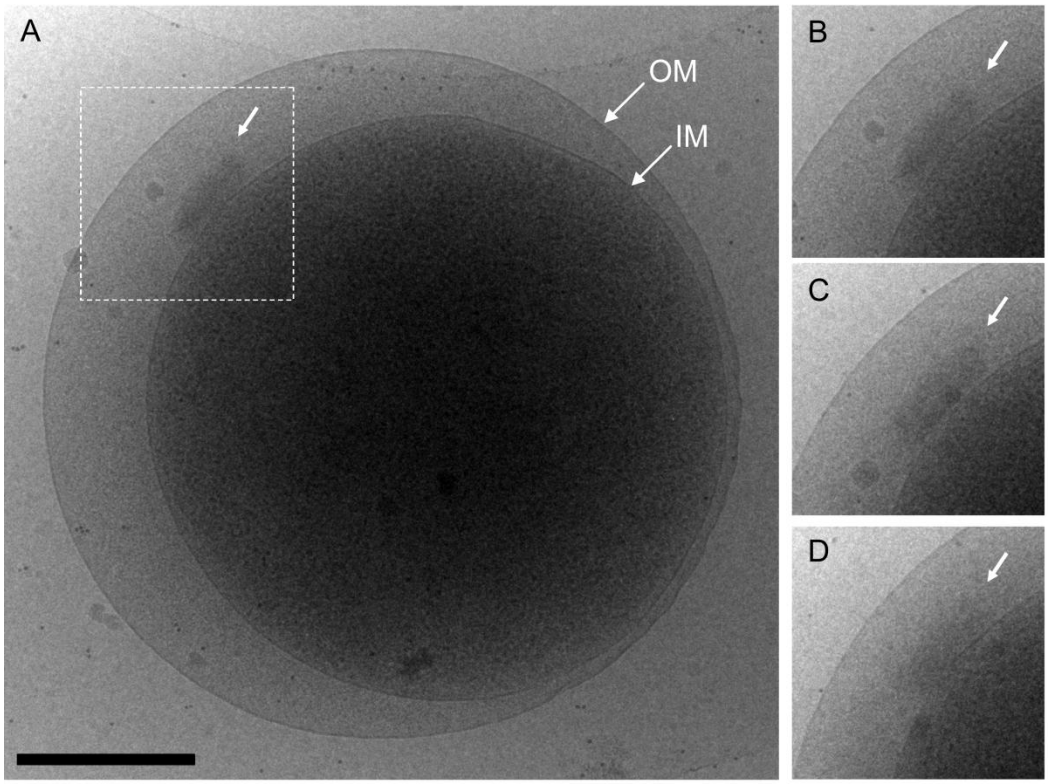

Figure 4.12. Early stages of cytoplasmic leakage from a cell co-expressing *S105* and *R*. The 0º image indicates a cloud of density escaping from the cytoplasm (A, B). Tilting of the stage by 20º (C) and 30º (D) revealed the membrane lesion from which the leakage originated. Scale bar corresponds to 500 nm.

considering that throughout the infection cycle until the moment of triggering a few seconds before lysis, the accumulation of S105 in the host membrane has no effect on the integrity of the membrane or its energy-generating capacity (38). This reflects the extreme, but opposed, selection pressures on holin function as the timer for the latent period; i.e, the holin should not compromise the capacity of the host for macromolecular synthesis until the programmed instant of triggering. However, after triggering, it should effect a rapid, efficient release of the cytoplasmic endolysin and thus minimize the delay between triggering, which terminates macromolecular synthesis, and the liberation of the progeny virions. It is even more remarkable that the timing of this all or nothing event can be adjusted drastically with a single missense change throughout the sequence of the λ holin (11, 16), and, indeed, of other unrelated holins (35, 96), of which there is staggering diversity of sequence and topology (6).

Although the molecular basis of holin triggering is still unknown, the results presented here provide a clear basis for the oldest observation about holin physiology, that bacterial respiration and macromolecular synthesis cease when S triggers (81, 97-98). A single hole of this size would be incompatible with the maintenance of either process. Importantly, although the formation of these holes and its temporal scheduling are unambiguously and solely dependent on holin function (6), the role of the S105 protein in the structure of the large lesions is not established. The 8 - 9 nm ring structures formed by purified S105 in detergent (25) are orders of magnitude too small to represent the membrane lesions described here. Although we as yet have no direct evidence addressing whether S105 participates directly in the holes, alternatives are

more difficult conceptually. One extreme alternative is that the triggering of S105 causes a small channel to form, perhaps on the scale of the detergent rings, resulting in collapse of the membrane energization, a local disruption in the organization of the lipid, and then propagation of that distortion due to loss of tensile strength of the bilayer, perhaps forcing the imposition of hexagonal phase at the edges of the hole. In support of this notion, transmembrane domains have been shown to stabilize non-bilayer lipid structures (99); however, such transitions require a relatively high protein to lipid ratio, whereas holins trigger at low protein concentrations (on the order of 10^3 per cell for S105) (6). Alternatively, the triggering of S105 could suddenly template the oligomerization and conformational change of unidentified host proteins. This notion is problematic, in view of the fact that S105 is also lethal when induced in yeast (100) and mammalian cells (101). In addition, even at these enormous sizes, the perimeters of the holes are consistent with the numbers of S105 holins present at the time of lysis. Since each holin has three TMDs, which as alpha-helices are ~1 nm in diameter, current estimates of ~1000 S105 molecules (18, 62) could correspond to ~3 μm of perimeter, if all the proteins are in the perimeter and each TMD participates. To settle this issue, the ideal approach would be to tag S105 with a fluorescent moiety and use correlative microscopy to demonstrate the presence of the holin in the lesion. However, to date, this technology has not been successfully applied to *E. coli*.

Assuming the simplest idea, that, like all other cytolytic membrane proteins, S105 actually forms the walls of the hole, it is conceivable that smaller S105 rings do form first in the membrane and then coalesce into the macroscopic lesions observed

here. Suggestive evidence for this can be seen in the perforated appearance of certain lesions (Fig. 2B). Genetic, physiological and biochemical data have led to a model in which the S105 holin forms large two-dimensional aggregates, or "death rafts", during the lysis pathway (20). The large holes described here can be viewed as supporting the notion that at the time of lethal triggering, the S105 holin exists in such large aggregates, leading to one or a small number of holes, rather than many smaller holes distributed throughout the membrane. Current work is aimed at generalizing the observation to other, unrelated holins and developing in vitro hole-formation methodology using purifed S105 holin and liposomes. Hopefully these approaches will provide further insight into the mysterious mechanism by which the holin manages the temporally-scheduled transition between the perfectly maintained membrane integrity of the pre-hole state and the massive membrane holes described here.

Materials and Methods

Plasmids and strains. The plasmid pSRRzRz1 is identical to pS105 (2) and carries the λ lysis gene cassette, *S105RRzRz1*, under the control of the native λ late promoter, pR'; *S105* is an *S* allele which produces S105, the holin, but not S107, the antiholin, by virtue of the conversion of codon 1 from ATG to CTG. The plasmid pSR is isogenic to pSRRzRz1 but carries the nonsense alleles *RzQ100amRz1W38am.* The plasmid pS is isogenic to pSR, except that it carries a silent mutation (C to T at λ nt 44594, which ablates an AatII site) and two nonsense mutations, Q26am and W73am, (previously identified as *Rsus54sus60*) (102), in *R.* p0 is isogenic to pS except that the *S105* allele is

replaced by the nonsense allele *Sam7* (39). The plasmid pQ is a single-copy vector with λ gene *Q* cloned under the control of P*ara-lac* (38); pQc is isogenic to pQ except that the kan^R marker was replaced by cam^R, for use in kan^R hosts. The hosts used were derivatives of the sequenced *E. coli* K-12 strain, MG1655 (103). A Δ*lacY* derivative was constructed by replacing the *lacY* gene in MG1655 Δ*fhuA* $lacI^q$ with Δ*lacY*::*kan*, in which a *kan* cassette flanked by Flp recombinase sites is substituted for the entire *lacY* reading frame (104). MG1655 Δ*fhuA* $lacI^q$ Δ*lacY*::*kan* was transformed with pQc, creating RY16505. RY16504 is isogenic to RY16505 except it carries pQ instead of pQc and the *kan* cassette was excised from Δ*lacY*::*kan* by Flp recombinase (104).

Growth conditions and monitoring. For all experiments except those shown in Figs. 4.10-4.12, the bacterial host used was RY16504. For Figs.4.10-412, the host was RY16505. Cultures were supplemented with 100 μg/ml ampicillin and either 40 μg/ml kanamycin (RY16504) or 10 μg/ml chloramphenicol (RY16505). In addition, pSR cultures were supplemented with 10 mM $MgCl_2$, which stabilizes the outer membrane in the absence of *RzRz1* function. For cultures grown in LB, 100 μl of overnight cultures grown in LB supplemented with the appropriate antibiotics, harboring the indicated plasmids, were used to inoculate 25 ml of LB. The identical procedure was used for succinate minimal media, except 10 μl of overnight cultures were used for inoculation. All cultures were induced with 1 mM IPTG at A_{550} = 0.2 (for lysis curves) or A_{550} = 0.4 (for cryo-EM).

Cryo-electron microscopy and cryo-tomography. For cryo-EM, cells were withdrawn at 60 min after induction, mixed with BSA-coated gold tracer (10 or 25 nm) and immediately applied to C-FLAT (CF-4/2-2C) or home-made lacey carbon-coated grids that had been glow-discharged just prior to use. Grids were then plunge-frozen in ethane using an FEI Vitrobot. Specimens were loaded into a GATAN 626 cryo-holder and observed with an FEI Tecnai G^2 F20 TEM equipped with a GATAN Tridiem imaging filter using zero-loss imaging and low-dose conditions with typical doses of 3-5 $e^-/Å^2$ per image. For cryo-electron tomography, specimens were prepared as above but cells were gently concentrated 20-fold by vacuum filtration through a 0.22 μm filter. Tilt-series were acquired automatically using the FEI Xplore3D software and the Saxton tilt scheme (105). The tilt range varied from +/- 53° to +/- 60° and the total electron dose for each series was kept below 100 $e^-/Å^2$. Tilt-series alignments, 3D reconstructions and tomogram segmentations were carried out using the IMOD (106) tomography package. Tomograms were filtered using nonlinear anisotropic diffusion (107) as implemented in the IMOD package.

Geometry of the lesions and probability of observation. A lesion in the inner membrane can be observed in the transmission electron microscope if part of the lesion is located at the edge of the cell and perpendicular to the optical axis in a given cell orientation. Assuming a circular hole with a diameter of 340 nm, the probability of its visualization can be approximately calculated from the angle formed by the edges of the hole and the center of mass of the cell (Fig. 4.4). This calculation results in a 40° angle for an average

cell width of 1000 nm. Thus the probability of observing such a hole is ~ 22%. (40°/180°, where 180° is the image projection range on one side of the cell). Since holes are observed in 48% of the cells, these data suggest that ~2 holes are created on average in a cell induced for *S105* expression; see Fig. 4.3A.

CHAPTER V

CHARACTERIZATION OF BACTERIOPHAGE HOLINS AND THEIR LESIONS

Part I: Characterization of the P2 Y Holin

The lysis cassette of bacteriophage P2 contains the following genes: *Y, K, lysA, lysB,* and *lysC* (26, 108). The P2 lysis genes were initially identified and analyzed based on sequence similarities to other phage lysis genes. In addition, conditional and nonsense mutants of each gene were isolated and analyzed in terms of their lysis behavior, and the mutant phenotypes were used to ascribe functions to the proteins they encode. It was determined that genes *Y* and *K* were necessary and essential for P2 lysis, whereas genes *lysA* and *lysB* were nonessential (26).

Y, which is the subject of this chapter, is the P2 holin gene, and it encodes a 93 amino acid protein. The Y protein is responsible for permeabilization of the *E. coli* cytoplasmic membrane by forming lesions which are believed to be similar to those of the lambda holin, during late gene expression. Although P2 Y and lambda S do not share any sequence similarity, the predicted overall topologies of the two proteins, as well as the amino acid charge distributions, are the same. Both have three regions of hydrophobic residues which are believed to comprise TMDs as well as charged termini and loop regions (Fig. 5.1). K is the P2 endolysin which degrades the cell wall layer after crossing the inner membrane barrier through the Y-lesion. The sequence of P2 K

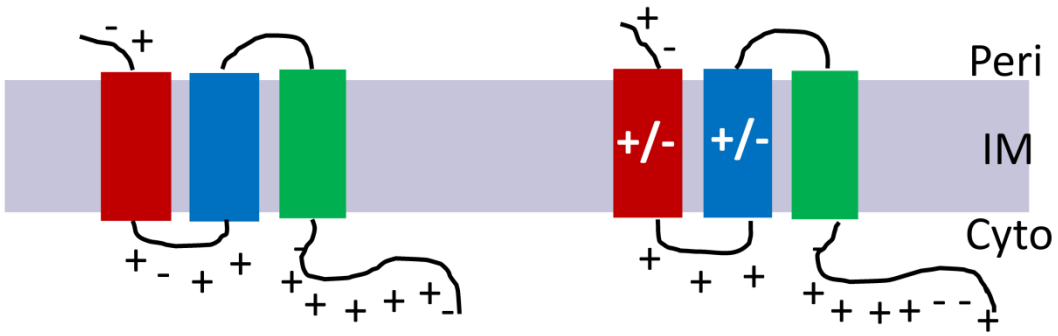

Figure 5.1. Comparison of predicted topology for P2 Y (left) and known topology for lambda S105 (right). The charged side chains of amino acids are indicated by plus signs (positively-charged residues) and minus signs (negatively-charged residues).

shares 57% identity (69% similarity) with lambda R (26). *lys A*, which encodes a 141 amino acid protein, has been shown to delay lysis when expressed with the holin, and so it is considered the P2 antiholin (26). Unlike lambda, the P2 holin and antiholin are encoded by two separate genes, instead of a single gene with a dual-start motif. Finally, *lysB* and *lysC* encode *Rz* and *Rz1*-like spanin proteins (13), respectively, and are thought to play a role in outer membrane destabilization during host cell lysis (108).

Results

Genetics of Y lysis timing. Several missense mutations were made within the 93 amino acid sequence of P2 Y to determine whether single amino acid changes would affect the timing of lysis, as is characteristic of the lambda holin and other holins (see Chapter I). Site-directed mutagenesis, or Quickchange, was used to convert the following residues: S46C, A49T, G50A, G50C, G50V, G50S, and C65G. These missense mutants were then tested for lysis behavior by monitoring their growth in liquid cultures (Fig. 5.2). The results showed that the mutant A49T, as well as all of the G50 mutants thus far tested, were non-functional, indicating that these residues within TMD2 were important in helical interactions. In contrast, mutants S46C and C65G were lytic and the timing of lysis was similar to that of wild-type Y. SDS-PAGE and Western blotting with an antibody directed at the C–terminus of Y were used to determine whether the single missense changes affected protein expression. The results showed that all of the missense mutants expressed Y protein (Fig. 5.3).

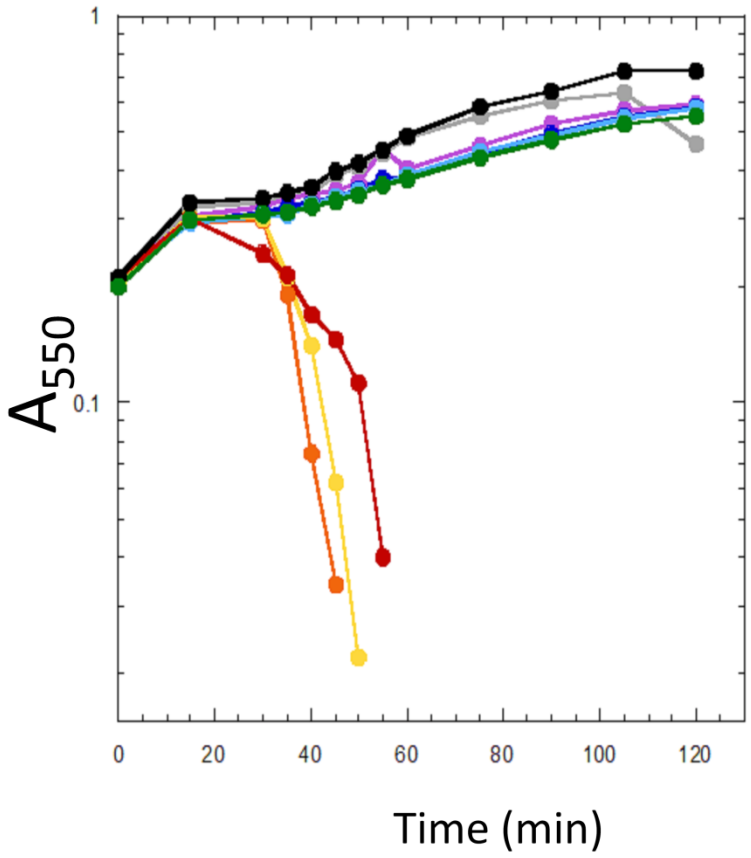

Figure 5.2. Lysis behavior of P2 Y mutants. Strain MC4100 Δ*tonA* (λCamΔ*SR*) was used for all curves, and Y mutants are expressed *in trans* from plasmid pY(mut)RRzRz1; pY_{wt}RRzRz1 (orange), pY_{S46A}RRzRz1 (yellow), pY_{C65G}RRzRz1 (red), pY_{am}RRzRz1 (green), pY_{G50C}RRzRz1 (light blue), pY_{G50V}RRzRz1 (dark blue), pY_{G50S}RRzRz1 (purple), pY_{G50A}RRzRz1 (gray), pY_{A49T}RRzRz1 (black).

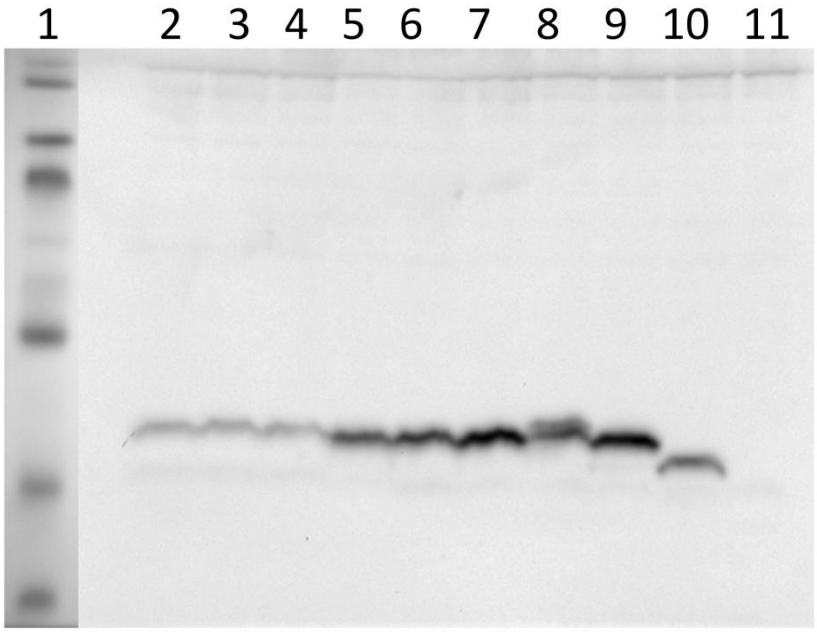

Figure 5.3. Western blot of Y mutant protein expression. Protein was expressed from a plasmid, along with the lambda lysis genes *R*, *Rz*, and *Rz1*, and transformed into the strain MC4100 Δ*tonA* (λCamΔ*SR*). Whole cell samples were collected for TCA precipitation 1-2 min prior to lysis or at 60 min for the non-lysing mutants. Lane 1: molecular weight marker; lane 2: Y_{wt}; lane 3: Y_{C65G}; lane 4: Y_{S46A}; lane 5: Y_{G50S}; lane 6: Y_{G50A}; lane 7: Y_{G50V}; lane 8: Y_{G50C}; lane 9: Y_{A49T}; lane 10: $Y_{\Delta TM1}$; lane 11: Y_{am}.

A truncation mutant of the lambda holin, $S105_{\Delta TM1}$, in which the entire first TMD has been deleted, was shown to function as an antiholin when expressed *in trans* to S105 (65). To determine whether this was a unique characteristic of the lambda holin, or an observation common with other class I holins, we sought to create the corresponding mutant for P2 Y, $Y_{\Delta TM1}$. This new mutant, which lacks the residues comprising the putative first TMD of P2Y, Ser7-Lys22, was expressed on a plasmid *in trans* to full-length Y that was expressed from a prophage (Fig. 5.4). The results show that $Y_{\Delta TM1}$ delays lysis by full-length Y when the two proteins are co-expressed in liquid culture. Again, SDS-PAGE followed by Western blotting with an antibody specific to the Y C-terminus were used to show that the truncation mutant $Y_{\Delta TM1}$ does in fact express protein (Fig. 5.3).

A third type of mutation was created via site-directed mutagenesis in which the C-terminal tail of P2 Y was truncated. Like S105, Y appears to have a highly charged C-terminal tail (Fig. 5.1). For cells expressing the lambda holin, it has been shown that the basic C-terminus of the S protein is not necessary for host cell lysis (17, 71-72). In fact, it was shown to play only a regulatory role in lysis timing, and was characterized as a cytoplasmic regulatory domain. As long as one positive charge remained at the C-terminus, lysis occurred; however, changing the number of basic residues varied lysis timing considerably by making lysis faster or slower than full-length, or wild-type, S (71). We sought to determine whether the C-terminal tail of Y is required for lysis and whether it too regulates lysis timing for phage P2. Residues R86-Q93 were deleted

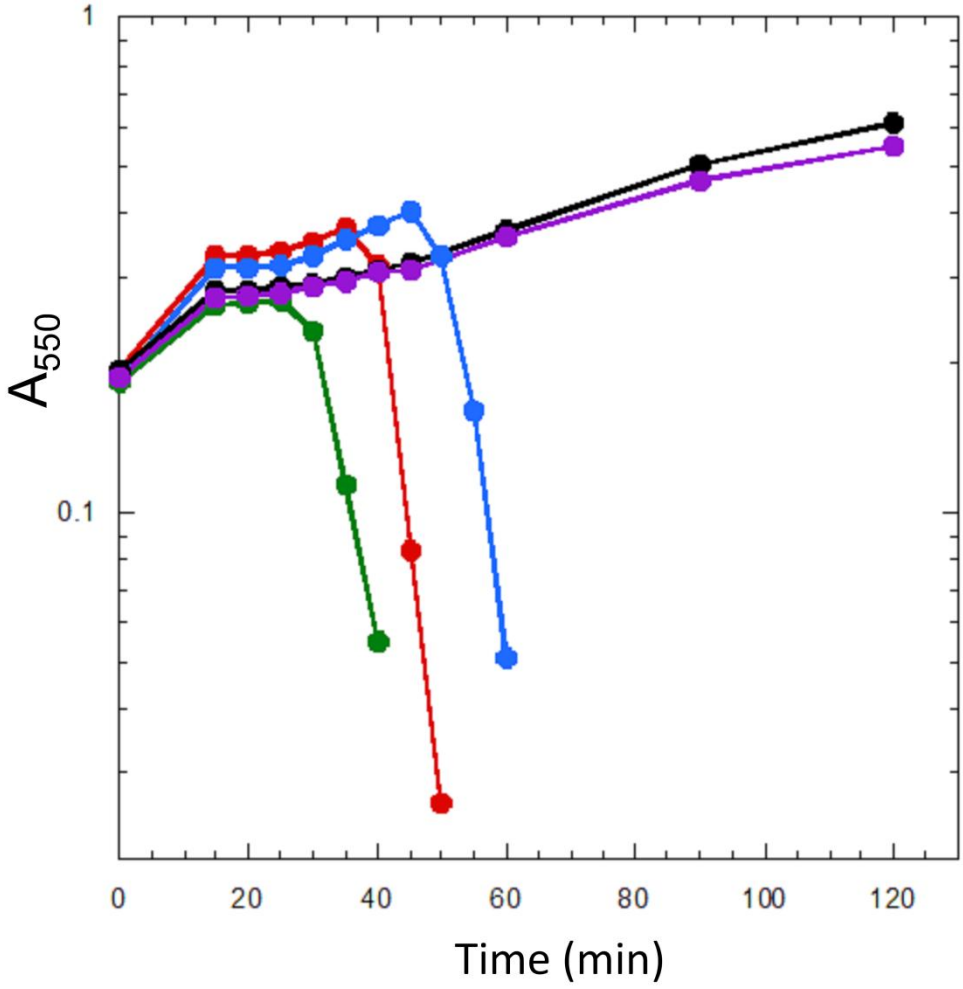

Figure 5.4. $Y_{\Delta TM1}$ delays Y-mediated lysis. $Y_{\Delta TM1}$ was expressed *in trans* to full-length Y. Two lysogenic strains were used for expression of *Y;* MC4100 *ΔtonA* (λCamΔ*SR*) was used for expression of *Y* and the lambda lysis genes *R*, *Rz*, and *Rz1* from a plasmid, and MC4100 (λ-*Y*) was used for expression of *Y* and the lambda lysis genes *R*, *Rz*, and *Rz1* from the integrated prophage. $Y_{\Delta TM1}$ was expressed from a plasmid. The lysis curves correspond to the following strains: MC4100 (λCam*ΔSR*) (black), MC4100 (λCamΔ*SR)* + $pY_{\Delta TM1}$ (purple), MC4100 (λCamΔ*SR*) + pYRRzRz1 (green), MC4100 (λ-*Y*) (red), and MC4100 (λ-*Y)* + $pY_{\Delta TM1}$ (blue).

leaving only a single basic residue at the C-terminus of the protein, and the mutant was named $Y_{\Delta C\text{-term}}$. The results suggest that residues 86-93 are in fact necessary for host cell lysis and/or proper protein expression because induction of the mutant, $Y_{\Delta C\text{-term}}$, resulted in a non-functional protein (Fig. 5.5). The results do not rule out the possibility that deletion of the C-terminus negatively affects expression of the Y protein. Since the available Y antibody recognizes the C-terminus of the protein, we were not able to determine whether Y is actually being made properly when the C-terminus is deleted. To determine the integrity of the protein in its truncated form, a tag should be fused to the protein so that an antibody that specifically recognizes the fusion tag can be used to verify protein expression with a Western blot.

Purification of the Y protein. Biochemical characterization of the P2 holin protein required that we successfully over-express and purify it. Because Y shares so many characteristics with S105, another class I holin for which a purification scheme has already been determined (2), the same strategy was applied to the P2 holin protein. The construct pET30b Y was made and transformed into competent cells for over-expression. Once induced for 45-50 min, the cells were harvested and lysed via passage through a French pressure cell. The membranes were pelleted, and the membrane proteins were extracted with detergent, then purified over a Talon resin column.

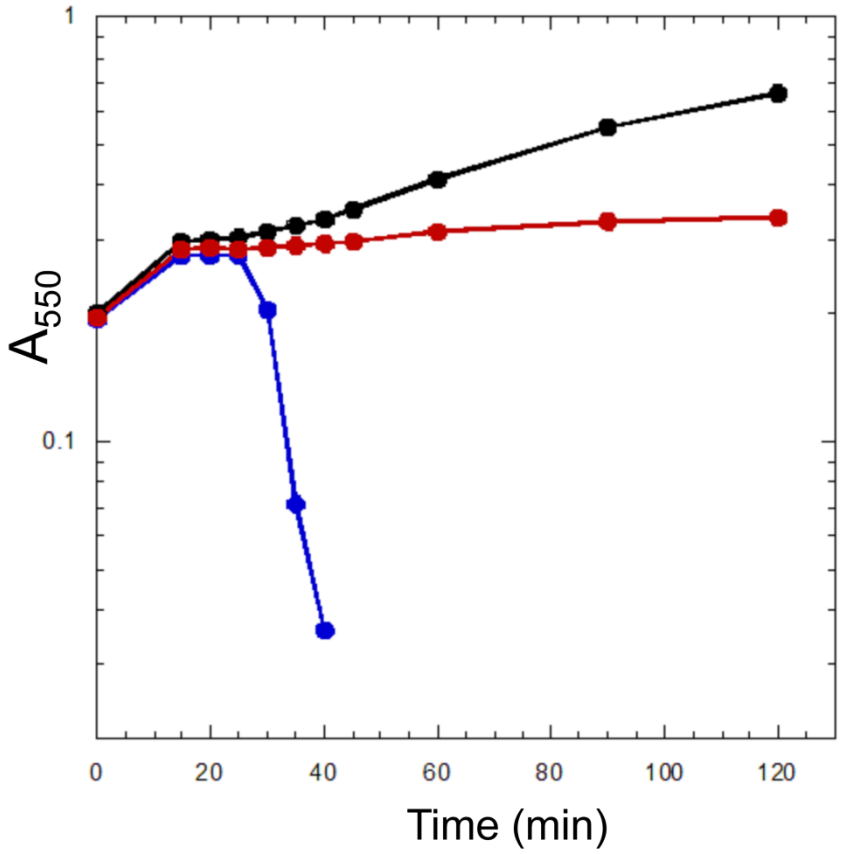

Figure 5.5. Deletion of C-terminal Y residues resulted in a non-functional mutant. The following strains were used: MC4100 Δ*tonA* (λCamΔ*SR*) (black), MC4100 Δ*tonA* (λCamΔ*SR*) + pYRRzRz1 (blue), MC4100 Δ*tonA* (λCamΔ*SR)* + $pY_{\Delta C\text{-term}}$ RRzRz1 (red).

Although the overall approach described above was the same as was used for purification of S105, some optimization was required. Specifically, the choice of detergent and conditions for membrane extraction required some trouble-shooting in order to obtain the most protein possible. The following detergents were used in the extraction and purification of P2 Y: DDM, EBB, octylglucoside, and LDAO. Also, the length of time and temperature at which membranes were extracted was optimized. It was determined that extraction with DDM for 2 hours at 37 °C was the appropriate condition for purification of Y protein (Fig. 5.6).

Directly following Talon purification, the protein was further analyzed via gel permeation chromatography, and the major protein peak was collected for negative-stain electron microscopy (EM). As shown in Fig. 5.7, the purified protein formed regular structures which were ~18 nm wide. However, the majority of the protein in the sample did not form the spiral-shaped structures. In an effort to obtain a homogeneous sample, Y was extracted from the membrane in the presence of 2,2' dithiodipyridine, or DTDP, to protect the cysteine sulfhydryl at position 65 from modification (64), and purified as described above. As a result of the thiol protection, the majority of the protein formed regular structures in the electron microscope viewing field (Fig. 5.8). To determine whether these structures were relevant and not just artifacts of the purification, we also purified a His_6-tagged product of Y_{A49T}, a non-functional allele of *Y*. The negative-stain EM images of purified Y_{A49T} contained structures, but the structures were irregular and much longer than those in the wild-type images (Fig. 5.9). Also, the structures appeared to be interconnected, as if they were aggregated together.

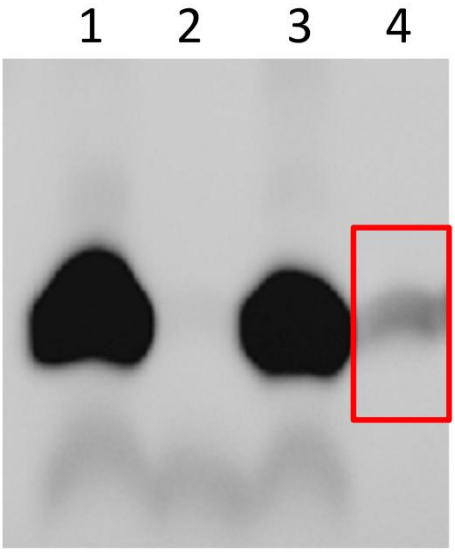

Figure 5.6. Purification results for P2 Y. Purified Y protein remained in the membrane pellet from ultracentrifugation spin at 100,000 x g for 1.5 h at 4 °C, directly following detergent extraction step. Western blot of samples from Y purification: total membranes (lane 1), extracted protein (lane 2), extraction spin pellet (lane 3), and eluted protein from Talon purification (lane 4). The antibody used was commercial α-His_6 from Amersham.

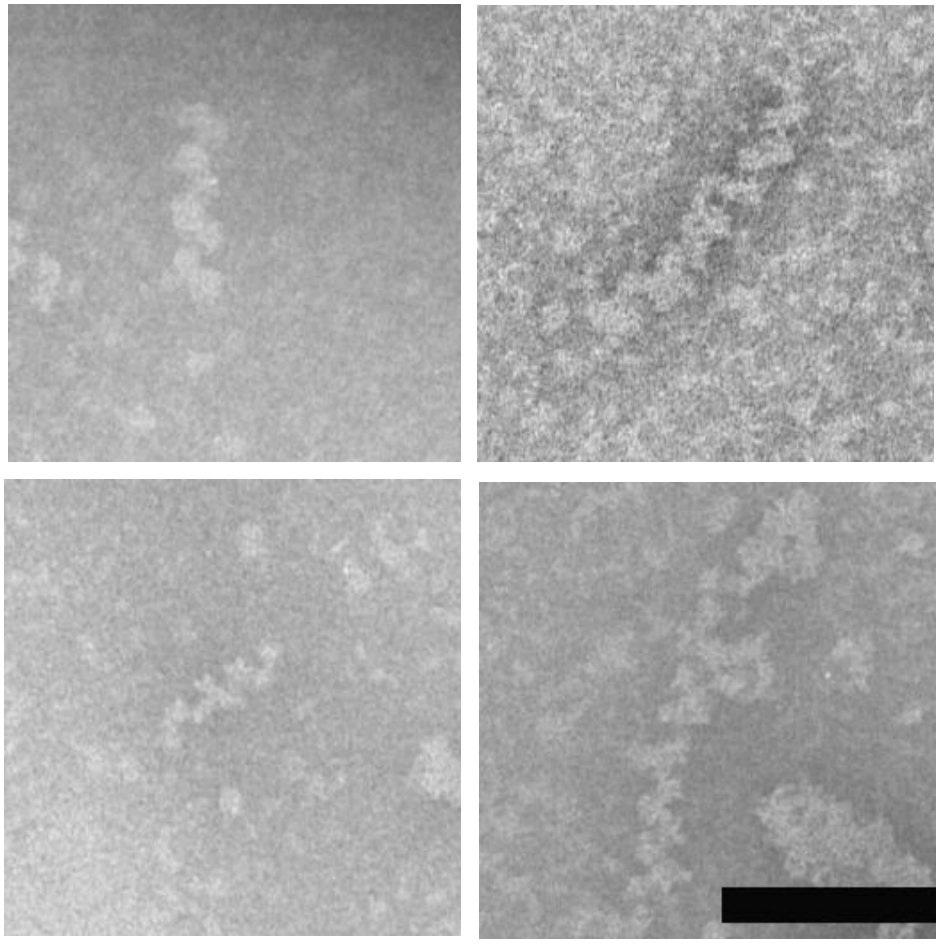

Figure 5.7. Negative-stain EM images of gel filtration fraction containing purified Y protein. The scale bar corresponds to 100 nm.

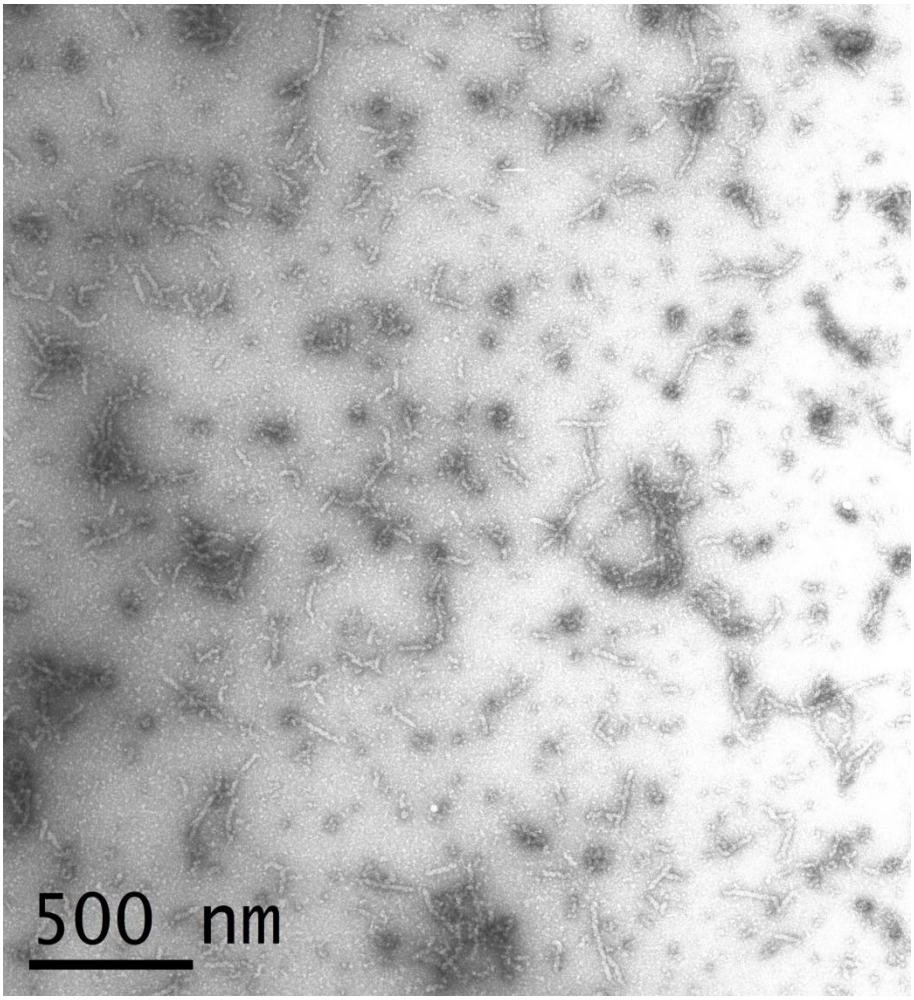

Figure 5.8. Negative-stain EM image of purified Y protein extracted from the membrane in the presence of thiol-protecting agent, DTDP. The sample appeared to be homogeneous because the majority of the protein participated in the formation of regular structures.

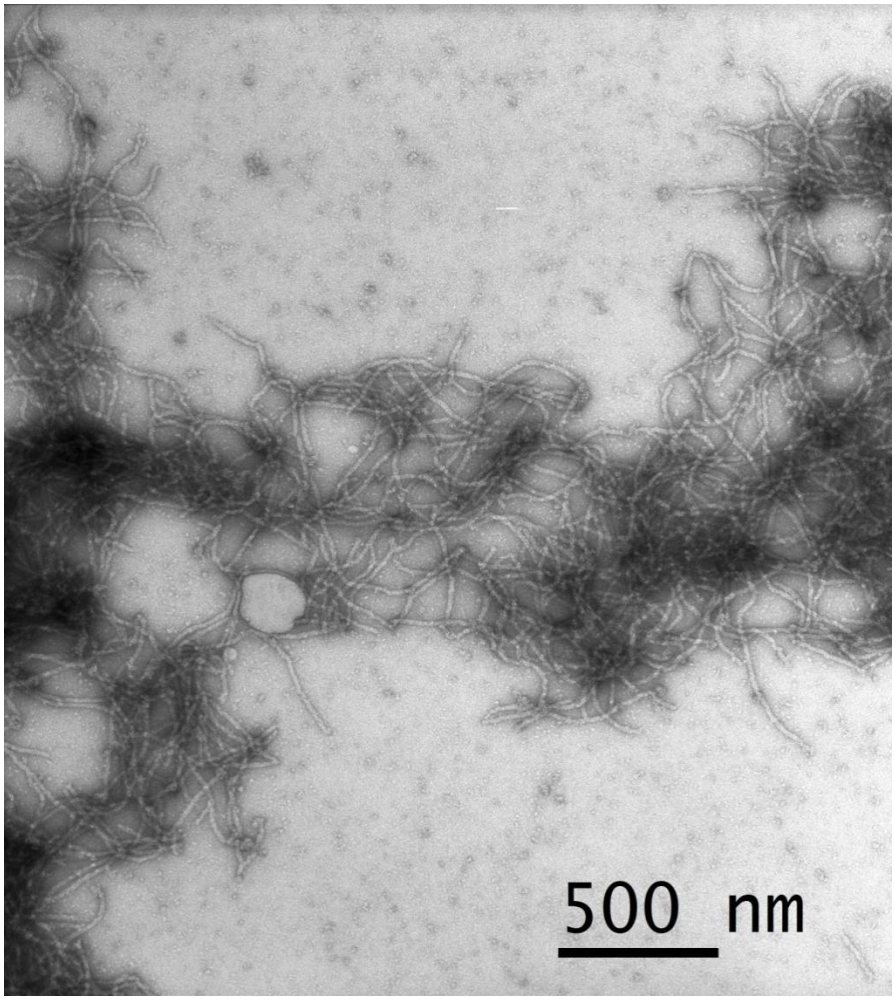

Figure 5.9. Negative-stain EM image of purified Y non-lytic mutant, Y_{A49T}. The mutant forms irregular, longer, and branched structures, as compared to the wt protein.

Discussion

P2 Y shares many characteristics with the lambda holin. S105 has been studied extensively by genetic means, and as a result, there are many S105 mutants which vary in terms of lysis timing, dominance/recessiveness, and oligomerization patterns by cross-linking (7, 14-16). In addition, S105 has been characterized biochemically. Detergent-purified lambda holin protein has been shown to make regular structures, or rings, which can stack to form higher order structures (25).

In this work, we sought to characterize Y genetically and biochemically, pointing out along the way its similarities to S105. First, Y was shown to exhibit sharp lysis at the time of triggering for hole formation. In addition, Y was subjected to site-directed mutagenesis, during which single missense mutants were made, as well as an N-terminal truncation mutant and a C-terminal truncation mutant. The N-terminal truncation mutant, in which the putative first TMD was deleted, caused a delay in lysis by full-length P2 Y. This result suggests that $Y_{\Delta TM1}$ exhibits antiholin character, much like the N-terminal truncation mutant of S105, $S105_{\Delta TM1}$(65). In contrast, the C-terminal truncation mutant of Y did not behave like its counterpart for S105. $Y_{\Delta C\text{-}term}$, which has a single positive charge at its C-terminus, did not cause lysis; whereas, the S105 mutant which had a single positive charge at its C-terminus, did cause lysis (71). For S105, these experiments, together with other results, showed that the C-terminal domain of the lambda holin has a regulatory function and is not required for host cell lysis (17, 71-72).

Y was purified according to the protocol for S105 purification, with a few minor changes. The purified holin of phage P2 forms higher-order helical structures, as visualized by negative-stain EM. These structures may be analogous to the stacks of rings formed by detergent-purified S105 (25), however, we were not able to isolate ring-like subunits as were seen with S105.

Materials and Methods

Plasmids and strains. The plasmids used in this work were pYRRzRz1 and associated mutants which were made by site-directed mutagenesis, or Quickchange. All of these plasmids are derivatives of pS105 (2), and have ampicillin resistance. The strain used for expression was MC4100 Δ*tonA* (λCamΔ*SR*) (2).

Growth conditions and TCA precipitation. For lysis curves and protein expression experiments, overnight cultures were used to inoculate ~25 ml cultures of LB supplemented with the appropriate antibiotic. The cells were grown at 30 °C to OD ~0.2 (for lysis curves) and OD ~0.4 (for protein expression experiments) for thermal induction at 42 °C for 15 min. Then, the cultures were shifted to 37 °C for the remaining time. For protein expression experiments, 1 ml samples were removed from the growing cultures and added to 100% TCA on ice. The samples were incubated for 30 min, then centrifuged at maximum speed in a tabletop microfuge at 4 °C. The supernatant was removed and the pellet was resuspended in 1 ml cold acetone, vortexed, and spun at maximum speed in the tabletop microfuge at 4 °C. The acetone wash was repeated and

the supernatant was removed carefully after the final spin. The pellet was air-dried overnight and resuspended in 2X reducing sample loading buffer for SDS-PAGE. Western blotting was done with an antibody directed against the C-terminus of Y (Genscript).

Protein purification. P2 Y was purified according to the protocol used for over-expression and purification of S105 (1, 25, 64), with the following exceptions. Tris was used for all buffers, and DDM detergent was used in the membrane extraction and subsequent purification buffers at final concentrations of 1% (w/v) and 0.1% (w/v), respectively. Membrane extraction was carried out at 37 °C for 2 hours with gentle shaking. Protein detection was carried out with SDS-PAGE followed by Western blotting using the commercially available His_6 antibody (Amersham).

Electron microscopy. EM grids were glow-discharged prior to use. Five microliters of 0.05 - 0.1 mg/ml purified protein was applied to the grid. After ~1 min, the excess liquid was removed carefully with filter paper. The grid was placed face-down on a drop of 2% (w/v) uranyl acetate, then carefully blotted dry. Specimens were observed in a JEOL 1200 EX TEM (MIC, Texas A&M University). Micrographs were recorded at calibrated magnifications.

Part II: Holin Lesions

The determinative step in the pathway to bacteriophage lysis is the formation of a holin-mediated lesion within the cytoplasmic membrane of the host cell. Recently, cryo-EM was used to visualize the lambda S105 hole in the inner membrane of *E.coli*, thus providing the first direct evidence of the holin lesion (3). The holes were characterized in terms of their size and localization throughout the membrane, and cryo-electron tomography was used to create three-dimensional reconstructions, or tomograms, of the S105 hole. The lesions were found to be much larger than anticipated with an average diameter of ~340 nm, and they were localized throughout the periphery of the cell (3). Although many aspects of the lambda holin were realized as a result of this data, many questions about holin lesions remained. First, we sought to determine whether the S105 holes were stable at their original size. Second, we raised the question as to whether the large lesions are specific to the class I holin S105. Third, we endeavored to correlate hole size with lysis timing.

There are three classes of holin proteins: class I, class II, and class III. The classes differ according to size, number of TMDs, and topology. Since lambda S105 is a class I holin and the large lesions were visualized in cells expressing lambda S105, we wondered if the massive membrane holes were common among other class I holins. To test this, we used cryo-EM to visualize cells expressing another class I holin, P2 Y. In addition, we also imaged cells expressing class II holin S^{68} from phage 21 and class III holin T from the well-studied phage T4.

The large collection of S105 mutants available provided a means to address the final question concerning these holin lesions, that is the relationship between hole size and lysis timing. Over the years, S105 alleles have arisen from a variety of methods, including genetic selection following chemical mutagenesis, cysteine-scanning mutagenesis, and site-directed mutagenesis (14-16). These mutants have been used to determine the topology of S105, verify the positions of the three TMDs, and determine oligomerization patterns for testing the hole formation pathway. Here we have used site-directed mutagenesis to convert two residues within the second TMD of S105 to all possible amino acids. Cys51 contains the only cysteine residue within the protein. The residue was mutated for cysteine scanning mutagenesis to determine the topology of S105, and was shown to be non-essential for S105 function (16). Its neighboring residue, Ala52, was mutated to glycine and valine many years ago. Although these two substituted residues are somewhat conservative changes in terms of side chain size and chemical composition, the mutants have opposing lysis profiles. $S105_{A52G}$ lyses very early, while $S105_{A52V}$ is completely non-functional in lysis. Cryo-EM was used to image cells expressing an early lysing S105 allele as well as a nonlytic mutant, and the data were assembled to form the current model for S105 hole formation.

Results

Determining the stability of S105 hole size. The lambda holin S105 was shown to form extremely large lesions, or holes, in the inner membranes of its host cell (see Chapter IV) (3). The holes were an average diameter of ~340 nm, which is much larger than any

known membrane channel in biology (3, 21-22). This raised the question of whether the holes are initially formed at this massive size. A timecourse experiment was used to determine whether the lambda holin lesions grow in size following triggering for hole formation. Samples were taken from a growing culture induced for expression of S105 at various times following the time of triggering. The hypothesis was that if the holes were not stable at the original size and they became larger over time, then the early timepoint samples would exhibit small hole formation and the later timepoint samples would show larger lesion formation. The results, however, clearly showed that the major size class of holes was the same, regardless of the time the samples were removed from the culture post triggering (Fig. 5.10). Over 50 cells were imaged for each timepoint, and in all cases, the major hole size class was 200 - 400 nm. Therefore, the holes did not grow and appear to be stable at their original size.

Visualizing cells expressing the class I holin, lambda S105. All of the cryo-EM experiments described thus far were done with an *E. coli* strain transformed with two separate plasmids: pS105 R_{am} Rz_{am} $Rz1_{am}$, which produces functional holin but non-functional endolysin and spanin proteins, and pQ (3). In order to visualize cells

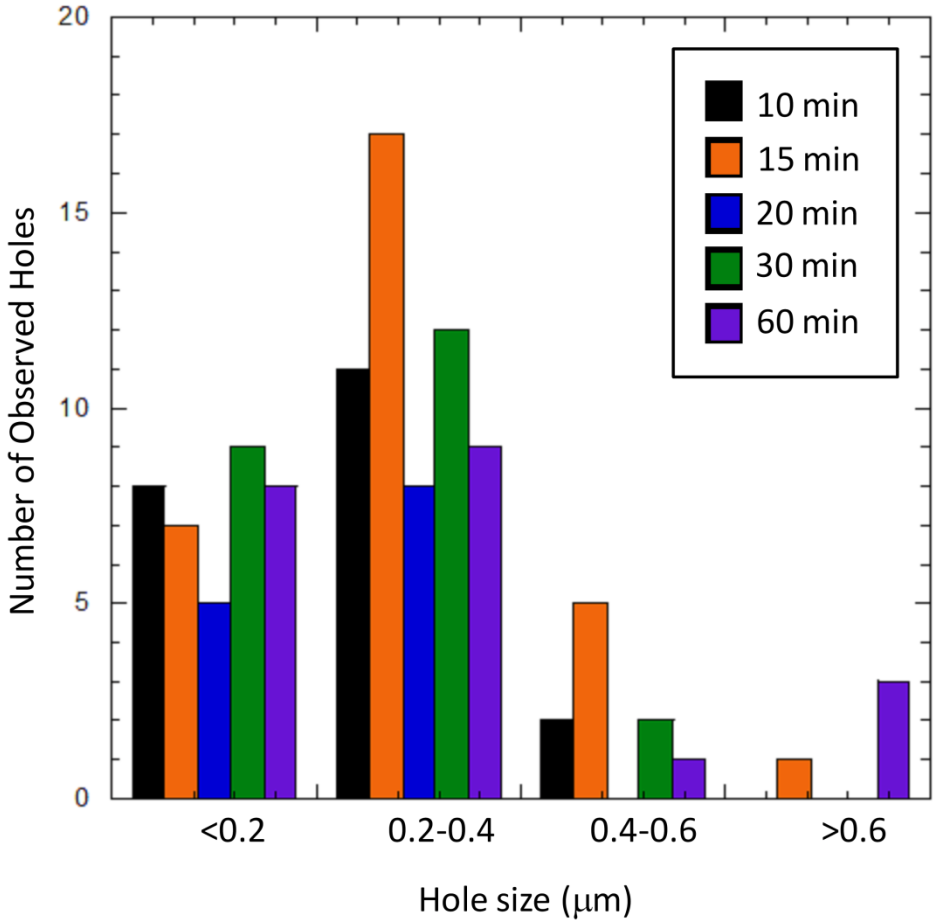

Figure 5.10. Cryo-EM timecourse to determine if S105 lesions increase in size over time. Cells were frozen on grids at 10 min (black), 15 min (orange), 20 min (blue), 30 min (green), and 60 min (purple) post triggering and imaged.

expressing other phage holins, we used a different strain background, an *E.coli* strain containing the lambda lysogen, λCamΔ*SR*, which was transformed with plasmids containing the functional holin gene and R_{am}, Rz_{am}, and $Rz1_{am}$ downstream of the lambda late promoter P_R'. The major difference between the two strains involves the source of *Q*, which is the antiterminator gene. *Q* allows for expression of the lambda late genes by repressing the terminator t_R' located just downstream of the late promoter P_R'. For the strains containing pQ, the antiterminator is supplied by a plasmid, and it is induced by the addition of IPTG. In contrast, the lysogenic strain containing λCamΔ*SR* supplies *Q* from the prophage and the gene is expressed upon thermal induction.

Lambda holin lesions were visualized again, this time in the λCamΔ*SR* lysogenic strain, expressing *S105* in the absence of other lysis genes. Fifty-two cells were imaged with cryo-EM, and 31, or ~60%, had visible lesions. The holes ranged in size from 86 - 989 nm, with the major size class being 200 - 400 nm (Fig. 5.11A). The majority of cells with holes had single visible lesions, but there were instances of multiple visible holes per cell (Fig. 5.11B). As in the S105 holes visualized in the other strain background, the visiblility of the cell membrane was limited by the position and orientation of the specimen on the EM grid, and geometry together with the viewing angle can be used to calculate the actual number of holes per cell (see Chapter IV) (3). The holes were localized throughout the membrane, and there was no correlation between hole size and hole localization (Fig. 5.11C). In conclusion, the data from both expression systems used for visualizing S105 lesions agreed that holes are present within the inner membrane following lambda holin expression and that these holes are

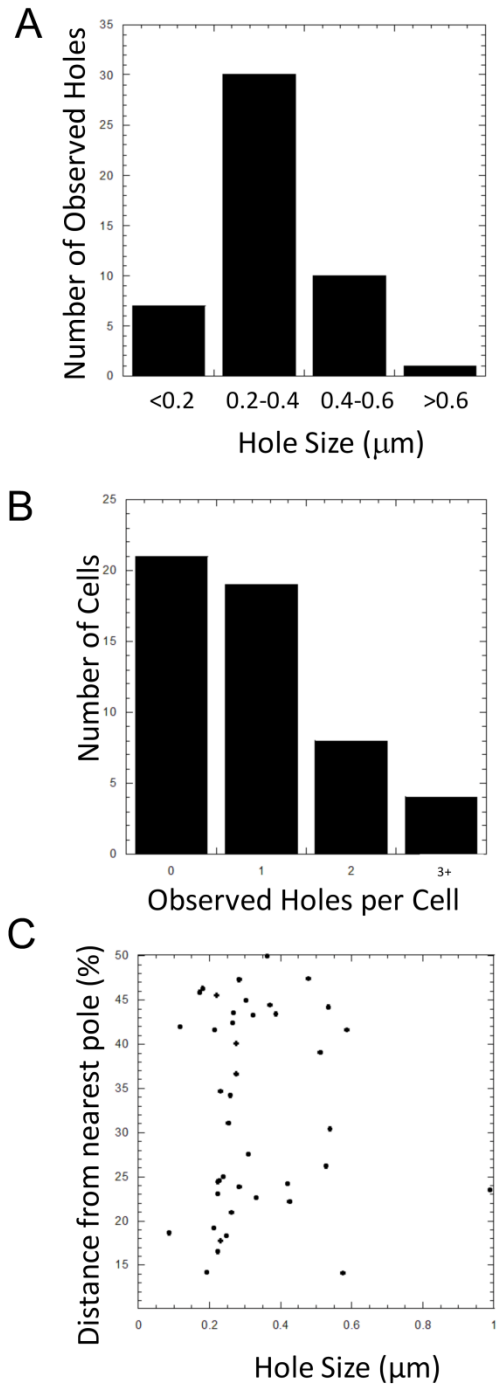

Figure 5.11. Statistics for cryo-EM visualized holin lesions in MC4100 Δ*tonA* (λCamΔ*SR*) pS105 cells. (A) Hole size, (B) Number of holes per cell, (C) Hole localization versus hole size.

extremely massive compared to other known membrane channels.

S105 Cys51 and Ala52 missense mutants. Site-directed mutagenesis was used to create single missense mutations at positions 51 and 52 within TMD2 of S105. Specifically, Cys51 and Ala52 were mutated to all possible amino acids, and the alleles were analyzed in terms of lysis behavior, protein accumulation, and hole size. The main question for the lysis timing analysis of these missense mutants was to determine whether side chain size correlated with lysis timing. Some of the original S105 mutants suggested such a correlation. For example, A52V has a larger side chain compared to wt (A52), which has a larger side chain than A52G. According to the lysis profiles of these proteins, increasing side chain size resulted in prolonged or no lysis, since A52V is non-lytic and wt lyses later than A52G. In the case of the C51 mutants, wt (C51) has a larger side chain than C51S, and again the large side chain of wt appears to inhibit or delay lysis timing compared to C51S, since it lyses much later. Figure 5.12 shows the lysis profiles for all of the missense mutants created, and there does not appear to be a correlation between the substituted amino acid and the resulting lysis time as suggested by the lysis profiles of some original S105 mutants. Preliminary versions of these lysis curves also appear in Dr. Rebecca White's dissertation, but have been repeated and shown here for the purposes of relating protein accumulation and hole size to lysis timing (109).

With regard to correlating lysis timing with protein accumulation for the C51 and A52 mutants, we determined whether early or late lysis was caused by different rates of synthesis for these proteins. In prior work, systems with increased amounts of S

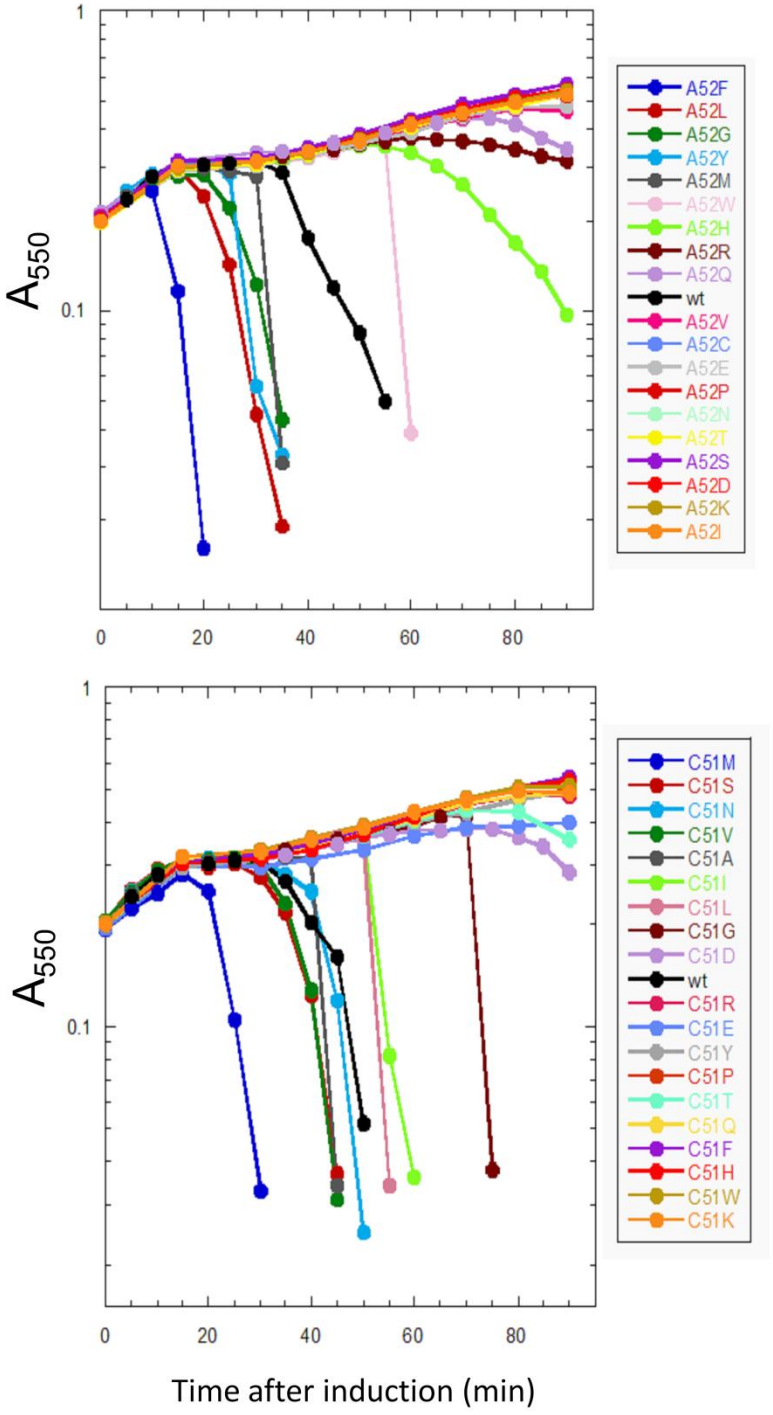

Figure 5.12. Lysis curves of A52 (top) and C51 (bottom) missense mutants. The substituted amino acids are indicated beside their respective curves in corresponding colors.

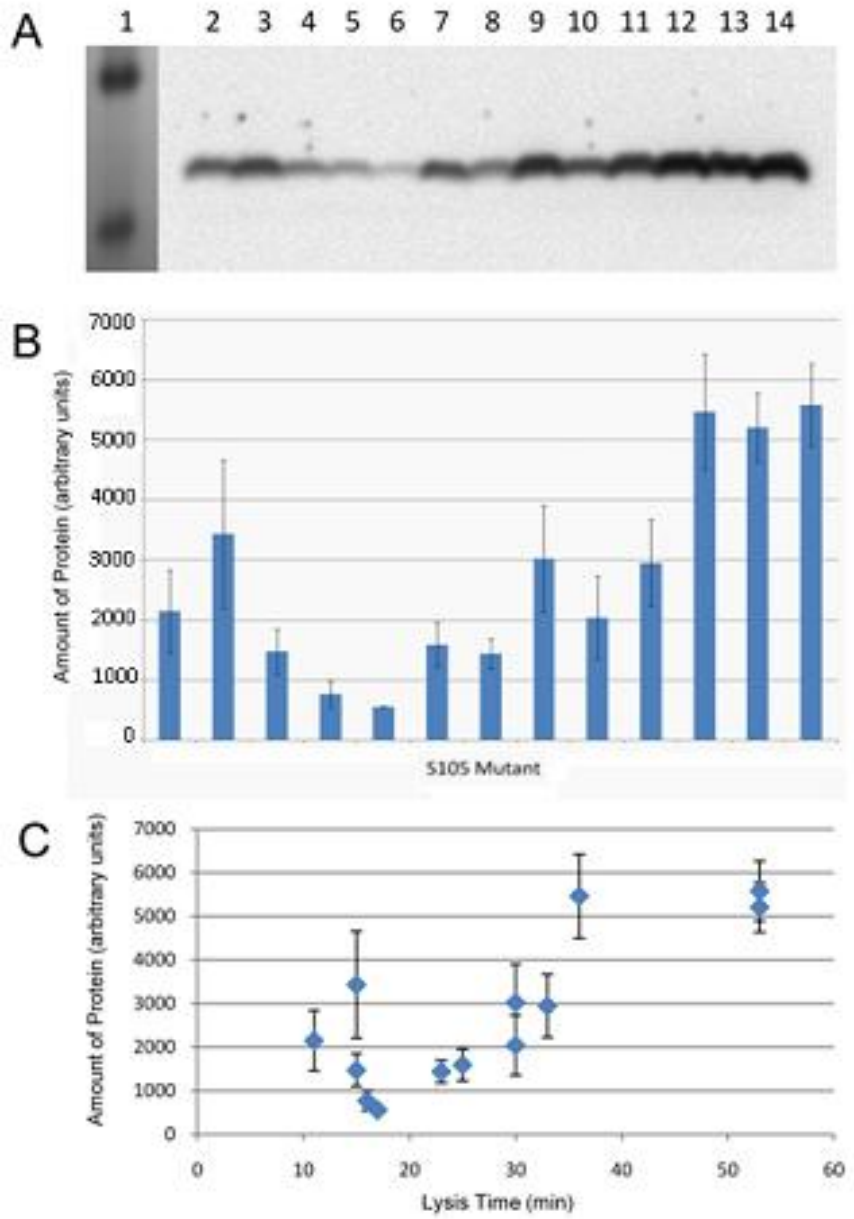

Figure 5.13. Western blot results of C51 and A52 lysing mutants. Representative Western blot of protein accumulation for lysing S105 mutants (in order of increasing lysis time, except lanes 7 and 8, which were inadvertently switched). Lane 1: molecular weight marker; lane 2: A52F, lane 3: A52L, lane 4: A52Y, lane 5: C51M, lane 6: A52G, lane 7: C51S, lane 8: A52M, lane 9: WT, lane 10: C51N, lane 11: C51V, lane 12: C51A, lane 13: C51I, lane 14: C51L. (B) Protein accumulation for S105 mutants (mutants are shown in the same order as (A)), as determined by densitometry from three Western blots. (C) Scatter plot of protein versus lysis time for S105 mutants, as determined by densitometry from three Western blots.

protein caused earlier lysis, such as with the pQ system, which has been shown to accumulate more protein and lyse earlier, compared to systems with phage induction (109). So, one reason for early lysis may be increased protein translation. Samples were taken just minutes prior to lysis for each mutant and whole cell samples were TCA precipitated and analyzed by SDS-PAGE and Western blotting (Fig. 5.13). The lytic mutants have varying amounts of protein accumulation prior to lysis, with early lysing mutants accumulating less protein and later lysing mutants accumulating more protein (Fig. 5.13). The early lysing mutants seem to require a lower concentration of holin protein in the membrane prior to lysis. This is opposed to a previous model which suggested that early lysing mutants triggered earlier because they reached a critical concentration of S105 more quickly than their later lysing counterparts. In general, the triggering concentration of S105 is allele-specific.

Cells which expressed S105 missense mutants, $S105_{A52I}$ and $S105_{A52F}$ were imaged. $S105_{A52I}$ is a non-lytic allele (Fig. 5.12A), and there were no visible lesions in ~50 cells that we imaged with cryo-EM. $S105_{A52F}$, on the other hand, is an early lysing mutant, which triggers for hole formation at ~11 min following induction (Fig. 5.12A), and was shown to form inner membrane holes with cryo-EM. The sizes of the holes in cells expressing the early-lysing mutant were smaller than the diameters of holes in $S105_{wt}$ cells, with the major size class being only 100 – 200 nm (Fig. 5.14).

Prior work suggested that cells prematurely triggered for hole formation with the addition of an energy poison to artificially depolarize the membrane would have small

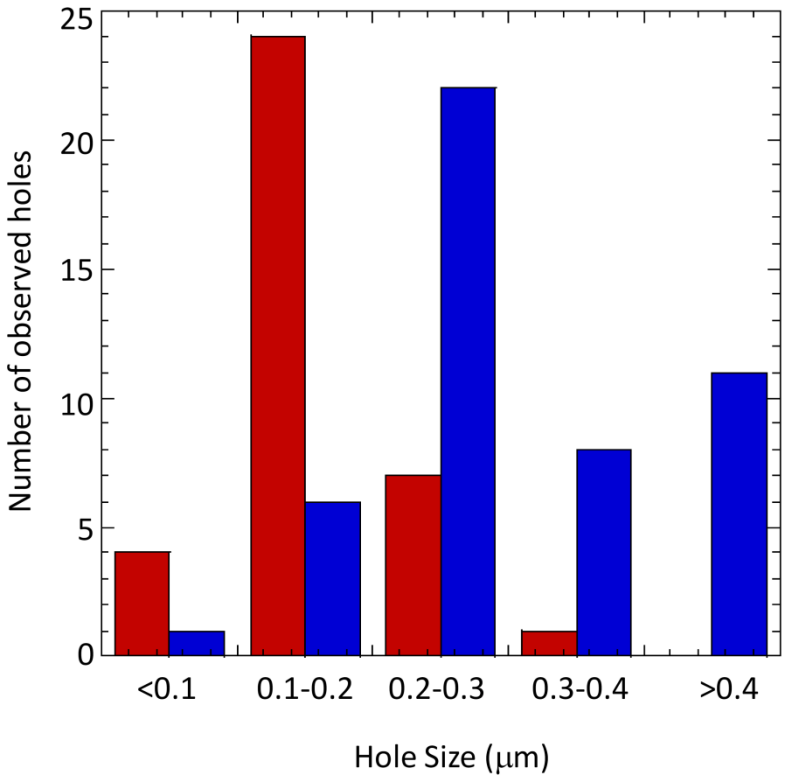

Figure 5.14. Hole size distribution for cells expressing early lysing mutant $S105_{A52F}$ (red). The sizes are compared to cells expressing $S105_{wt}$ (blue). The Student's T-test was applied to this data and the following values were calculated: t-value = 5.22 and p-value = <0.0001, indicating a significant difference between these two data sets.

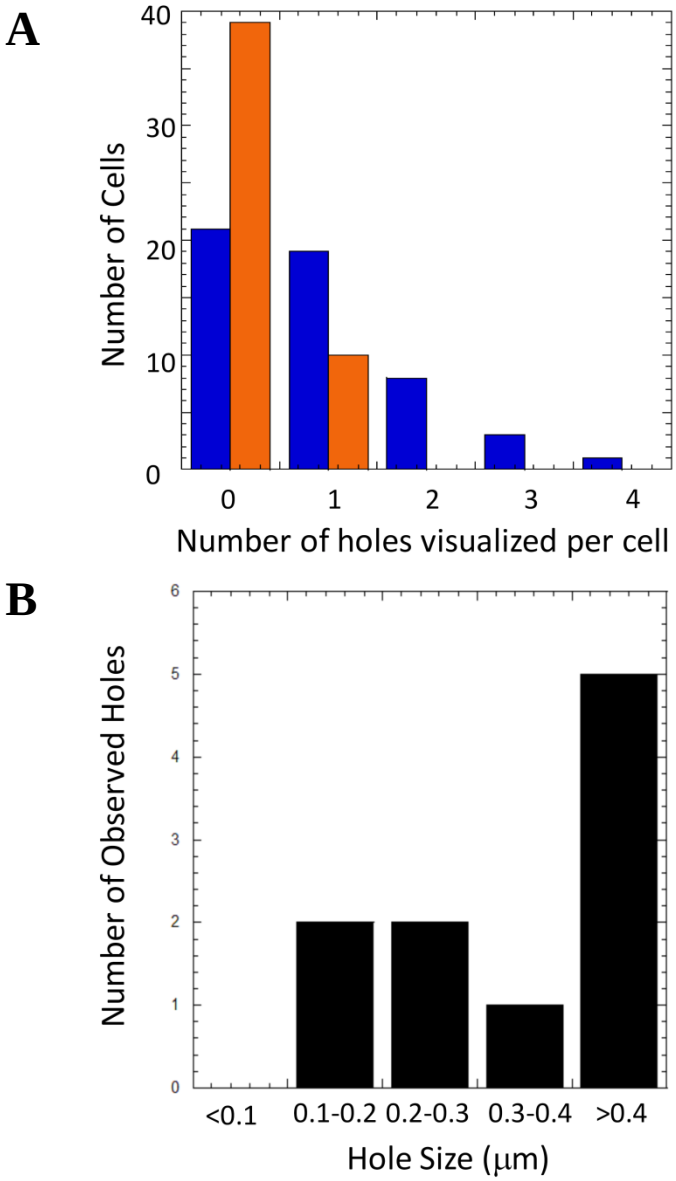

Figure 5.15. Cryo-EM of cells with prematurely triggered holins. (A) Number of holes per cell for wild-type S105 untreated (blue) and wild-type S105 + 10 mM KCN (orange). (B) Average hole size of prematurely triggered holins.

sized holes, as well. Cells expressing S105 were prematurely triggered at 15 minutes post induction with 10 mM potassium cyanide (KCN) and imaged with cryo-EM. Only 20% of the cells had visible inner membrane lesions, and those visible holes were variable in size (Figs. 5.15). The majority of the cells did not have visible lesions, which suggests that the holes may be so small that we were unable to visualize them with our current system. As a control, cells expressing *Sam7* were prematurely triggered with 10 mM KCN at 30 minutes post induction, and 98% of the cells, or 49 out of 50, did not have visible lesions.

Visualizing cells expressing the class I holin P2 Y. Cryo-EM was used to visualize cells expressing another class I holin, P2 Y, in an effort to determine whether large lesions are formed. MC4100 Δ*tonA* (λCamΔ*SR*) competent cells transformed with the plasmid $pYR_{am}Rz_{am}Rz1_{am}$ were induced for expression of Y. The cells were collected, concentrated, and applied to prepared EM grids, then plunge-frozen into liquid ethane to fix the cells in a thin layer of vitreous ice. The cells were visualized by cryo-EM, and 65 cells were imaged. Fig. 5.16 shows a cell induced for expression of Y. Of the cells that were imaged, 30, or 46%, had visible inner membrane lesions. Hole size ranged from ~114 nm to ~1.3 μm, and the major size class was 200 – 400 nm (Fig. 5.17A). In addition, the majority of cells with holes had a single visible hole, but there were instances where cells had multiple visible holes (Fig. 5.17B), and the geometry can be

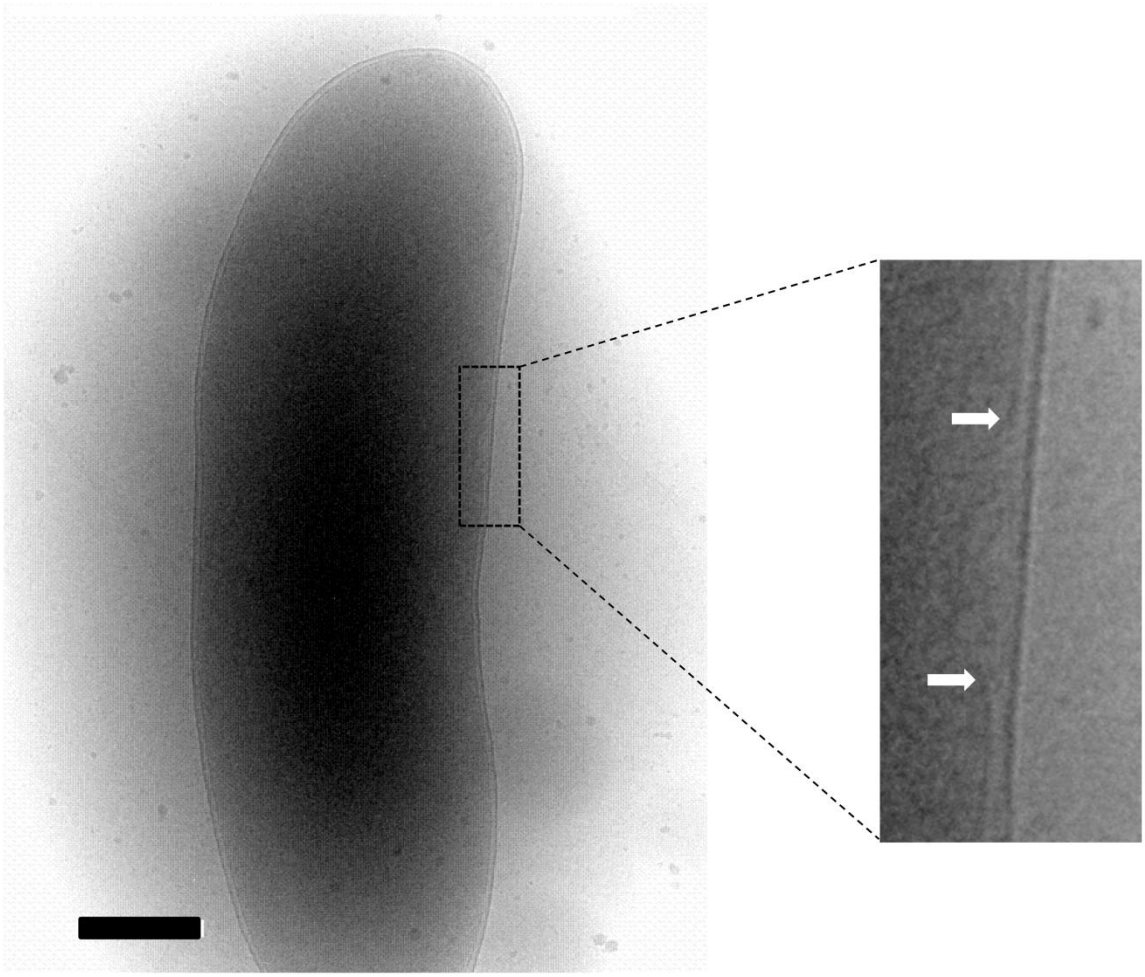

Figure 5.16. *E.coli* cell expressing P2 *Y*. The enlarged region shows a disruption in the inner membrane which is the holin-mediated lesion. White arrows indicate the discontinuity in the cytoplasmic membrane. The scale bar corresponds to 0.5 μm.

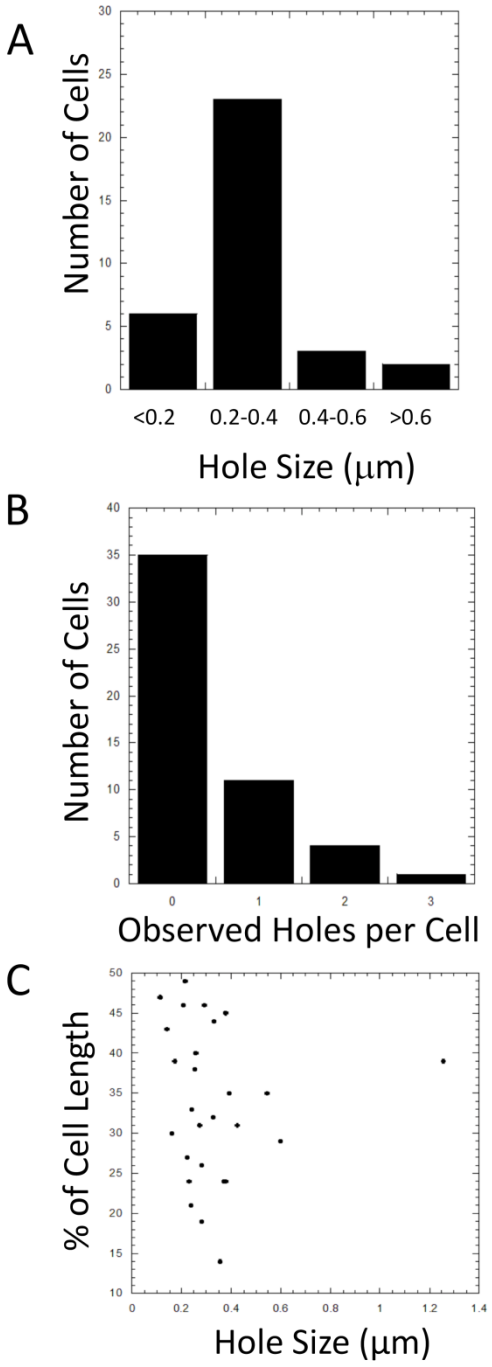

Figure 5.17. Statistics for cells expressing *Y*, including hole size (A), number of holes per cell (B), and hole localization with respect to hole size (C).

used to calculate the predicted actual number of holes per cell. As in the case of λ S, Y holes were not localized to a specific region of the membrane, nor was there a correlation between hole size and localization within the membrane (Fig. 5.17C).

Visualizing cells expressing class II and class III holins. To address the question of whether the large lesions are characteristic of only class I holins, we imaged cells expressing the class II holin, $S^{21}68$, and the class III holin, T4 T. $S^{21}68$ is a pinholin, so named because it forms very small holes in the inner membrane of its host cell (30). A plasmid, containing $S^{21}68$ just upstream of nonsense mutant lambda lysis genes R_{am}, Rz_{am}, and $Rz1_{am}$, was transformed into lysogenic cells containing λCamΔ*SR*, and $S^{21}68$ was thermally induced for expression. As expected, there were no visible holes in the inner membrane of these cells because the pinholes, which are estimated to be 1-2 nm in diameter (110), would be too small to be seen with our current system. Efforts were made to visualize cells expressing another class II holin, 17.5 from phage T7; however, expression problems made this project unsuccessful. When *17.5* upstream of R_{am}, Rz_{am}, and $Rz1_{am}$ was expressed in a lysogenic strain, the holin did not trigger hole formation.

Cells expressing the class III holin T4 T were visualized with cryo-EM in collaboration with Samir Moussa. A plasmid containing *T* upstream of the non-functional lambda lysis genes, R_{am}, Rz_{am}, and $Rz1_{am}$ was transformed into the lysogenic strain containing λCamΔ*SR*, and the T4 holin was thermally induced for expression. The results showed that cells expressing *T* did in fact have large inner membrane lesions

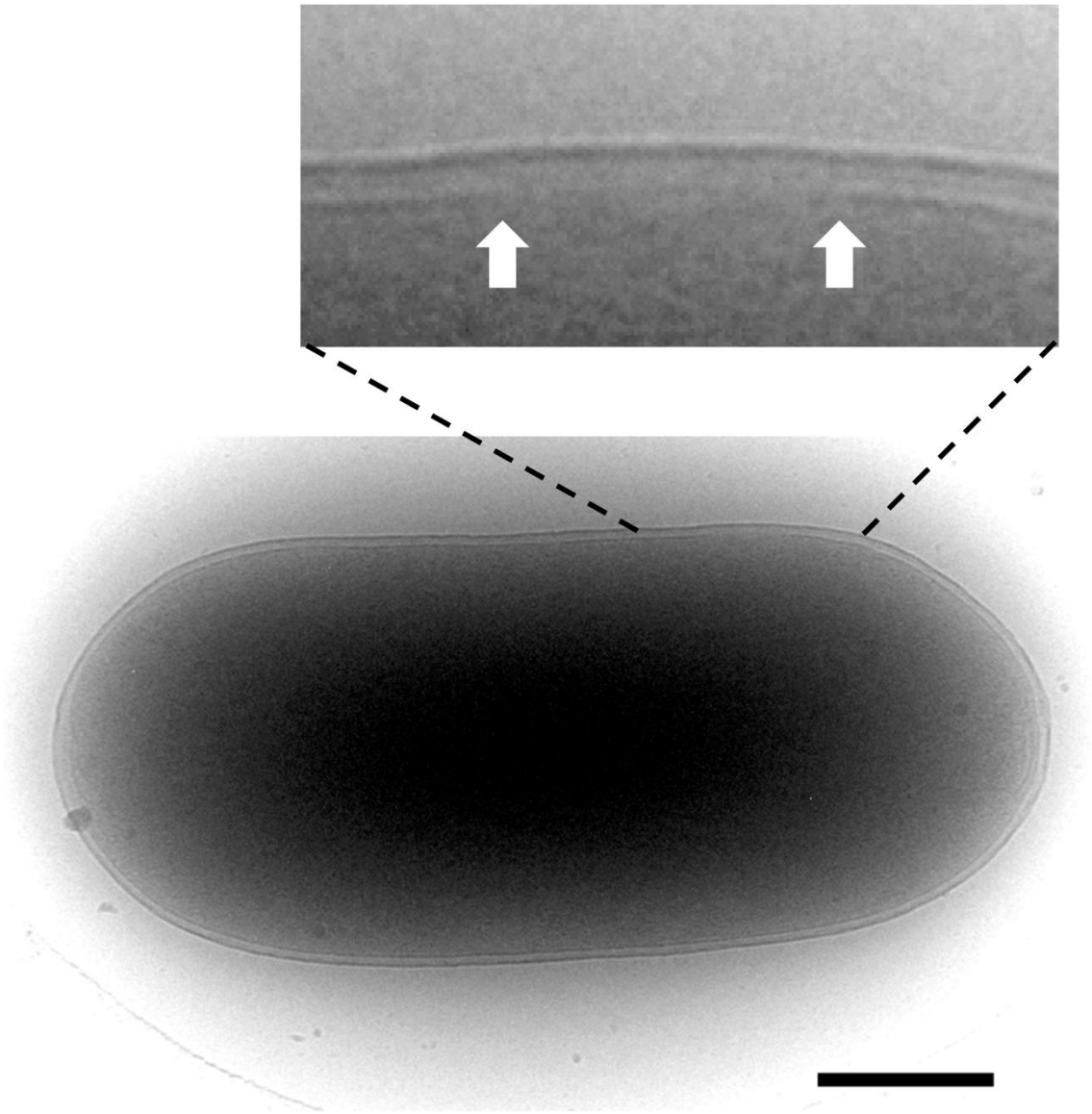

Figure 5.18. *E.coli* cell expressing T4 *T*. The region of the cytoplasmic membrane with a lesion is shown enlarged. The arrows indicate the region of dicontinuity in the inner membrane. The scale bar corresponds to 0.5 μm.

(Fig. 5.18). Cells expressing the T_{am} mutant had continuous membranes in 98%, or 50 out of 51, of the cells imaged. Of the 55 cells expressing *T*, 19, or 35%, had inner membrane lesions. Hole size ranged from 99 nm to 704 nm, with the majority of lesions in either the <200 nm class or the 200 – 400 nm class (Fig. 5.19A). With the current system, the minimum hole size visualized and measured was ~80 nm, so the smallest size class was actually 80 - 200 nm. Most of the cells with holes had a single visible lesion, but there were instances where cells had multiple visible holes (Fig. 5.19B), and the geometry can again be used to calculate the predicted actual number of holes per cell. Finally, the holes were located throughout the cell periphery, and there was no apparent correlation between hole size and localization (Fig. 5.19C).

Discussion

The massive holes visualized in cells expressing S105 are not limited to one bacteriophage holin, nor to one class of holin proteins. Instead, we have shown that the large lesions are present in the cytoplasmic membranes of cells expressing the class I holin protein Y from phage P2 and the class III holin protein T from the well-studied phage T4. Over 50 cells were imaged for all holins, and the hole sizes and localization patterns were analyzed. For these experiments, lysogenic strains were used and the holin was thermally induced. The holes were found to be somewhat similar in size for all holins. The major size class for λ S105 and P2 Y was 200 - 400 nm, but with T holes, the major size classes were <200 nm and 200 - 400 nm. With the current system, the minimum hole size visualized and measured was ~80 nm, so the smallest size class is

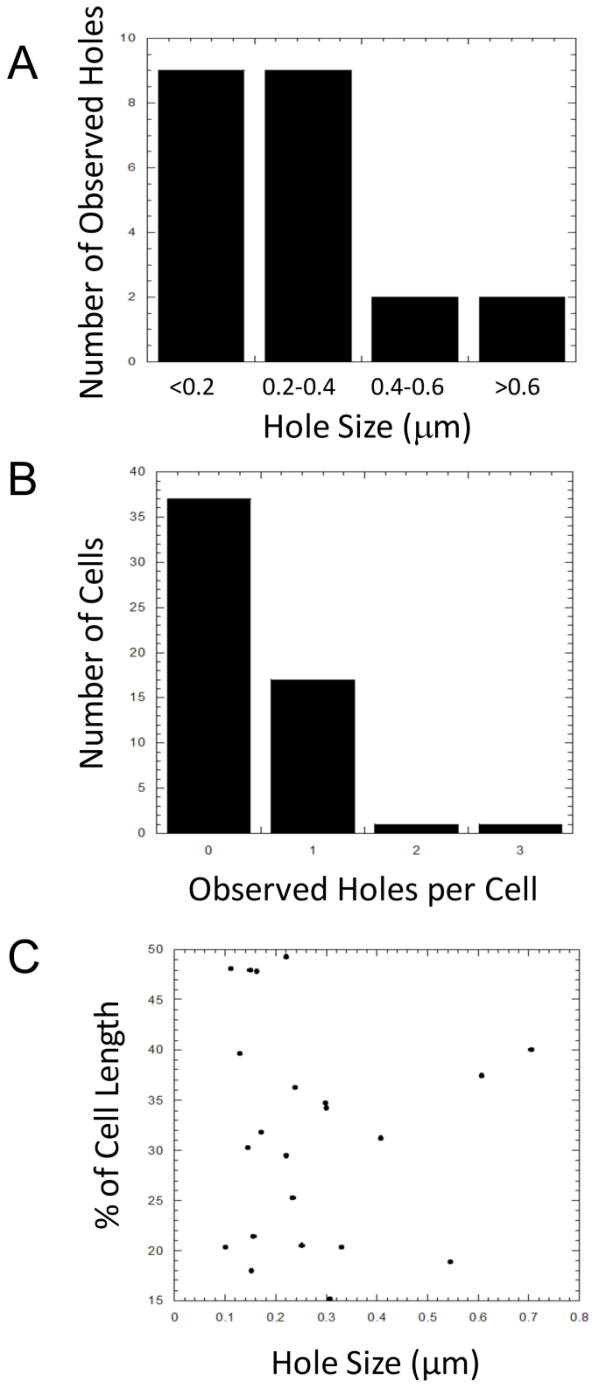

Figure 5.19. Statistics of cells expressing *T*, including hole size (A), number of holes per cell (B) , and hole localization with respect to hole size (C).

actually 80 - 200 nm. In all cases, the holes were localized randomly throughout the periphery of the cell, and there was no correlation between hole size and hole location. Finally, in all cases, most cells with holes had a single visible hole per cell, but the geometry and viewing angle must be accounted for in determining the actual number of holes per cell because we are limited by the position and orientation of the cells on the grid during the freezing process.

Single amino acid S105 missense mutants were analyzed in terms of lysis timing, protein accumulation, and hole size. The results indicated that lysis timing cannot be correlated with side chain size, composition, or branching pattern, nor is it the effect of protein translation levels. Instead, we found that the protein concentration at the time of triggering is allele-specific, with early lysing mutants accumulating less protein and late lysing mutants accumulating more protein prior to lysis. This conclusion is opposed to the former belief that early lysing mutants make more protein faster to reach the critical concentration necessary for hole formation. An early lysing S105 mutant, A52F, was expressed in cells and shown to form lesions which were smaller in diameter than wild-type cells. When cells expressing wild-type S105 were prematurely triggered with an energy poison, only 20% of the cells had visible lesions, indicating that most of the holes were too small to visualize with our system.

Materials and Methods

Plasmids and strains. The plasmids used for C51 and A52 site-directed mutagenesis are derivatives of pS105 (2). The plasmids used for cryo-EM were $pYR_{am}Rz_{am}Rz1_{am}$,

pS105$R_{am}Rz_{am}Rz1_{am}$ (and missense mutants), $pS^{21}R_{am}Rz_{am}Rz1_{am}$, and $pTR_{am}Rz_{am}Rz1_{am}$. All of these plasmids are derivatives of pS105 (2), and have ampicillin resistance. The strains used for expression include MC4100 Δ*tonA* (λCamΔ*SR*) (2) and MG1655 Δ*tonA* $lacI^q$ Δ*lacY* pQ (3).

Growth conditions and monitoring. Growth conditions and TCA precipitation of whole cell samples for lysis curves and protein expression experiments, respectively, were the same as described in Chapter V, Part I.

Electron microscopy. Cryo-EM grids were prepared and imaged as previously described, except cultures were concentrated gently prior to liquid ethane fixation. Specifically, cells were vacuum filtered with a 0.45 μm filter and resuspended in ~1 ml of LB (3). Three to five microliters of this sample was applied to C-flat or homemade holey carbon grids.

CHAPTER VI

CONCLUSIONS

The lambda holin has been studied extensively by a combination of genetic and biochemical approaches over the years. This work describes additional characterization of the lambda holin S105, as well as its inner membrane lesion and the lesions of other bacteriophage holins. During late gene expression, the lambda holin accumulates in the inner membrane of its host, *E. coli*. Chemical crosslinking experiments were used to show that the protein dimerizes and oligomerizes upon accumulation (16). Specifically, non-functional missense mutants were blocked in various stages of the hole formation pathway. The current model for hole formation suggests that the S105 oligomers, which are two-dimensional arrays or aggregates termed "rafts", spontaneously trigger to form holes in the cytoplasmic membrane. The holes allow the endolysin to pass through the inner membrane and degrade the peptidoglycan layer of the cell wall. After cell wall degradation, the spanin proteins, Rz and Rz1, destabilize the outer membrane, and lysis occurs (13). Until now, nothing was known about the structure of the holin-mediated membrane hole that forms during late gene expression just before phage lysis of its host cell. In this work, we have visualized holin lesions for the very first time, and determined that they represent the largest membrane lesions ever observed, by at least an order of magnitude (3). In addition, they are irregular in shape, and present in cells expressing at least two of the classes of holin proteins.

With regard to in vitro characterization of the lambda holin, this work describes advances in two important aspects of S105 research: in vitro reconstitution of the hole formation pathway and structural studies. A completely in vitro system including purified lambda holin and artificial membrane vesicles would be the ideal system for testing the current model for S105 hole formation. Such a system has been implemented (1-2), and in this work, some progress was made to improve it. The vesicles, or liposomes, were loaded with the self-quenching fluorophore calcein, and upon addition of purified S105, hole formation was assayed by an increase in fluorescence. Using cysteine-less, guanidine-solubilized purified lambda holin in the fluorescence assay resulted in improved yields of calcein release.

In addition to in vitro reconstitution of hole formation, structural studies of the lambda holin would also provide valuable information about S105 function in the lytic pathway. In collaboration with the Hilty lab (Texas A&M, Chemistry Department), we have embarked on structural analysis of a lambda holin mutant by optimizing the processes involved in sample preparation and NMR assays. In addition, TMD residues were shown to be involved in lipid micelle interactions, while the C-terminal tail residues were primarily involved in interactions with water. These NMR studies have resulted in chemical shift assignments for most of the residues within the protein, and have provided preliminary data for obtaining structural information for the holin mutant. In addition, the sample preparation and NMR optimization in this work may be applicable to structural studies of other S105 mutants and other phage holin proteins.

Finally, this work has provided the first direct evidence of the inner membrane holin-mediated lesion. In collaboration with Dr. Christos Savva and Dr. Andreas Holzenburg (Texas A&M, MIC), we used cryo-EM to visualize cells expressing the following holins: lambda S105, P2 Y, $S^{21}68$, and T4 T. Large holes were imaged in the cytoplasmic membranes of cells expressing the class I holins S105 and Y, as well as the class III holin T. The S105 holes were much larger than anticipated with an average diameter of ~340 nm (3). Most of the cells with holes had only a single visible lesion, but multiple holes per cell were seen in some cases. The geometry, together with the viewing angle, can be used to determine the actual number of holes per cell since the number of visible holes is limited by the position and orientation of the cells on the EM grid. In addition, the holes were localized randomly throughout the membrane, and there was no correlation between hole localization and hole size. Cryo-electron tomography was also used to create three-dimensional reconstructions of the S105 membrane hole, providing information on the overall extent of hole formation and the somewhat irregular shape of the hole (3).

The holin-mediated lesions described in this work were extremely large. In fact, the average hole size was ten-fold greater than the largest known membrane channels in biology, the cholesterol-dependent cytolysins (3, 21-22). Why are the holes so big? One answer to this question may be considered in an evolutionary context. Consider, for example, the bacterial holin encoded by *tcdE,* which is found in *Clostridium difficile* (111). This particular holin gene is located between two toxin genes called *tcdA* and *tcdB*. These toxin genes encode two of the largest known bacterial toxins (112), with

TcdA and TcdB being 308 kDa and 269 kDa in size, respectively (113). Interestingly, these two proteins do not have signal sequences (111, 114), so there is no obvious pathway for their extracellular release, except lysis. Since these proteins are so large, it has been hypothesized that TcdA and TcdB may exit the cell via the TcdE holin lesion (111, 115). In this context, the inner membrane hole must be large enough to accommodate these massive proteins.

The current model for S105 function suggests that a lesion spontaneously forms in the cytoplasmic membrane of *E.coli* from a two-dimensional aggregate, or raft, at the triggering time. The timing is allele-specific and the critical concentration of S105 molecules in the membrane at the triggering time is also allele-specific, such that early lysing mutants have less protein in the membrane at the time of lysis, and later lysing mutants have more protein in the membrane at the time of lysis. There is biological precedence for such an allele-specific critical concentration model which involves the integral membrane protein bacteriorhodopsin, or BR. This protein, together with lipid, forms the two-dimensional lattice purple membrane of *Halobacterium salinarum* (116-117). BR has seven α-helical TMDs, and was used to study membrane protein oligomerization. Mutations were made at the residues involved in helical interactions within the oligomerized protein complex, and the stability of the BR-lipid lattice was assayed for the mutant proteins. In each case, the mutants either increased or decreased the stability of the lattice (116). In other words, there was an allele-specific effect which resulted in changes in the self-assembly of BR in the membrane.

According to the current model, the S105 raft reaches a critical concentration, after which the protein undergoes conformational changes leading to hole formation and dissipation of the pmf. Therefore, the holin critical concentration and subsequent timing of lysis are directly related to protein interactions in the membrane. This model infers that individual phage holins would have different intermolecular interactions and therefore, different critical concentrations. In addition, the timing of hole formation and lysis would vary among these holins. However, a surprising result showed that lambda S and T4 T holins are additive, i.e. when these holins were co-expressed, lysis occurred sooner than when they are each expressed alone (34). Since S and T do not share any sequence similarity, it is unlikely that these two proteins interact to form rafts and holes together. In addition, there is no effect on the membrane potential prior to the instant of triggering for lysis (38), indicating that the pmf remains intact and is not titrated out by oligomerized holins. Instead, there may be a host inhibitory protein blocking hole formation. Prior to this shocking result of the additive hole formation by S and T (34), the host inhibitory protein model seemed unlikely given the diversity of holins and their function in both yeast and mammalian cells, but it cannot be excluded as a possibility.

The phage-shock-protein, or Psp, functions in extracytoplasmic stress response (118), and may be an example of a host protein that inhibits hole formation. These proteins are common to many types of bacteria, including *E. coli*, and in many bacterial genomes, there are two or more adjacent Psp proteins which together comprise a Psp system (118). It is believed that dissipation of the membrane pmf is an inducing signal for the Psp system. Therefore, these proteins may be induced after holin lesion

formation, which is accompanied by depolarization of the membrane. In this context, the Psp system would serve to counteract the dissipation of the pmf, thus prolonging lysis timing. In the example above where *S* and *T* are co-expressed, lysis may have occurred earlier because there was simply not enough Psp to block hole formation by both functional holins.

The formation of S105 rafts was visualized by Dr. Rebecca White when she expressed S105-GFP in cells and imaged them with fluorescence microscopy (109, 119). Prior to the triggering time, S105-GFP was localized throughout the membrane of the cells, and after the triggering time, there were punctuate spots, or patches, of fluorescence in specific regions of the membrane. Correlative microscopy is currently underway to co-localize the S105-GFP rafts visualized with fluorescence microscopy and the membrane holes visualized with cryo- EM. Currently, there is no direct evidence that S105 is lining the holes, or lesions, although the current model suggests that is in fact the case. Co-localization of the protein around the edges of the membrane hole would provide indisputable evidence that the lesions we have visualized here for the first time are a direct result of S105 accumulation in the membrane.

REFERENCES

1. Deaton J, Savva CG, Sun J, Holzenburg A, Berry J, et al. (2004) Solubilization and delivery by GroEL of megadalton complexes of the lambda holin. *Protein Sci* 13(7):1778-1786.

2. Smith DL, Struck DK, Scholtz JM, & Young R (1998) Purification and biochemical characterization of the lambda holin. *J Bacteriol* 180(9):2531-2540.

3. Dewey JS, Savva CG, White RL, Vitha S, Holzenburg A, et al. (2010) Micron-scale holes terminate the phage infection cycle. *Proc Natl Acad Sci U S A* 107(5):2219-2223.

4. Wang I & Young R (2006) Phage lysis. *The Bacteriophages*, 2nd Ed, ed Calendar R (Oxford University Press, New York), pp 104-128.

5. Young R (1992) Bacteriophage lysis: mechanism and regulation. *Microbiol Rev* 56(3):430-481.

6. Wang IN, Smith DL, & Young R (2000) Holins: the protein clocks of bacteriophage infections. *Annu Rev Microbiol* 54:799-825.

7. Young R (2002) Bacteriophage holins: deadly diversity. *J Mol Microbiol Biotechnol* 4(1):21-36.

8. Bernhardt TG, Roof WD, & Young R (2000) Genetic evidence that the bacteriophage phi X174 lysis protein inhibits cell wall synthesis. *Proc Natl Acad Sci U S A* 97(8):4297-4302.

9. Altman E, Altman RK, Garrett JM, Grimaila RJ, & Young R (1983) *S* gene product: identification and membrane localization of a lysis control protein. *J Bacteriol* 155(3):1130-1137.

10. Blasi U, Chang CY, Zagotta MT, Nam KB, & Young R (1990) The lethal lambda *S* gene encodes its own inhibitor. *EMBO J* 9(4):981-989.

11. Raab R, Neal G, Sohaskey C, Smith J, & Young R (1988) Dominance in lambda *S* mutations and evidence for translational control. *J Mol Biol* 199(1):95-105.

12. Bienkowska-Szewczyk K & Taylor A (1980) Murein transglycosylase from phage lambda lysate. Purification and properties. *Biochim Biophys Acta* 615(2):489-496.

13. Berry J, Summer EJ, Struck DK, & Young R (2008) The final step in the phage infection cycle: the Rz and Rz1 lysis proteins link the inner and outer membranes. *Mol Microbiol* 70(2):341-351.

14. Grundling A, Blasi U, & Young R (2000) Biochemical and genetic evidence for three transmembrane domains in the class I holin, lambda S. *J Biol Chem* 275(2):769-776.

15. Raab R, Neal G, Garrett J, Grimaila R, Fusselman R, et al. (1986) Mutational analysis of bacteriophage lambda lysis gene *S*. *J Bacteriol* 167(3):1035-1042.

16. Grundling A, Blasi U, & Young R (2000) Genetic and biochemical analysis of dimer and oligomer interactions of the lambda S holin. *J Bacteriol* 182(21):6082-6090.

17. Johnson-Boaz R, Chang CY, & Young R (1994) A dominant mutation in the bacteriophage lambda *S* gene causes premature lysis and an absolute defective plating phenotype. *Mol Microbiol* 13(3):495-504.

18. Zagotta MT & Wilson DB (1990) Oligomerization of the bacteriophage lambda S protein in the inner membrane of *Escherichia coli*. *J Bacteriol* 172(2):912-921.

19. Ryan GL & Rutenberg AD (2007) Clocking out: modeling phage-induced lysis of *Escherichia coli*. *J Bacteriol* 189(13):4749-4755.

20. Wang IN, Deaton J, & Young R (2003) Sizing the holin lesion with an endolysin-beta-galactosidase fusion. *J Bacteriol* 185(3):779-787.

21. Tweten RK (2005) Cholesterol-dependent cytolysins, a family of versatile pore-forming toxins. *Infect Immun* 73(10):6199-6209.

22. Tilley SJ & Saibil HR (2006) The mechanism of pore formation by bacterial toxins. *Curr Opin Struct Biol* 16(2):230-236.

23. Smith DL, Chang CY, & Young R (1998) The lambda holin accumulates beyond the lethal triggering concentration under hyperexpression conditions. *Gene Expr* 7(1):39-52.

24. Smith DL & Young R (1998) Oligohistidine tag mutagenesis of the lambda holin gene. *J Bacteriol* 180(16):4199-4211.

25. Savva CG, Dewey JS, Deaton J, White RL, Struck DK, et al. (2008) The holin of bacteriophage lambda forms rings with large diameter. *Mol Microbiol* 69(4):784-793.

26. Ziermann R, Bartlett B, Calendar R, & Christie GE (1994) Functions involved in bacteriophage P2-induced host cell lysis and identification of a new tail gene. *J Bacteriol* 176(16):4974-4984.

27. Blasi U & Young R (1996) Two beginnings for a single purpose: the dual-start holins in the regulation of phage lysis. *Mol Microbiol* 21(4):675-682.

28. Vukov N, Scherer S, Hibbert E, & Loessner MJ (2000) Functional analysis of heterologous holin proteins in a λΔ*S* genetic background. *FEMS Microbiol Lett* 184(2):179-186.

29. Heineman RH, Bull JJ, & Molineux IJ (2009) Layers of evolvability in a bacteriophage life history trait. *Mol Biol Evol* 26(6):1289-1298.

30. Park T, Struck DK, Dankenbring CA, & Young R (2007) The pinholin of lambdoid phage 21: control of lysis by membrane depolarization. *J Bacteriol* 189(24):9135-9139.

31. Park T, Struck DK, Deaton JF, & Young R (2006) Topological dynamics of holins in programmed bacterial lysis. *Proc Natl Acad Sci U S A* 103(52):19713-19718.

32. Sun Q, Kuty GF, Arockiasamy A, Xu M, Young R, et al. (2009) Regulation of a muralytic enzyme by dynamic membrane topology. *Nat Struct Mol Biol* 16(11):1192-1194.

33. Xu M, Struck DK, Deaton J, Wang IN, & Young R (2004) A signal-arrest-release sequence mediates export and control of the phage P1 endolysin. *Proc Natl Acad Sci U S A* 101(17):6415-6420.

34. Ramanculov E & Young R (2001) Functional analysis of the phage T4 holin in a lambda context. *Mol Genet Genomics* 265(2):345-353.

35. Ramanculov E & Young R (2001) Genetic analysis of the T4 holin: timing and topology. *Gene* 265(1-2):25-36.

36. Paddison P, Abedon ST, Dressman HK, Gailbreath K, Tracy J, et al. (1998) The roles of the bacteriophage T4 *r* genes in lysis inhibition and fine-structure genetics: a new perspective. *Genetics* 148(4):1539-1550.

37. Tran TA, Struck DK, & Young R (2005) Periplasmic domains define holin-antiholin interactions in T4 lysis inhibition. *J Bacteriol* 187(19):6631-6640.

38. Grundling A, Manson MD, & Young R (2001) Holins kill without warning. *Proc Natl Acad Sci U S A* 98(16):9348-9352.

39. Goldberg AR & Howe M (1969) New mutations in the *S* cistron of bacteriophage lambda affecting host cell lysis. *Virology* 38(1):200-202.

40. Kropinski AM, Kovalyova IV, Billington SJ, Patrick AN, Butts BD, et al. (2007) The genome of epsilon15, a serotype-converting, Group E1 *Salmonella enterica*-specific bacteriophage. *Virology* 369(2):234-244.

41. Srividhya KV & Krishnaswamy S (2007) Subclassification and targeted characterization of prophage-encoded two-component cell lysis cassette. *J Biosci* 32(5):979-990.

42. Krupovic M, Daugelavicius R, & Bamford DH (2007) A novel lysis system in PM2, a lipid-containing marine double-stranded DNA bacteriophage. *Mol Microbiol* 64(6):1635-1648.

43. Haro A, Velez M, Goormaghtigh E, Lago S, Vazquez J, et al. (2003) Reconstitution of holin activity with a synthetic peptide containing the 1-32 sequence region of EJh, the EJ-1 phage holin. *J Biol Chem* 278(6):3929-3936.

44. Diaz E, Munthali M, Lunsdorf H, Holtje JV, & Timmis KN (1996) The two-step lysis system of pneumococcal bacteriophage EJ-1 is functional in gram-negative bacteria: triggering of the major pneumococcal autolysin in *Escherichia coli*. *Mol Microbiol* 19(4):667-681.

45. Sao-Jose C, Santos S, Nascimento J, Brito-Madurro AG, Parreira R, et al. (2004) Diversity in the lysis-integration region of oenophage genomes and evidence for multiple tRNA loci, as targets for prophage integration in *Oenococcus oeni*. *Virology* 325(1):82-95.

46. Labrie S, Vukov N, Loessner MJ, & Moineau S (2004) Distribution and composition of the lysis cassette of *Lactococcus lactis* phages and functional analysis of bacteriophage ul36 holin. *FEMS Microbiol Lett* 233(1):37-43.

47. Yokoi KJ, Shinohara M, Kawahigashi N, Nakagawa K, Kawasaki K, et al. (2005) Molecular properties of the two-component cell lysis system encoded by prophage phigaY of *Lactobacillus gasseri* JCM 1131T: cloning, sequencing, and expression in *Escherichia coli*. *Int J Food Microbiol* 99(3):297-308.

48. Yokoi KJ, Kawahigashi N, Uchida M, Sugahara K, Shinohara M, et al. (2005) The two-component cell lysis genes *holWMY* and *lysWMY* of the *Staphylococcus*

warneri M phage varphiWMY: cloning, sequencing, expression, and mutational analysis in *Escherichia coli*. *Gene* 351:97-108.

49. Rice KC, Mann EE, Endres JL, Weiss EC, Cassat JE, et al. (2007) The cidA murein hydrolase regulator contributes to DNA release and biofilm development in *Staphylococcus aureus*. *Proc Natl Acad Sci U S A* 104(19):8113-8118.

50. Takac M, Witte A, & Blasi U (2005) Functional analysis of the lysis genes of *Staphylococcus aureus* phage P68 in *Escherichia coli*. *Microbiology* 151(Pt 7):2331-2342.

51. Habeeb AF (1972) Reaction of protein sulfhydryl groups with Ellman's reagent. *Meth Enzymol* 25:457-464.

52. Riddles PW, Blakeley RL, & Zerner B (1979) Ellman's reagent: 5,5'-dithiobis(2-nitrobenzoic acid)--a reexamination. *Anal Biochem* 94(1):75-81.

53. Riddles PW, Blakeley RL, & Zerner B (1983) Reassessment of Ellman's reagent. *Methods Enzymol* 91:49-60.

54. Grassetti DR & Murray JF, Jr. (1967) Determination of sulfhydryl groups with 2,2'- or 4,4'-dithiodipyridine. *Arch Biochem Biophys* 119(1):41-49.

55. Bonovich MT & Young R (1991) Dual start motif in two lambdoid *S* genes unrelated to lambda *S*. *J Bacteriol* 173(9):2897-2905.

56. Faulstich H, Tews P, & Heintz D (1993) Determination and derivatization of protein thiols by n-octyldithionitrobenzoic acid. *Anal Biochem* 208(2):357-362.

57. Cartwright T, Senussi O, & Grady D (1977) Reagents which inhibit disulphide bond formation stabilize human fibroblast interferon. *J Gen Virol* 36(2):323-327.

58. Murphy ME, Scholich H, & Sies H (1992) Protection by glutathione and other thiol compounds against the loss of protein thiols and tocopherol homologs during microsomal lipid peroxidation. *Eur J Biochem* 210(1):139-146.

59. Hochgrafe F, Mostertz J, Pother DC, Becher D, Helmann JD, et al. (2007) S-cysteinylation is a general mechanism for thiol protection of *Bacillus subtilis* proteins after oxidative stress. *J Biol Chem* 282(36):25981-25985.

60. Britto PJ, Knipling L, McPhie P, & Wolff J (2005) Thiol-disulphide interchange in tubulin: kinetics and the effect on polymerization. *Biochem J* 389(Pt 2):549-558.

61. Miroux B & Walker JE (1996) Over-production of proteins in *Escherichia coli*: mutant hosts that allow synthesis of some membrane proteins and globular proteins at high levels. *J Mol Biol* 260(3):289-298.

62. Chang CY, Nam K, & Young R (1995) *S* gene expression and the timing of lysis by bacteriophage lambda. *J Bacteriol* 177(11):3283-3294.

63. Harris AW, Mount DW, Fuerst CR, & Siminovitch L (1967) Mutations in bacteriophage lambda affecting host cell lysis. *Virology* 32(4):553-569.

64. Dewey JS, Struck DK, & Young R (2009) Thiol protection in membrane protein purifications: a study with phage holins. *Anal Biochem* 390(2):221-223.

65. White R, Tran TA, Dankenbring CA, Deaton J, & Young R (2010) The N-terminal transmembrane domain of lambda S is required for holin but not antiholin function. *J Bacteriol* 192(3):725-733.

66. Fernandez C & Wider G (2003) TROSY in NMR studies of the structure and function of large biological macromolecules. *Curr Opin Struct Biol* 13(5):570-580.

67. Roosild TP, Greenwald J, Vega M, Castronovo S, Riek R, et al. (2005) NMR structure of Mistic, a membrane-integrating protein for membrane protein expression. *Science* 307(5713):1317-1321.

68. Hiller S, Garces RG, Malia TJ, Orekhov VY, Colombini M, et al. (2008) Solution structure of the integral human membrane protein VDAC-1 in detergent micelles. *Science* 321(5893):1206-1210.

69. Wider G (2000) Structure determination of biological macromolecules in solution using nuclear magnetic resonance spectroscopy. *Biotechniques* 29(6):1278-1282, 1284-1290, 1292 passim.

70. Lee Y, Dewey JS, Young R, & Hilty C (2010) NMR studies of a helical membrane protein, $S105_{\Delta TM1}$. Manuscript in preparation.

71. Blasi U, Fraisl P, Chang CY, Zhang N, & Young R (1999) The C-terminal sequence of the lambda holin constitutes a cytoplasmic regulatory domain. *J Bacteriol* 181(9):2922-2929.

72. Rietsch A, Fraisl P, Graschopf A, & Blasi U (1997) The hydrophilic C-terminal part of the lambda S holin is non-essential for intermolecular interactions. *FEMS Microbiol Lett* 153(2):393-398.

73. Wishart DS & Sykes BD (1994) The 13C chemical-shift index: a simple method for the identification of protein secondary structure using 13C chemical-shift data. *J Biomol NMR* 4(2):171-180.

74. Wuthrich K, Billeter M, & Braun W (1984) Polypeptide secondary structure determination by nuclear magnetic resonance observation of short proton-proton distances. *J Mol Biol* 180(3):715-740.

75. Kay LE, Torchia DA, & Bax A (1989) Backbone dynamics of proteins as studied by 15N inverse detected heteronuclear NMR spectroscopy: application to staphylococcal nuclease. *Biochemistry* 28(23):8972-8979.

76. LeMaster DM & Richards FM (1988) NMR sequential assignment of *Escherichia coli* thioredoxin utilizing random fractional deuteriation. *Biochemistry* 27(1):142-150.

77. McIntosh LP & Dahlquist FW (1990) Biosynthetic incorporation of 15N and 13C for assignment and interpretation of nuclear magnetic resonance spectra of proteins. *Q Rev Biophys* 23(1):1-38.

78. Delaglio F, Grzesiek S, Vuister GW, Zhu G, Pfeifer J, et al. (1995) NMRPipe: a multidimensional spectral processing system based on UNIX pipes. *Journal of Biomolecular NMR* 6:277-293.

79. Masse JE & Keller R (2005) AutoLink: Automated sequential resonance assignment of biopolymers from NMR data by relative-hypothesis-prioritization-based simulated logic. *Journal of Magnetic Resonance* 174(1):133-151.

80. Summer EJ, Berry J, Tran TA, Niu L, Struck DK, et al. (2007) *Rz/Rz1* lysis gene equivalents in phages of Gram-negative hosts. *J Mol Biol* 373(5):1098-1112.

81. Reader RW & Siminovitch L (1971) Lysis defective mutants of bacteriophage lambda: on the role of the *S* function in lysis. *Virology* 43(3):623-637.

82. Kellenberger E, Johansen R, Maeder M, Bohrmann B, Stauffer E, et al. (1992) Artefacts and morphological changes during chemical fixation. *J Microsc* 168(Pt 2):181-201.

83. McIntosh R, Nicastro D, & Mastronarde D (2005) New views of cells in 3D: an introduction to electron tomography. *Trends Cell Biol* 15(1):43-51.

84. Dubochet J, Adrian M, Chang JJ, Homo JC, Lepault J, et al. (1988) Cryo-electron microscopy of vitrified specimens. *Q Rev Biophys* 21(2):129-228.

85. Berriman J & Unwin N (1994) Analysis of transient structures by cryo-microscopy combined with rapid mixing of spray droplets. *Ultramicroscopy* 56(4):241-252.

86. Bremer H & Dennis PP (1996) Modulation of chemical composition and other parameters of the cell by growth rate. *Escherichia coli and Salmonella: Cellular and Molecular Biology*, 2nd Ed, ed Neidhart FC (ASM Press, Washington D. C.), pp 1527-1542.

87. Pierucci O (1978) Dimensions of *Escherichia coli* at various growth rates: model for envelope growth. *J Bacteriol* 135(2):559-574.

88. Radermacher M (1992) Weighted back-projection methods. *Electron Tomography*, ed Frank J (Plenum, New York), pp 245-273.

89. Ford RC & Holzenburg A (2008) Electron crystallography of biomolecules: mysterious membranes and missing cones. *Trends Biochem Sci* 33(1):38-43.

90. Casjens S, Eppler K, Parr R, & Poteete AR (1989) Nucleotide sequence of the bacteriophage P22 gene *19* to *3* region: identification of a new gene required for lysis. *Virology* 171(2):588-598.

91. Young R, Way J, Way S, Yin J, & Syvanen M (1979) Transposition mutagenesis of bacteriophage lambda: a new gene affecting cell lysis. *J Mol Biol* 132(3):307-322.

92. Bayer ME (1968) Areas of adhesion between wall and membrane of *Escherichia coli*. *J Gen Microbiol* 53(3):395-404.

93. Bayer ME (1974) Ultrastructure and organization of the bacterial envelope. *Ann N Y Acad Sci* 235(0):6-28.

94. Hobot JA, Carlemalm E, Villiger W, & Kellenberger E (1984) Periplasmic gel: new concept resulting from the reinvestigation of bacterial cell envelope ultrastructure by new methods. *J Bacteriol* 160(1):143-152.

95. Tilley SJ, Orlova EV, Gilbert RJ, Andrew PW, & Saibil HR (2005) Structural basis of pore formation by the bacterial toxin pneumolysin. *Cell* 121(2):247-256.

96. Rydman PS & Bamford DH (2003) Identification and mutational analysis of bacteriophage PRD1 holin protein P35. *J Bacteriol* 185(13):3795-3803.

97. Adhya S, Sen A, & Mitra S (1971) *The Role of Gene S* (Cold Spring Harbor Laboratory Press, Cold Spring Harbor, New York).

98. Josslin R (1971) The effect of phage T4 infection on phospholipid hydrolysis in *Escherichia coli*. *Virology* 44(1):94-100.

99. Siegel DP, Cherezov V, Greathouse DV, Koeppe RE, 2nd, Killian JA, et al. (2006) Transmembrane peptides stabilize inverted cubic phases in a biphasic length-dependent manner: implications for protein-induced membrane fusion. *Biophys J* 90(1):200-211.

100. Garrett J, Bruno C, & Young R (1990) Lysis protein S of phage lambda functions in *Saccharomyces cerevisiae*. *J Bacteriol* 172(12):7275-7277.

101. Agu CA, Klein R, Lengler J, Schilcher F, Gregor W, et al. (2007) Bacteriophage-encoded toxins: the lambda-holin protein causes caspase-independent non-apoptotic cell death of eukaryotic cells. *Cell Microbiol* 9(7):1753-1765.

102. Campbell A (1961) Sensitive mutants of bacteriophage lambda. *Virology* 14:22-32.

103. Blattner FR, Plunkett G, 3rd, Bloch CA, Perna NT, Burland V, et al. (1997) The complete genome sequence of *Escherichia coli* K-12. *Science* 277(5331):1453-1474.

104. Datsenko KA & Wanner BL (2000) One-step inactivation of chromosomal genes in *Escherichia coli* K-12 using PCR products. *Proc Natl Acad Sci U S A* 97(12):6640-6645.

105. Saxton WO, Baumeister W, & Hahn M (1984) Three-dimensional reconstruction of imperfect two-dimensional crystals. *Ultramicroscopy* 13(1-2):57-70.

106. Kremer JR, Mastronarde DN, & McIntosh JR (1996) Computer visualization of three-dimensional image data using IMOD. *J Struct Biol* 116(1):71-76.

107. Frangakis AS & Hegerl R (2001) Noise reduction in electron tomographic reconstructions using nonlinear anisotropic diffusion. *J Struct Biol* 135(3):239-250.

108. Markov D, Christie GE, Sauer B, Calendar R, Park T, et al. (2004) P2 growth restriction on an *rpoC* mutant is suppressed by alleles of the *Rz1* homolog *lysC*. *J Bacteriol* 186(14):4628-4637.

109. White RL (2008) What makes the lysis clock tick? A study of the bacteriophage lambda holin. Ph.D. Dissertation (Texas A&M University, College Station, TX).

110. Pang T, Savva CG, Fleming KG, Struck DK, & Young R (2009) Structure of the lethal phage pinhole. *Proc Natl Acad Sci U S A* 106(45):18966-18971.

111. Tan KS, Wee BY, & Song KP (2001) Evidence for holin function of *tcdE* gene in the pathogenicity of *Clostridium difficile*. *J Med Microbiol* 50(7):613-619.

112. Ackermann G, Loffler B, Tang-Feldman YJ, Cohen SH, Silva J, Jr., et al. (2004) Cloning and expression of *Clostridium difficile* toxin A gene (tcdA) by PCR amplification and use of an expression vector. *Mol Cell Probes* 18(4):271-274.

113. Yang G, Zhou B, Wang J, He X, Sun X, et al. (2008) Expression of recombinant *Clostridium difficile* toxin A and B in *Bacillus megaterium*. *BMC Microbiol* 8:192.

114. Aktories K (1997) Rho proteins: targets for bacterial toxins. *Trends Microbiol* 5(7):282-288.

115. von Eichel-Streiber C & Sauerborn M (1990) *Clostridium difficile* toxin A carries a C-terminal repetitive structure homologous to the carbohydrate binding region of streptococcal glycosyltransferases. *Gene* 96(1):107-113.

116. Isenbarger TA & Krebs MP (1999) Role of helix-helix interactions in assembly of the bacteriorhodopsin lattice. *Biochemistry* 38(28):9023-9030.

117. Isenbarger TA & Krebs MP (2001) Thermodynamic stability of the bacteriorhodopsin lattice as measured by lipid dilution. *Biochemistry* 40(39):11923-11931.

118. Darwin AJ (2005) The phage-shock-protein response. *Mol Microbiol* 57(3):621-628.

119. White R, Chiba S, Pang T, Dewey JS, Savva CG, et al. (2010) The instant of death: holin triggering in real time. Manuscript in preparation.

VITA

Name: Jill Sayes Dewey

Address: Texas A&M University, Department of Biochemistry and Biophysics, TAMU 2128, Bio/Bio 311, College Station, TX 77843-2128

Email Address: jilldewey@gmail.com

Education: B.S., Biochemistry, Louisiana State University, 2003
graduated *summa cum laude*

Publications: Savva CG, **Dewey JS**, Deaton J, White RL, Struck DK, Holzenburg A, Young R (2008) The holin of bacteriophage lambda forms rings with large diameter. *Mol Microbiol* 69(4):784-793.

Dewey JS, Struck DK, and Young R (2009) Thiol protection in membrane protein purification: a study with bacteriophage holins. *Anal Biochem* 390(2):221-223.

Dewey JS, Savva CG, White RL, Vitha S, Holzenburg A, and Young R (2009) Micron-scale holes terminate the phage infection cycle. *Proc Natl Acad Sci U S A* 107(5):2219-2223.